

Cover Page



Universiteit Leiden



The handle <http://hdl.handle.net/1887/138650> holds various files of this Leiden University dissertation.

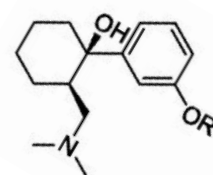
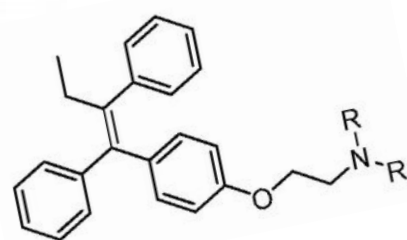
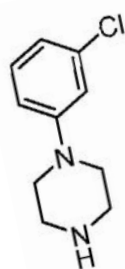
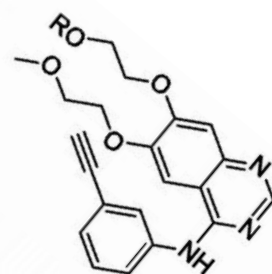
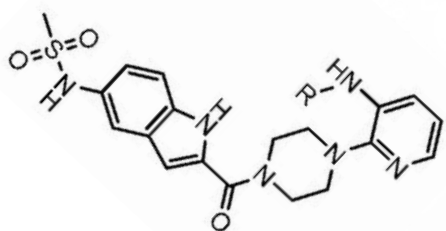
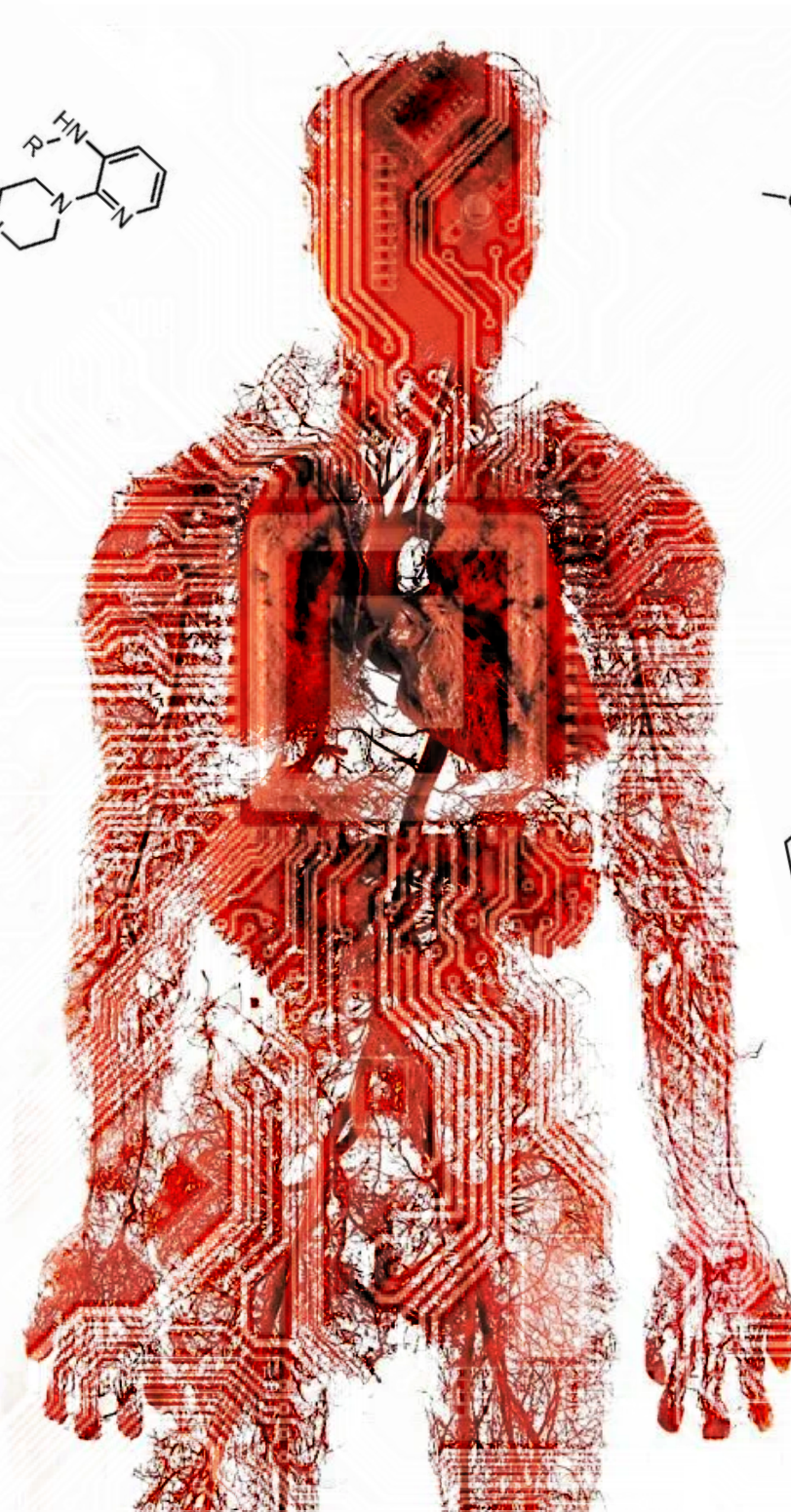
Author: Junaid, A.O.

Title: Microengineered human blood vessels for next generation drug discovery

Issue date: 2020-12-16

Microengineered Human Blood Vessels For Next Generation Drug Discovery

Abidemi Olakunle Junaid



***Microengineered Human
Blood Vessels For Next
Generation Drug Discovery***

ISBN: 978-90-831117-1-1

© Abidemi Olakunle Junaid

Printed by: Print Service Ede

Microengineered Human Blood Vessels For Next Generation Drug Discovery

PROEFSCHRIFT

ter verkrijging van
de graad van Doctor aan de Universiteit Leiden,
op gezag van Rector Magnificus prof. mr. C. J. J. M. Stolker,
volgens besluit van het College voor Promoties
te verdedigen op woensdag 16 december 2020
klokke 12.30 uur

door

Abidemi Olakunle Junaid

geboren te Ibadan, Nigeria
in 1990

PROMOTOR

Prof. dr. Thomas Hankemeier

Prof. dr. Anton Jan van Zonneveld

CO-PROMOTOR

Dr. Janine van Gils

Dr. Alireza Mashaghi

PROMOTIECOMMISSIE

Prof. dr. Hubertus Irth (voorzitter)

Leiden University, the Netherlands

Prof. dr. Joke Bouwstra (secretaries)

Leiden University, the Netherlands

Prof. dr. Gerald Urban

University of Freiburg, Germany

Prof. dr. Dirk Jan Duncker

Erasmus University Medical Center, the Netherlands

Prof. dr. Marie-José Goumans

Leiden University Medical Center, the Netherlands

Prof. dr. Bob van de Water

Leiden University, the Netherlands

Financial support by the Dutch Heart Foundation for the publication of this thesis is gratefully acknowledged.

The research described in this thesis was supported by a grant of the Dutch Heart Foundation (DHF CVON 2014-11 RECONNECT).

Contents

Chapter I	
General Introduction	7
Chapter II	
An End-User Perspective on Organ-on-a-Chip: Assays and Usability Aspects	19
Chapter III	
Microengineered human blood vessel to study microvascular destabilization <i>in vivo</i>	47
Chapter IV	
Ebola hemorrhagic shock syndrome-on-a-chip	69
Chapter V	
Metabolic response of blood vessels to TNF α	95
Chapter VI	
An integrated microvessels-on-a-chip platform for automated multi-channel perfusion and continual <i>in situ</i> oxygen monitoring	125
Chapter VII	
Discussion and Conclusion	143
Chapter VIII	
Summary	156
Nederlandse samenvatting	159
Acknowledgements	162
Curriculum Vitae	163
List of Publications	164

Chapter I

General Introduction

General Introduction

Microvascular diseases

In the last decades, great progress has been made in the treatment of the atherosclerosis-driven macrovascular diseases that are a leading cause of death worldwide. However, it is now well established that diseases of the microvasculature contribute to mortality in equal proportions.

In the cardiovascular field, heart failure (HF) is a major global health care problem with high morbidity and mortality, already affecting more than 23 million people worldwide [1]. Traditionally, most attention was paid to HF with reduced myocardial contractile function, left ventricular dilatation and reduced ejection blood volume (HFrEF) as the main feature. However, it is now clear that 50% of HF patients demonstrate symptoms of HF with preserved ejection fraction (HFpEF) [2]. It was established that HFpEF involves the progressive loss of myocardial microvascular integrity leading to an ischemia- and inflammation related fibrotic response that results to increased left ventricular stiffness [3]. While treatment options and subsequent clinical outcome have been improved over the years in patients with HFrEF, this is not true for patients with HFpEF, for whom therapeutic options remain limited [4].

Additionally, in ischemic heart disease, 20-30% of patients undergoing coronary angiography for evaluation of angina-like chest pain may suffer from non-obstructive coronary artery disease, also denoted as 'microvascular angina'. This condition is associated with low-grade chronic inflammation and coronary microvascular dysfunction [5, 6].

The worldwide increase of obesity is directly related to the prevalence of patients with type 2 diabetes mellitus (DM) [7]. These patients develop severe microvascular complications, including diabetic retinopathy, nephropathy and neuropathy [8]. Patients with diabetes and chronic renal failure also have a high risk to develop HFpEF and microvascular angina.

Microvascular involvement is also largely underestimated in patients with autoimmune disease. Systemic sclerosis (SSc) is an autoimmune disease that is characterized by microvascular damage, dysregulation of innate and adaptive immunity and fibrosis in multiple organs. The estimated prevalence ranges from 50 to 300 cases per 1 million persons and an

incidences ranging from 2.3 to 22.8 cases per 1 million persons per year [9]. The events initiating SSc are unknown. In the nailfold capillaries of SSc patients, enlarged capillaries and capillary loss can be found. This suggest that microvascular malfunction is involved in the early development of SSc [10].

The human microvessels

Mechanistically, the endothelial cells (ECs) from the microvasculature are key drivers and targets of inflammatory and thrombotic processes in microvascular diseases. They are the inner surface of the blood vessels in contact with blood and mural cells that interact with the outer surface of ECs. Mural cells most often are smooth muscle cells (SMCs) or pericytes. Larger blood vessels, in the range of 100 μm , such as the arterioles, arteries and veins, are invested with single layer of ECs, surrounding layer of SMCs, outside layer of fibroblasts and extracellular matrix (ECM) components. The microvessels, in the range of 10 μm , which are the capillaries, consist of single layer ECs, underlying basal lamina and surrounded by pericytes (Figure 1) [11, 12].

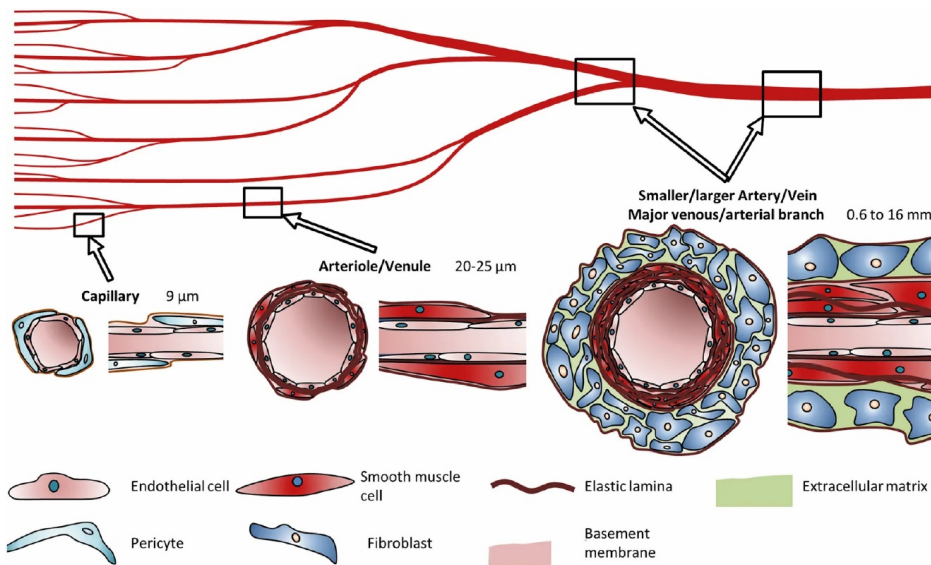


Figure 1 | Schematic of the human blood vessel. Arterioles/venules are invested with endothelial cells, smooth muscle cells and enclosed layer of fibroblasts. The capillaries, which comprise the microvessels, consists of endothelial cells surrounded by pericytes [11].

The ECs regulate blood flow, modulate coagulation, inflammation and vascular permeability in the capillaries. Destabilization of the microvessels is initiated by chronic activation of the ECs by cardiovascular risk factors that inflict the loss of pericytes, followed by the loss of EC cell-cell junctions, microvascular leakage and induction of a pro-angiogenic response [13, 14]. These processes are mediated by several angioregulatory factors, including pericyte-expressed anti-inflammatory factor Angiopoietin-1 (Ang-1) and the EC-derived pro-inflammatory factor Angiopoietin-2 (Ang-2). In normal physiological condition, Ang-1 binds to its main receptor, Tie2, that is predominantly expressed on ECs [14]. This mediates microvessel maturation and stability and reduce vascular leakage. However, in microvascular diseases such as diabetic nephropathy, Ang-2 competes for binding to the same Tie-2 receptor as Ang-1 and elicits inflammation, microvascular destabilization and leakage [15].

Insufficient diagnostic and prognostic tools for microvascular diseases

Microvascular disease has an unmet clinical need for new therapeutics, with few to no therapies available. Unfortunately, microvascular disease cannot be studied in a physiologically relevant way using static cell cultures, because current two-dimensional (2D) human models with cultured ECs lack sufficient complexity to assess the functionality of the microvascular system. Therefore, microvascular disease has been predominantly studied in experimental animal models. However, recent publications have emphasized the differences between human diseases and animal models of diseases, and how this led to failure in predicting therapeutic safety and efficacy [16]. Moreover, animal models are limited in the number of individual parameters that can be assessed at cell-type specific levels. Some have recommended abandoning animal studies and focusing more on clinical trials in patients. However, the ethic and financial burdens behind this concept is too great to overcome. Clinical trials must be conducted in agreement with ethical standards, coherent scientific proof and benefit outweigh risk [17]. On average, it takes between 10-12 years and \$1.5-\$3 billion to bring a new drug to the market. This is to a large extent as less than 10% of drugs that enter clinical trials end up making it to the market [18].

The use of organs-on-chips to study microvascular diseases

The development of relevant micro-physiological systems could benefit the investigation of human-specific molecular mechanisms of microvascular destabilization. The 'organs-on-chips' are proposed to serve as advanced micro-physiological systems that can mimic key features of microvascular homeostasis. These are biomimetic microfluidic cell culture devices with microchannels consisting of glass or silicon-based, often made with microfabrication methods that were initially designed for the electronics industry [19].

An organ-on-a-chip platform makes it possible to co-culture cells and study cell-cell interactions, such as the culture of ECs with pericytes [20]. It can provide native microvessel function in an intricate three-dimensional (3D) environment with intimate interactions between ECs and pericytes (Figure 2) [21]. Moreover, with the perfusion of whole blood or blood particles, the organs-on-chips feature laminar shear stress in order for the ECs to

maintain a quiescent anti-inflammatory phenotype. The lack of laminar shear stress in static cell cultures converts ECs to maintain a pro-inflammatory “diseased” phenotype [22]. ECs are usually cultured on surfaces such as plastics and glass that are much stiffer than ECM. Unfortunately, the cells on such hard substrate also adopt a pro-inflammatory phenotype [23]. On the contrary, in the organs-on-chips, ECs can be cultured on ECM with a modifiable physiological stiffness, forming a microvessel that is uniquely suited to study microvascular disease.

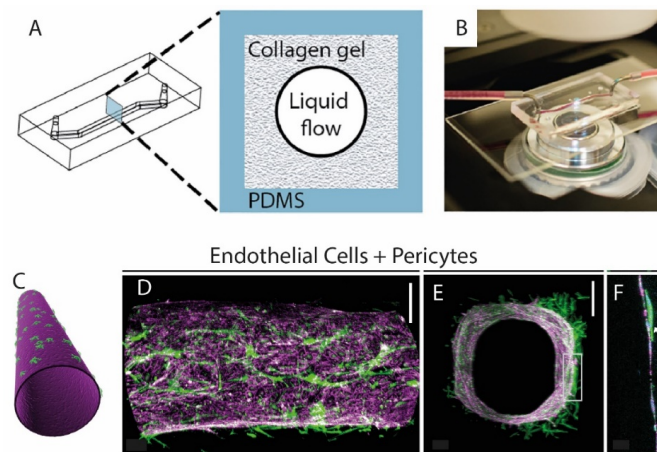


Figure 2 | The 3D human blood-brain barrier (BBB) on a chip. (A) Schematic diagram of the organ-on-a-chip showing the microchannel containing extracellular matrix (collagen) and a central lumen for generating a 3D BBB on a chip. (B) Photograph of the 3D BBB on a chip on the stage of a microscope. (C-F) The fluorescence micrographs of the brain microvascular endothelium invested with brain pericytes in surrounding extracellular matrix (bars, 200 μm in D, E and 30 μm in F). Magenta corresponds to VE-Cadherin staining of endothelial cells and green represents F-actin staining of pericytes [21].

Advancements in organs-on-chips has also enabled the production of multi-organs-on-chips. In this platform, cells are co-cultured in several organ chambers and are connected by microfluidic channels. These organ chambers can interact with each other through the flow of culture medium, simulating blood circulation. This allows investigation of pharmacokinetic and pharmacodynamic (PK/PD) parameters [24]. To fully mimic human organismal homeostasis, blood circulation through ECs-lined microfluidic channels connecting organ

equivalents with each other in a physiological order is needed [25]. In one study, a chip model was developed that connects induced pluripotent stem cells (iPSCs)-derived cardiomyocytes and hepatocytes by 3D-printed rigid filament networks of a carbohydrate glass lined with ECs and perfused with blood under high-pressure pulsatile flow [26]. This platform may serve as a unique tool for toxicology studies as well as for the development of novel therapeutic strategies to combat loss on microvascular integrity.

Various functional and biochemical read-outs can be used to gain information on the health status of the microvessel, depending on the choice of organ-on-a-chip platform. It is very common to utilize immunostaining and imaging to assess the structure and viability of the miniaturized vessel [27, 28]. In order to investigate vessel permeability or leakage, micro-structured electrodes are integrated in the microfluidic chip to measure the trans-endothelial electrical resistance (TEER) that allows continuous and non-invasive evaluation of the endothelial barrier function [29]. Another method is to quantify the diffusion of fluorescent molecules, with physiological relevant sizes, through the vessel wall [30]. This assay can be used to optimize the culture conditions for robust and long-term culture of the vessels at a low cost.

Cell metabolism in the organs-on-chips can also be used to understand the health condition of the vascular tissue model. To analyze metabolism of cells, often small molecules, i.e., metabolites and lipids such as amines and modified fatty acids are measured with metabolomics, thus providing additional information to standard end-point assays such as immunostainings, permeability assay and quantitative polymerase chain reaction (qPCR). The integration of both functional and biochemical measurements makes the read-out of the microvessel *in vitro* more accurate and informative.

With the functional and biochemical read-outs, the organ-on-a-chip platform may facilitate the identification of disease-associated circulating factors in blood that cause microvascular destabilization and help diagnosis and clinical management of patients at risk for microvascular disease related complications such as HFpEF, microvascular angina and diabetic nephropathy. It may serve to assess the functional impact of adverse circulating factors and facilitate the identification of the affected biological pathways and processes and identify potential novel therapeutic targets with sufficient efficacy and safety.

Outline of this thesis

In recent years, a wide range of perfusable microvessel models have been developed exploiting advances in microfluidics, biomaterials and tissue engineering. Therefore, the research question that is discussed in this thesis:

How can we use a microfluidic 3D cell culture platform to develop a reliable robust and physiological relevant ‘microvessel-on-a-chip’ platform, that may serve as an attractive and versatile replacement for a significant fraction of animal models in vascular homeostasis?

To answer this question, the comparability of the physiology of the *in vitro* system with human situation is hereby essential. The conditions of blood plasma have to be matched and a sensitive read-out of small changes is needed. Metabolomics as read-out could be suited for this. Most importantly, the microvessel-on-a-chip should be optimally suited to model human microvessels and possess the ability to measure the presence of inflammatory leakage factors in patient-derived blood, thereby opening up the options to study loss of microvascular integrity, and ultimately allowing to perform “clinical trial on-a-chip”. As microfluidic 3D cell culture platform, we have chosen the OrganoPlate because of its high-throughput capabilities [31]. This device enables the culture of endothelial cells as 96 3D and perfusable microvessels (Figure 3) [30].

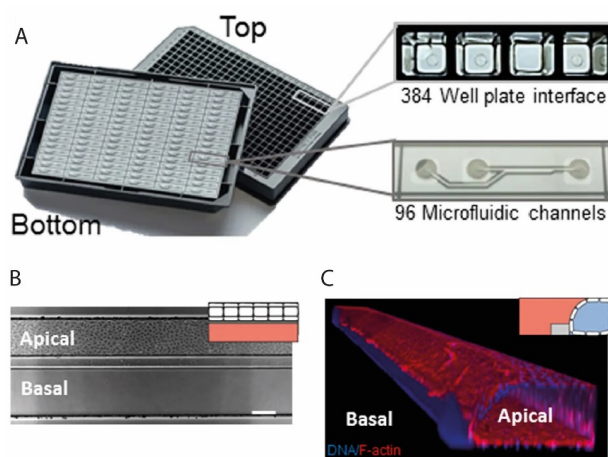


Figure 3 | Microfluidic cell culture device: OrganoPlate. (A) Photograph of bottom and top views of an OrganoPlate. The device consists of a 384 wells plate interface on top and 96 microfluidic chips integrated in the bottom. (B) Phase contrast image and (C) 3D reconstruction of a microvessel in the OrganoPlate [30].

Chapter II summarizes the current state of the art of organ-on-a-chip systems and especially evaluates the efforts put in the development of these systems in the light of end-user adoption aspects. We made an inventory of instrument compatibility, ease of handling, and adoption readiness aspects. In addition, we considered the type of assays that are typically carried out in, or on samples from, these systems, providing insight in the spectrum of techniques that can be deployed for assessing biological properties and responses, and to answer biological, clinical or pharmacological questions. The results clearly identified that the elements that bring organs-on-chips to end-users are in place, but only few systems have succeeded in applying them in order to answer biological questions.

Chapter III reports the development of a perfusable high-throughput microvessel-on-a-chip platform to study microvascular diseases, featuring a collagen hydrogel that minimally mimics the ECM. The microengineered human blood vessel allows quantitative and parallel testing of microvascular leakage. Exposure of the microvessels to VEGF, histamine and TNF α led to albumin leakage, reconstituting the microvascular leakage seen *in vivo*. Moreover, we demonstrated that this process involves changes in cellular mechanics and our findings were confirmed with TEER measurements. Especially, we developed a method to screen blood samples for vascular destabilizing factors in our device. Plasma samples were prepared from whole blood and treated with hirudin, corn trypsin inhibitor (CTI) and compstatin. Subsequently, the samples were spiked with VEGF, histamine and TNF α and perfused through the microvessels-on-chips, which showed increase in vessel permeability and confirmed the effect of destabilizing factors in blood to induce microvascular leakage in a physiological relevant *in vitro* setting. The screening of effect of plasma samples on microvessels-on-chips can be used for the development of therapeutic strategies to combat microvascular destabilization.

With the microvessels that were developed in chapter III, we show in **Chapter IV** the first chip-based model for studying mechanisms in the vascular pathophysiology associated with Ebola virus disease and provides an *in vitro* platform for drug studies. Luminal infusion of Ebola virus-like particles (VLPs) consisting of the Ebola virus matrix protein VP40 and Ebola glycoprotein (GP_{1,2}) leads to albumin leakage from the engineered vessels. This process involves the activation of the Rho/ROCK pathway. Moreover, VLP-induced vessel permeability is associated with changes in cellular mechanics and Ebola virus GP_{1,2} in its particle associated form

mediates endothelial cell activation and increased vessel permeability. We demonstrated the utility of our platform for Ebola drug therapy by studying the recently developed experimental drug FX06 and melatonin, that strongly suppressed Ebola-induced vascular destabilization.

In **Chapter V**, we applied metabolomics to measure the metabolic state of the microvessels. To assess whether the microvessels display a less inflammatory phenotype, we used an optimized targeted liquid chromatography–tandem mass spectrometry to measure a panel of pro- and anti-inflammatory bioactive lipids to generate expression profiles in TNF α treated microvessels. We demonstrated that bioactive lipid profiles can be readily detected from the microvessels-on-a-chip. Moreover, the metabolic profile of the microvessels were compared to 2D endothelial cell cultures. The results showed that the micro-physiological system actually display a more dynamic, less inflammatory response to TNF α , that resembles more the human situation, compared to classical 2D endothelial cell cultures.

In **Chapter VI**, we developed a multi-channel microfluidic pump and *in situ* oxygen monitoring system for the microvessels-on-chips. The integrated microvessels-on-chips platform is a fully closed system and the oxygen concentration was constantly monitored in order to be sure of a constant oxygen level due to gas permeability of the tubings. The cytoskeleton remodeling of the endothelial cells under unidirectional flow with the microfluidic pump, bidirectional flow with the Mimetas perfusion rocker and static condition was quantified. Cells under static condition and bidirectional flow were more randomly orientated, whereas cells under unidirectional flow were uniformly orientated and aligned in one direction. Moreover, the microvessels under shear stress with the microfluidic pump show high expression of *Klf2* and *Klf4* compared to bidirectional flow and static condition. Our results demonstrated that the generated shear stress changes the morphology and gene expression of the microvessels-on-chips to what is found *in vivo* and deviate significantly from models without shear stress.

Finally, **Chapter VII** provides discussions and conclusions of this thesis. A critical evaluation of the research is revealed together with a discussion about the future perspective and directions of the field of organs-on-chips to study microvascular diseases.

References

1. McMurray, J.J., et al., *Clinical epidemiology of heart failure: public and private health burden*. Eur Heart J, 1998. **19 Suppl P**: p. P9-16.
2. Owan, T.E., et al., *Trends in prevalence and outcome of heart failure with preserved ejection fraction*. N Engl J Med, 2006. **355**(3): p. 251-9.
3. Paulus, W.J. and C. Tschope, *A novel paradigm for heart failure with preserved ejection fraction: comorbidities drive myocardial dysfunction and remodeling through coronary microvascular endothelial inflammation*. J Am Coll Cardiol, 2013. **62**(4): p. 263-71.
4. Cleland, J.G., P. Pellicori, and R. Dierckx, *Clinical trials in patients with heart failure and preserved left ventricular ejection fraction*. Heart Fail Clin, 2014. **10**(3): p. 511-23.
5. Lichtlen, P.R., K. Bargheer, and P. Wenzlaff, *Long-term prognosis of patients with anginalike chest pain and normal coronary angiographic findings*. J Am Coll Cardiol, 1995. **25**(5): p. 1013-8.
6. Crea, F., P.G. Camici, and C.N. Bairey Merz, *Coronary microvascular dysfunction: an update*. Eur Heart J, 2014. **35**(17): p. 1101-11.
7. Danaei, G., et al., *National, regional, and global trends in fasting plasma glucose and diabetes prevalence since 1980: systematic analysis of health examination surveys and epidemiological studies with 370 country-years and 2.7 million participants*. Lancet, 2011. **378**(9785): p. 31-40.
8. Fowler, M.J., *Microvascular and Macrovascular Complications of Diabetes*. Clinical Diabetes, 2008. **26**(2): p. 77.
9. Gabrielli, A., E.V. Avvedimento, and T. Krieg, *Scleroderma*. New England Journal of Medicine, 2009. **360**(19): p. 1989-2003.
10. Furue, M., et al., *Pathogenesis of systemic sclerosis-current concept and emerging treatments*. Immunologic Research, 2017. **65**(4): p. 790-797.
11. Schoneberg, J., et al., *Engineering biofunctional in vitro vessel models using a multilayer bioprinting technique*. Scientific Reports, 2018. **8**.
12. Bautch, V.L., *Stem cells and the vasculature*. Nature Medicine, 2011. **17**(11): p. 1437-1443.
13. Rabelink, T.J., H.C. de Boer, and A.J. van Zonneveld, *Endothelial activation and circulating markers of endothelial activation in kidney disease*. Nature Reviews Nephrology, 2010. **6**(7): p. 404-414.
14. Armulik, A., G. Genove, and C. Betsholtz, *Pericytes: Developmental, Physiological, and Pathological Perspectives, Problems, and Promises*. Developmental Cell, 2011. **21**(2): p. 193-215.
15. Khairoun, M., et al., *Microvascular Damage in Type 1 Diabetic Patients Is Reversed in the First Year After Simultaneous Pancreas-Kidney Transplantation*. American Journal of Transplantation, 2013. **13**(5): p. 1272-1281.
16. van Esbroeck, A.C.M., et al., *Activity-based protein profiling reveals off-target proteins of the FAAH inhibitor BIA 10-2474*. Science, 2017. **356**(6342): p. 1084-1087.

17. Muthuswamy, V., *Ethical issues in clinical research*. *Perspect Clin Res*, 2013. **4**(1): p. 9-13.
18. Thomas, K. *The price of health: the cost of developing new medicines* 2016 [cited 2019 11-08-2019]; Available from: <https://www.theguardian.com/healthcare-network/2016/mar/30/new-drugs-development-costs-pharma>.
19. Novak, R., et al., *Scalable Fabrication of Stretchable, Dual Channel, Microfluidic Organ Chips*. *Jove-Journal of Visualized Experiments*, 2018(140).
20. Junaid, A., et al., *An end-user perspective on Organ-on-a-Chip: Assays and usability aspects*. *Current Opinion in Biomedical Engineering*, 2017. **1**: p. 15-22.
21. Herland, A., et al., *Distinct Contributions of Astrocytes and Pericytes to Neuroinflammation Identified in a 3D Human Blood-Brain Barrier on a Chip*. *Plos One*, 2016. **11**(3).
22. Baeyens, N., et al., *Endothelial fluid shear stress sensing in vascular health and disease*. *J Clin Invest*, 2016. **126**(3): p. 821-8.
23. Sack, K.D., M. Teran, and M.A. Nugent, *Extracellular Matrix Stiffness Controls VEGF Signaling and Processing in Endothelial Cells*. *J Cell Physiol*, 2016. **231**(9): p. 2026-39.
24. Zhao, Y., et al., *Multi-Organs-on-Chips: Towards Long-Term Biomedical Investigations*. *Molecules*, 2019. **24**(4).
25. Schimek, K., et al., *Integrating biological vasculature into a multi-organ-chip microsystem*. *Lab on a Chip*, 2013. **13**(18): p. 3588-3598.
26. Vunjak-Novakovic, G., et al., *HeLiVa platform: integrated heart-liver-vascular systems for drug testing in human health and disease*. *Stem Cell Research & Therapy*, 2013. **4**.
27. Yasotharan, S., et al., *Artery-on-a-chip platform for automated, multimodal assessment of cerebral blood vessel structure and function*. *Lab Chip*, 2015. **15**(12): p. 2660-9.
28. Jung, Y., et al., *Scaffold-free, Human Mesenchymal Stem Cell-Based Tissue Engineered Blood Vessels*. *Sci Rep*, 2015. **5**: p. 15116.
29. Kratz, S.R.A., et al., *Latest Trends in Biosensing for Microphysiological Organs-on-a-Chip and Body-on-a-Chip Systems*. *Biosensors (Basel)*, 2019. **9**(3).
30. van Duinen, V., et al., *96 perfusable blood vessels to study vascular permeability in vitro*. *Scientific Reports*, 2017. **7**(1): p. 18071.
31. Trietsch, S.J., et al., *Membrane-free culture and real-time barrier integrity assessment of perfused intestinal epithelium tubes*. *Nature Communications*, 2017. **8**(1): p. 262.

Chapter II


An End-User Perspective on Organ-on-a-Chip: Assays and Usability
Aspects

Abidemi Junaid, Alireza Mashaghi, Thomas Hankemeier, Paul Vulto

Current Opinion in Biomedical Engineering (2017) **1**, 15-22

Chapter II

Abstract



The field of Organ-on-a-Chip is rapidly shifting from academic proof-of-concept studies to real-world solutions. The challenge is now to enhance end-user adoption by improving user friendliness, compatibility, assay ability and product readiness of these solutions. This review evaluates Organ-on-a-Chip efforts published over the last two years in light of such end-user adoption aspects. Elegant platforms have been reported including a microtiter plate-based 3D cell culture platform and a platform of cantilevers with integrated gauge sensors for contractility measurement. Also functional assays for angiogenesis, calcium imaging of neurons and neuro-muscular contractility were reported. Compatibility with standard analysis techniques such as sequencing, fluorescent activated cell sorting and mass spectrometry were reported only in rare cases. It is concluded that the elements that enable the leap towards end-user adoption are in place, but only few systems have managed to incorporate all aspects, and are able to answer biological questions.

Introduction

Organ-on-a-Chip has recently emerged as a new paradigm in enhanced cell culture [1]. The field builds on almost 25 years of developments in microfluidic and associated microfabrication techniques on the one hand and an urge towards ever more physiologically relevant cell culture on the other hand [2, 3]. Application of microengineering techniques in cell culture enables the use of flow and associated sheer stress, mechanical strain and allows integration of sensors and systems such as, sample preparation aspects, automated dosing and dilution series preparation. It also facilitates co-culture, 3D culture and application of controlled gradients.

Earliest work in microfluidic cell culture appeared around the turn of the century and includes perfused Transwell systems, multi-organ systems and 3D liver tissue [4-7]. Although many applications have been developed over the last 15 years, it was not until the paradigm shifting Lung-on-a-Chip publication of the Ingber group in 2010 that one could identify Organs-on-Chips as a field in its own right [8]. Since then, the field has expanded tremendously, both in terms of academic publications as well as commercial offerings.

In our 2015 review article, we concluded that the field is currently shifting from a technology focus, aiming to develop prototypes and concepts, towards a biology focus, whereby validation of culture systems and integration of state-of-the-art stem cell and cell culture techniques are key [9]. With this transition towards an application focus, the question poses itself: what efforts are ongoing to promote end-user adoption?

In this critical review, we attempt to take an end-user perspective on Organ-on-a-Chip developments and make an inventory of instrument compatibility, ease of handling, and adoption readiness aspects. In addition, we consider the type of assays that are typically carried out in, or on samples from, these systems, providing insight in the spectrum of techniques that can be deployed for assessing biological properties and responses, and to answer biological, clinical or pharmacological questions.



Overview

In this review, we catalogued 77 research articles containing the keywords (Organ-on-a-chip) OR ("Organ on a chip") OR ("microfluidic" AND "cell culture"), which appeared since 2014 on PubMed. Papers that were not found with the search string, but were known to the authors as highly relevant were added to the database. The articles were categorized according to on-chip and off-chip assays, integration aspects, flow control and format in Figure 1 and supplementary info.

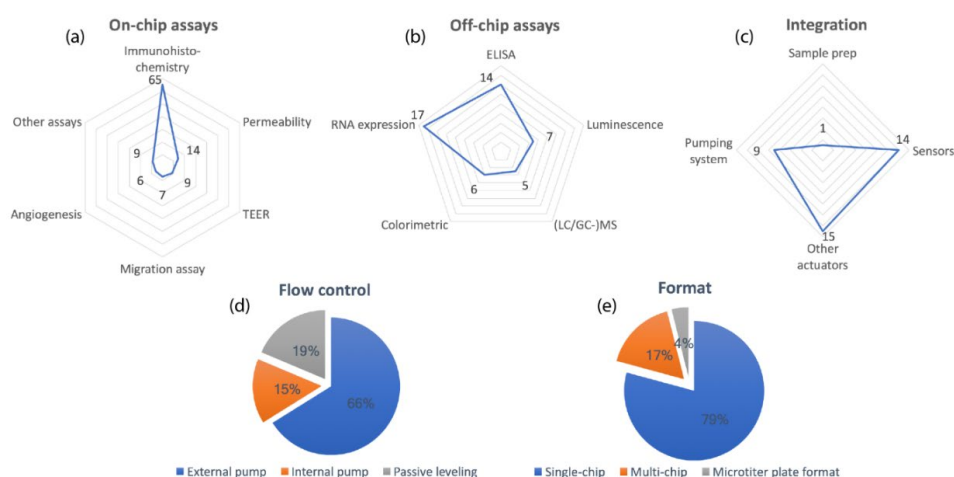


Figure 1 | Overview of assays and usability aspects of Organs-on-Chips since 2014. (a-c) Relative scores for the frequency of assays and integrations in Organs-on-Chips. On-chip assays: Immunohistochemistry scored the highest followed by permeability. Off-chip assays: RNA expression had the highest score, followed by ELISA. Integration: Other actuators and sensors scored the highest. **(d)** The distribution of different mechanisms of flow control in Organ-on-a-Chip. More than half of the developed microfluidic models had external pumps. **(e)** The distribution of different formats: The majority of Organ-on-a-Chip models is comprised of single chip concepts.

Although articles referenced in this paper describe many aspects of Organ-on-a-Chip systems, we have chosen to focus solely on usability and compatibility aspects of the solutions proposed. Physiological relevance of the various systems has been extensively reviewed elsewhere [1, 9-11].

Figure 1a and b show spider graphs of assays performed in Organs-on-Chips, categorized into on-chip and off-chip assays. On-chip assays include immunohistochemistry, permeability, trans epithelial electric resistance (TEER), migration assays, angiogenesis and other assays (e.g. calcium imaging, colorimetric and luminescence). Off-chip assays consist of enzyme-linked immunosorbent assays (ELISA), luminescence, liquid/gas chromatography–mass spectrometry ((LC/GC-) MS), RNA expression and colorimetric assays. Immunohistochemical staining is the dominant on-chip analysis technique. Almost all publications used immunohistochemical staining to characterize the physiology of their tissue or organ models. We assume that also phase-contrast microscopy is generically used for on-chip assessment of cell morphology and confluence during culturing, however we omitted this from our analysis as it is usually not used as an endpoint or quantified analyses.

RNA expression analysis and ELISA are often used for assessing cellular responses to flow, co-culture or drug compounds. Although very well possible to perform such techniques on chips, in our analysis we find PCRs and ELISA to be exclusively performed off-chip. Although being a highly generic analysis technique, (LC/GC-) MS is used as a readout for Organs-on-Chips only by few [12-16].

Off-chip assays have the benefit that they are readily available and standardized. However, a disadvantage arises in conjunction with microfluidic chips. Cell culture volumes are typically quite small and dead-volumes in comparison are large. This renders the signal-to-noise ratio low in comparison to classical cell culture techniques. This problem is largely solved by performing assays on the chip. It is for this reason that immunohistochemical staining and other optical readouts are highly popular. Not only is their implementation relatively straightforward, the microfluidic environment also assures excellent imaging quality. Other on-chip assays are reported less often, as they have the disadvantage that they need to be tailored to the microfluidic environment. This puts higher constraints on the engineering skills of the research team, potentially distracting from biological developments.

Microengineering techniques offer ample opportunities to integrate actuators, sensors and complex fluid handling modules on the same chip (see Figure 1c). In recent Organ-on-a-Chip publications, this is predominantly done for sensors and actuators. The trend to induce or measure mechanical strain has led to a relatively large number of publications that use actuators other than for integrated pumping [17-19]. Chip-integrated sensors are



predominantly electrochemical sensors [20-22]. Relatively few number of papers demonstrate integration of sample preparation aspects to improve the quality of the read out of assays of cell cultures [14].

Since the human physiology consists of a dynamic environment, flow control is a crucial requirement of Organs-on-Chips. While microengineering techniques offer ample precedents for integration of pumps on the chip, the majority of publications make use of external pumps to drive the flow (see Figure 1d). Although convenient in a proof-of-concept phase, none of the publications researched, showed an easy to use approach for connecting an external pump system by non-expert end-users. Passive levelling on the other hand is a very simple technique that is becoming rapidly more popular to drive flow in microfluidic systems [13, 23-26]. Although very simple to use for the non-expert end-user, the bidirectionality of the flow is seen as a disadvantage by some. Integration of pumps is an alternative solution to this [12, 27-31].

Strikingly, most publications show Organ-on-a-Chip concepts on single chips, although it is crucial for end-user acceptance to include dilution series, replica's and positive and negative controls (see Figure 1e). A small fraction incorporates multiple microfluidic networks on a single chip and yet in exceptional situations the microtiter plate standard is adopted to enable compatibility [26, 32].

Usability aspects

The usability aspects of microfluidic devices relate to aspects of compatibility to existing equipment, automation, ease of handling, possibility to generate multiple data points amongst others. We describe here some selected papers that we feel made particular progress on one or more of these aspects. For example, Birchler *et al.* created an open format hanging-droplet system for microfluidic handling, culturing of single cells and microtissue spheroids in multiple culture compartments (Figure 2a) [33]*. Noteworthy, their system was compatible with fluorescence-activated cell sorting (FACS) to directly sort cells, without the need of intermediate steps, into the desired microfluidic culture compartments. Cells were sorted corresponding to their light-scattering characteristics, which enabled the separation of single cells from cell clusters and assess the biological structure of cells during loading. The

open microfluidic chip of Birchler *et al.* gives an agreeable illustration of a system that is both high-throughput, compatible and can be coupled with standard cell biology tools.

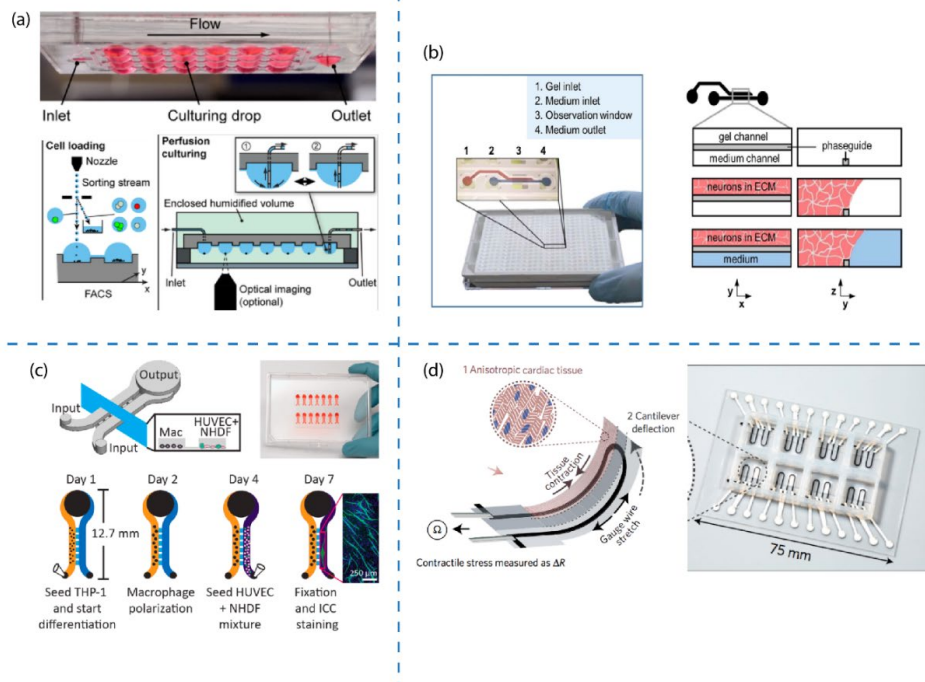



Figure 2 | Selection of Organ-on-a-Chip systems with particularly interesting usability aspects. (a) Hanging-drop chip network for loading, culturing and harvesting stem cells and microtissue spheroids. This system is compatible with optical imaging and fluidic pumps and was integrated with a FACS machine to accurately and directly sort cells into compartments of the microfluidic network [33]*. **(b)** The OrganoPlate®, a 384-well microtiter plate format that comprised 96 microfluidic networks for high-throughput assays. A capillary pressure barrier enables to pattern the extracellular matrix while leaving half the chamber for culture medium in a “membrane-free” manner. Microfluidic flow was induced by passive leveling [26]**. **(c)** Microfluidic device by Theberge *et al.* for parallel angiogenesis assays in co-culture. Flow was facilitated by passive pumping [32]*. **(d)** Microphysiological device with eight independent wells. The device was fully 3D printed and integrated with a strain sensor for continuous electronic readout of cardiac tissue contractions [18]**.

Similarly, Wevers *et al.* reported 3D culturing of neuronal and glial cells in a high throughput 3D cell culture platform using a modified 384-well plate to create 96 independent microfluidic



networks for 3D cell culture (Figure 2b) [26]**. The platform employs passive levelling for fluid exchange and 175 μm thin glass for enhanced microscopic imaging. The microtiter plate format renders the platform fully compatible with standard microscopes, automated readers and robot handling, an aspect that was utilized by Wevers *et al.* for generating dose response curves to toxic compounds. Moreno *et al.* also used the same platform to differentiate human iPSC-derived neuroepithelial stem cells into functional dopaminergic neurons [24]. Jang *et al.* used a similar platform for studying drug induced liver injury [34]. The fact that three different universities report use of the platform is a strong indication of transferability of the concept.

Another study reported a chip system for studying angiogenesis (Figure 2c) [32]*. The system consists of an array of 14 microfluidic networks perfused by passive pumping. Each microfluidic network has two main microfluidic channels that are interconnected through microchannels that are substantially lower than the main channels (30 μm vs. 330 μm) enabling exchange of soluble signalling molecules between cells grown in the two separated channels. The authors studied the effects of antiangiogenic factor MMP12 and proangiogenic factors secreted by macrophages on endothelial tubule formation. Pipette operation makes the microfluidic device simple to use and although not demonstrated in the publication, the system seems easily made compatible with liquid handling systems.

Lind *et al.* used 3D printing to develop an assay concept for measuring contractility of cardiac tissue (see Figure 2d) [18]**. The system has integrated soft strain gauge sensors to measure contractile stresses of multiple cardiac micro-tissues. Each device is composed of eight independent wells with multilayer cantilevers, a base layer, an embedded strain sensor, a tissue-guiding layer and electrical interconnects for readout. The tissue-guiding layer promotes the self-assembly of physio-mimetic laminar cardiac tissues. The system developed by Lind *et al.* enables non-invasive real-time electronic readout of contractile properties inside a cell incubator and can be used to study dose-response of drugs that influence contractile strength or beat rate.

An example of a more complex system is reported by Ramadan *et al.* [35]. This device contained three parallel cell culture chambers and Ag/AgCl electrode wires to measure TEER of the human skin *in vitro* under perfusion of culture media. The barrier integrity of human keratinocytes was measured in co-culture with monocytes. A chip comprised three such

devices, although due to external pump and open electrode wire connections, the operation of the device is primarily reserved for expert end-users.

Functional assays in Organ-on-a-Chip systems

In vitro microcirculation, induced by flow, is important to mimic organ physiology. Kim *et al.* demonstrated this with angiogenesis assays in their three-dimensional culture model [36] (see Figure 3a). Blood endothelial cells were cultured in a microfluidic platform and vasculogenesis was stimulated by fibroblast-secreted pro-angiogenic factors and flow-mediated mechanical stresses. They found that interstitial flow plays a significant role in the growth of angiogenic sprouts. It can either promote or suppress angiogenic sprouting depending on the direction of flow (Figure 3a). The control over gradients of angiogenic factors and application of interstitial flow for 3D angiogenic sprouting is a strong example of an assay that can be exclusively done by means of microfluidic techniques.

Wang *et al.* illustrated different stages of vascular development in a microfluidic system [37]. This system contained a well-defined hourglass shaped communication pore that pins fibrin gel at its vertexes and permits the formation of an endothelial cell monolayer on the fibrin gel interface. Subsequently, the authors induced vasculogenesis, endothelial cell lining, sprouting angiogenesis, and anastomosis by using an optimized interstitial flow and VEGF gradient. This finally enabled the formation of an intact and perfusable microvascular network. The system was used for co-culture with tumor cells for clinical applications [38]* (see Figure 3b). The impact of drugs was assessed on either the tumour directly or to the microvascular network. The growth and assaying of perfused 3D vascular networks is another example of tissue modelling that is inherently performed in a microfluidic setting.



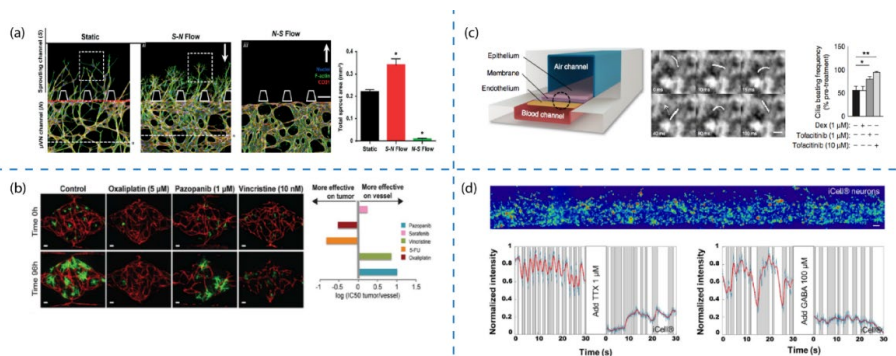


Figure 3 | Noteworthy assays in Organs-on-Chips. (a) Angiogenesis model developed by Kim *et al.*, showing directional prejudice in response to flow direction. *S-N*: Downward direction. *N-S*: Upward direction [36]. **(b)** Vascularized micro-tumors and their response to drugs. Human colorectal cancer cell line HCT116 (green) and endothelial cells (red) were visualized by confocal microscopy. The results were translated to IC50 ratios (tumor growth and total vessel length) [38]*. **(c)** Model of human Airway-on-a-Chip by Benam *et al.* High-speed microscopic imaging showed the beating activity of the cilia on the epithelium under healthy condition, asthmatic phenotype, COPD exacerbation and drug treatment [39]*. **(d)** Calcium imaging recordings to detect electrophysiological activity of neurons. This assay was used to evaluate compounds effect in the high-throughput 3D culture system of Wevers *et al.* [26]**.

Benam *et al.* elaborated on their initial Lung-on-a-Chip work to model small airway epithelium comprised of a co-culture of bronchial epithelium and microvascular endothelium separated by a membrane [39]*. A particularly elegant assay was implemented to measure the beating frequency of cilia in response to stimuli. Figure 3c shows the increase in cilia beating frequency in response to the drug Tofacitinib. The extra value of this work in comparison to classical Transwell system is to be sought in the perfusion of the basal compartment and the imaging, but this goes at the cost of ease of handling and throughput.

Wevers *et al.* demonstrated 3D culture of iPSC-derived neuronal-glia cells of healthy people and Huntington's disease patients in Matrigel, which they showed and quantified with immunohistochemistry [26]**. They measured cell viability following exposure to several neurotoxic compounds. Particularly interesting was the compound mediated modulation of electrophysiological activity that was visualized by calcium imaging (see Figure 3d).

A visualisation of electrophysiological activity was reported by Müller *et al.* who developed a CMOS chip with high density electrodes to measure spatial voltage distribution at a 17.5 μm resolution [40]. Each electrode was used to measure the electrical activity of individual neurons. Noteworthy, an elegant indirect readout for electrophysiological activity was reported by Uzel *et al.* that used photosensitized embryonic stem cells to differentiate into neurospheres and interact with muscle tissue [19]**. Photostimulation or glutamate addition caused the muscle to contract as a consequence of action potentials that could be measured by deflection of microfabricated pillars.

Herland *et al.* demonstrated a blood-brain barrier, the barrier function thereof could be interrogated by leakage of 3 kDa FITC labelled dextran and calculating the P_{app} value thereof [41].

Chen *et al.* reported a microfluidic cell culture chip, made of four microchannels and Petri dish-based cell medium supply system that was used to measure cell migration [42]. They were successful in screening highly metastatic sublines in their system. Interestingly, to perform parallel cell migration with different modes, Ma *et al.* created a microfluidic system that combines membrane-based cell migration and droplet-based techniques [43]*. Droplets were adjacently positioned on either side of a membrane, enabling gradient formation that was exploited in migration assays. Consequently, multi-parametric gradients were constructed for metastatic assays. The concept allowed multiple in-droplet operations in the nanoliter range and up to 81 assays in parallel.

Molecular assays in Organ-on-a-Chip systems

Organ-on-a-Chip based models have been extensively analysed with help of molecular assays such as ELISA, RNA expression analysis, probing metabolism and immunohistochemistry [14, 44-46]. A particular extensive analysis was done by Kamei *et al.* who performed global gene expression analysis on human embryonic stem cells and induced pluripotent stem cells that were cultured in a 3D thermo responsive hydrogel in a microfluidic channel [47].

Patra *et al.* analysed 5000 3D tumour spheroids using flow cytometry after dissociation of the tumour [25]*. In that context, they could perform single cell analysis which they correlated to



tumour size, 2D or 3D culture as well as therapy response based on Calcein AM (healthy) and 7-Amino-ActinomycinD (necrosis) and APC-Annexin V (apoptosis). The assays demonstrate the power of large numbers using flow-cytometry, which is a standard instrument in modern cell biology.

A compatible assay setup was demonstrated by Bavli *et al.* who could distinguish between cell death, healthy cells and on-set of mitochondrial dysfunction in real-time by measuring glucose, lactate and oxygen [48]*. Oxygen was measured by tissue embedded Ru-CPOx oxygen sensors, while glucose and lactate measured by amperometric detection of glucose and lactate oxidase mediated oxidation of H₂O₂. Time-resolved sampling was supported by an off-chip microfluidic switchboard. The switchboard also enabled automated calibration of the amperometric sensing scheme. Similar electrochemical recordings were demonstrated by Misun *et al.* in conjunction with hanging drop-based cell culture [22]. The authors project their setup for real-time monitoring applications of glucose and lactate in Body-on-a-Chip type setups.

A rare example of coupling LC/MS based metabolomics techniques with microfluidic cell culture is given by Filla *et al.* However, no in depth biological analysis was demonstrated in their report [14].

Although being impressive examples in terms of complexity of the assays, the added value of the microfluidics is still limited in many of the above examples. Kamei *et al.* did not use any of the flow aspects, while both Patra, Bavli and Kamei *et al.* did not consider co-culture or other aspects that render 3D cell culture more physiologically relevant [25, 47, 48]*.

Conclusions and future directions

In this article, we assessed usability, compatibility and assay ability aspects in recent Organ-on-a-Chip publications. We discussed examples of efforts to improve usability, incorporate unique assays, or informative analyses using standard laboratory techniques. However, only in rare examples an Organ-on-a-Chip concept ticks all the boxes and can be considered ready for transfer to an end-user. On the contrary, the majority of publications reported single chip-based models, external pumping and use immunohistochemical stains as primary readout. In

Chapter II

the review article of van Duinen *et al.* we concluded that with maturation of the microfluidics field, the focus in Organ-on-a-Chip studies will shift towards validation of models and integration of newest stem cell techniques [9]**. Thus, the multidisciplinary field will become more and more the realm of biologists. However, with an increasing role of biologists in the field, attention for usability aspects, throughput and compatibility is critical. Moreover, compatibility with the full width of biochemical analysis techniques is crucial in order to enhance end-user adoption and full validation of the models. Last but not least, availability of these systems, either in commercial form, or at least producible in significant numbers becomes critical, enabling the end-user to perform his/her optimisation research.

We envision that in coming years, the end-user aspects will dominate engineering aspects in the Organ-on-a-Chip field and that commercial providers will be playing an increasingly dominant role. The availability of easy-to-operate, mass produced systems will enable end-users to focus on what they do best: excellent biology, validation of the models and screening for better medicines. And this will require the availability of proper molecular or physiological read outs to answer clinical, biomedical or biological questions.

Acknowledgements

Abidemi Junaid was financially supported by the RECONNECT CVON Groot consortium, which is funded by the Dutch Heart Foundation. Thomas Hankemeier and Paul Vulto received funding from the European Union's Horizon 2020 research and innovation program under grant agreement No 668738 SysMedPD.

References

1. Esch, E.W., A. Bahinski, and D. Huh, *Organs-on-chips at the frontiers of drug discovery*. Nature Reviews Drug Discovery, 2015. **14**(4): p. 248-260.
2. Manz, A., N. Graber, and H.M. Widmer, *Miniaturized Total Chemical-Analysis Systems - a Novel Concept for Chemical Sensing*. Sensors and Actuators B-Chemical, 1990. **1**(1-6): p. 244-248.
3. Horvath, P., et al., *Screening out irrelevant cell-based models of disease*. Nature Reviews Drug Discovery, 2016. **15**(11): p. 751-769.

4. Powers, M.J., et al., *A microfabricated array bioreactor for perfused 3D liver culture*. *Biotechnology and Bioengineering*, 2002. **78**(3): p. 257-269.
5. Leclerc, E., Y. Sakai, and T. Fujii, *Cell culture in 3-dimensional microfluidic structure of PDMS (polydimethylsiloxane)*. *Biomedical Microdevices*, 2003. **5**(2): p. 109-114.
6. Hung, P.J., et al., *Continuous perfusion microfluidic cell culture array for high-throughput cell-based assays*. *Biotechnology and Bioengineering*, 2005. **89**(1): p. 1-8.
7. Viravaidya, K., A. Sin, and M.L. Shuler, *Development of a microscale cell culture analog to probe naphthalene toxicity*. *Biotechnology Progress*, 2004. **20**(1): p. 316-323.
8. Huh, D., et al., *Reconstituting Organ-Level Lung Functions on a Chip*. *Science*, 2010. **328**(5986): p. 1662-1668.
9. van Duinen, V., et al., *Microfluidic 3D cell culture: from tools to tissue models*. *Current Opinion in Biotechnology*, 2015. **35**: p. 118-126.
10. Caplin, J.D., et al., *Microfluidic Organ-on-a-Chip Technology for Advancement of Drug Development and Toxicology*. *Advanced Healthcare Materials*, 2015. **4**(10): p. 1426-1450.
11. Picollet-D'hahan, N., et al., *A 3D Toolbox to Enhance Physiological Relevance of Human Tissue Models*. *Trends Biotechnol*, 2016. **34**(9): p. 757-769.
12. Maschmeyer, I., et al., *Chip-based human liver-intestine and liver-skin co-cultures--A first step toward systemic repeated dose substance testing in vitro*. *Eur J Pharm Biopharm*, 2015. **95**(Pt A): p. 77-87.
13. Lee, H., et al., *A pumpless multi-organ-on-a-chip (MOC) combined with a pharmacokinetic-pharmacodynamic (PK-PD) model*. *Biotechnology and Bioengineering*, 2017. **114**(2): p. 432-443.
14. Filla, L.A., et al., *Automated sample preparation in a microfluidic culture device for cellular metabolomics*. *Analyst*, 2016. **141**(12): p. 3858-3865.
15. Zeller, P., et al., *Hepatocytes cocultured with Sertoli cells in bioreactor favors Sertoli barrier tightness in rat*. *Journal of Applied Toxicology*, 2017. **37**(3): p. 287-295.
16. Shah, P., et al., *A microfluidics-based in vitro model of the gastrointestinal human-microbe interface*. *Nature Communications*, 2016. **7**.
17. Gaio, N., et al., *Cytostretch, an Organ-on-Chip Platform*. *Micromachines*, 2016. **7**(7).
18. Lind, J.U., et al., *Instrumented cardiac microphysiological devices via multimaterial three-dimensional printing*. *Nature Materials*, 2017. **16**(3): p. 303-+.
19. Uzel, S.G.M., et al., *Microfluidic device for the formation of optically excitable, three-dimensional, compartmentalized motor units*. *Science Advances*, 2016. **2**(8): p. e1501429.
20. Bonk, S.M., et al., *Design and Characterization of a Sensorized Microfluidic Cell-Culture System with Electro-Thermal Micro-Pumps and Sensors for Cell Adhesion, Oxygen, and pH on a Glass Chip*. *Biosensors-Basel*, 2015. **5**(3): p. 513-536.
21. Zhou, Q., et al., *Liver injury-on-a-chip: microfluidic co-cultures with integrated biosensors for monitoring liver cell signaling during injury*. *Lab on a Chip*, 2015. **15**(23): p. 4467-4478.

22. Misun, P.M., et al., *Multi-analyte biosensor interface for real-time monitoring of 3D microtissue spheroids in hanging-drop networks*. *Microsystems & Nanoengineering*, 2016. **2**.
23. Esch, M.B., et al., *Modular, pumpless body-on-a-chip platform for the co-culture of GI tract epithelium and 3D primary liver tissue*. *Lab on a Chip*, 2016. **16**(14): p. 2719-2729.
24. Moreno, E.L., et al., *Differentiation of neuroepithelial stem cells into functional dopaminergic neurons in 3D microfluidic cell culture*. *Lab on a Chip*, 2015. **15**(11): p. 2419-2428.
25. Patra, B., et al., *Drug testing and flow cytometry analysis on a large number of uniform sized tumor spheroids using a microfluidic device*. *Scientific Reports*, 2016. **6**.
26. Wevers, N.R., et al., *High-throughput compound evaluation on 3D networks of neurons and glia in a microfluidic platform*. *Scientific Reports*, 2016. **6**.
27. Hasenberg, T., et al., *Emulating human microcapillaries in a multi-organ-chip platform*. *Journal of Biotechnology*, 2015. **216**: p. 1-10.
28. Chang, J.Y., et al., *A novel miniature dynamic microfluidic cell culture platform using electro-osmosis diode pumping*. *Biomicrofluidics*, 2014. **8**(4).
29. Maschmeyer, I., et al., *A four-organ-chip for interconnected long-term co-culture of human intestine, liver, skin and kidney equivalents*. *Lab on a Chip*, 2015. **15**(12): p. 2688-2699.
30. Ju, S.M., et al., *High-Throughput Cytotoxicity Testing System of Acetaminophen Using a Microfluidic Device (Mfd) in Hepg2 Cells*. *Journal of Toxicology and Environmental Health-Part a-Current Issues*, 2015. **78**(16): p. 1063-1072.
31. Yazdi, S.R., et al., *Adding the 'heart' to hanging drop networks for microphysiological multi-tissue experiments*. *Lab on a Chip*, 2015. **15**(21): p. 4138-4147.
32. Theberge, A.B., et al., *Microfluidic Multiculture Assay to Analyze Biomolecular Signaling in Angiogenesis*. *Analytical Chemistry*, 2015. **87**(6): p. 3239-3246.
33. Birchler, A., et al., *Seamless Combination of Fluorescence-Activated Cell Sorting and Hanging-Drop Networks for Individual Handling and Culturing of Stem Cells and Microtissue Spheroids*. *Analytical Chemistry*, 2016. **88**(2): p. 1222-1229.
34. Jang, M., et al., *On-chip three-dimensional cell culture in phaseguides improves hepatocyte functions in vitro*. *Biomicrofluidics*, 2015. **9**(3).
35. Ramadan, Q. and F.C.W. Ting, *In vitro micro-physiological immune-competent model of the human skin*. *Lab on a Chip*, 2016. **16**(10): p. 1899-1908.
36. Kim, S., et al., *Interstitial flow regulates the angiogenic response and phenotype of endothelial cells in a 3D culture model*. *Lab on a Chip*, 2016. **16**(21): p. 4189-4199.
37. Wang, X.L., et al., *Engineering anastomosis between living capillary networks and endothelial cell-lined microfluidic channels*. *Lab on a Chip*, 2016. **16**(2): p. 282-290.
38. Sobrino, A., et al., *3D microtumors in vitro supported by perfused vascular networks*. *Scientific Reports*, 2016. **6**.
39. Benam, K.H., et al., *Small airway-on-a-chip enables analysis of human lung inflammation and drug responses in vitro*. *Nature Methods*, 2016. **13**(2): p. 151-+.

40. Muller, J., et al., *High-resolution CMOS MEA platform to study neurons at subcellular, cellular, and network levels*. Lab on a Chip, 2015. **15**(13): p. 2767-2780.
41. Herland, A., et al., *Distinct Contributions of Astrocytes and Pericytes to Neuroinflammation Identified in a 3D Human Blood-Brain Barrier on a Chip*. Plos One, 2016. **11**(3).
42. Chen, Z.Z., et al., *Establishment of a gastric cancer subline with high metastatic potential using a novel microfluidic system*. Scientific Reports, 2016. **6**.
43. Ma, Y., et al., *Microdroplet chain array for cell migration assays*. Lab on a Chip, 2016. **16**(24): p. 4658-4665.
44. Chen, C.P., et al., *Use of electrospinning and dynamic air focusing to create three-dimensional cell culture scaffolds in microfluidic devices*. Analyst, 2016. **141**(18): p. 5311-5320.
45. Materne, E.M., et al., *The Multi-organ Chip - A Microfluidic Platform for Long-term Multi-tissue Coculture*. Jove-Journal of Visualized Experiments, 2015(98).
46. Wu, X.J., et al., *Exploring inflammatory disease drug effects on neutrophil function*. Analyst, 2014. **139**(16): p. 4056-4063.
47. Kamei, K., et al., *Characterization of Phenotypic and Transcriptional Differences in Human Pluripotent Stem Cells under 2D and 3D Culture Conditions*. Advanced Healthcare Materials, 2016. **5**(22): p. 2951-2958.
48. Bavli, D., et al., *Real-time monitoring of metabolic function in liver-on-chip microdevices tracks the dynamics of mitochondrial dysfunction*. Proceedings of the National Academy of Sciences of the United States of America, 2016. **113**(16): p. E2231-E2240.

Recommended reading

Papers of particular interest, published within the period of review, have been highlighted as:

- of special interest
- of outstanding interest

[9] van Duinen, V., et al., *Microfluidic 3D cell culture: from tools to tissue models*. Current Opinion in Biotechnology, 2015. **35**: p. 118-126.

(••) Comprehensive review on the developments of microfluidic 3D cell culture since 2012.

[33] Birchler, A., et al., *Seamless Combination of Fluorescence-Activated Cell Sorting and Hanging-Drop Networks for Individual Handling and Culturing of Stem Cells and Microtissue Spheroids*. Analytical Chemistry, 2016. **88**(2): p. 1222-1229.

(●) A workflow for microfluidic handling and culturing of cells, based on hanging-droplet concept. This system displays a nice example of throughput, compatibility and integration.

[26] Wevers, N.R., et al., *High-throughput compound evaluation on 3D networks of neurons and glia in a microfluidic platform*. Scientific Reports, 2016. **6**.

(●●) Noteworthy example of an Organ-on-a-Chip that is pre-clinically relevant, easy to use, high-throughput and modestly compatible with other systems in life sciences.

[32] Theberge, A.B., et al., *Microfluidic Multiculture Assay to Analyze Biomolecular Signaling in Angiogenesis*. Analytical Chemistry, 2015. **87**(6): p. 3239-3246.

(●) Microfluidic device to study angiogenesis by using segregated co-culture in simplest form.

[18] Lind, J.U., et al., *Instrumented cardiac microphysiological devices via multimaterial three-dimensional printing*. Nature Materials, 2017. **16**(3): p. 303-+.

(●●) An example of a complex assay in an easy to use format with electrical readout and automation.

[19] Uzel, S.G.M., et al., *Microfluidic device for the formation of optically excitable, three-dimensional, compartmentalized motor units*. Science Advances, 2016. **2**(8): p. e1501429.

(●●) Interesting article on the use of microfluidic device to measure electrophysiological activity of differentiated motor neurons.

[38] Sobrino, A., et al., *3D microtumors in vitro supported by perfused vascular networks*. Scientific Reports, 2016. **6**.

(●) This study demonstrated several bioassays to study drug responses of vascularized tumors in Organ-on-a-Chip, which can be used for drug screening.

[39] Benam, K.H., et al., *Small airway-on-a-chip enables analysis of human lung inflammation and drug responses in vitro*. Nature Methods, 2016. **13**(2): p. 151-+.

(●) *In vitro* model of human lung inflammatory disorders to study drug responses based on epithelium cilia activity in perfused co-culture format.

[25] Patra, B., et al., *Drug testing and flow cytometry analysis on a large number of uniform sized tumor spheroids using a microfluidic device*. Scientific Reports, 2016. **6**.

Chapter II

(●) A study on bridging 3D microfluidic cell culture with flow cytometry for drug screening applications.

[48] Bavli, D., et al., *Real-time monitoring of metabolic function in liver-on-chip microdevices tracks the dynamics of mitochondrial dysfunction*. Proceedings of the National Academy of Sciences of the United States of America, 2016. **113**(16): p. E2231-E2240.

(●) Authors show a setup for measuring the metabolic function of Liver-on-a-Chip in real-time. To accomplish this, their microfluidic device was compatible with various systems.

[43] Ma, Y., et al., *Microdroplet chain array for cell migration assays*. Lab on a Chip, 2016. **16**(24): p. 4658-4665.

(●) Cell migration assay in a microdroplet chain array with an adjustable concentration gradient that modulated biomimetic chemotaxis assay based on Organ-on-a-Chip concept.

Chapter II

Supplementary info: The categorization of articles published in the Organ-on-a-Chip field over the last two years

DOI	Assays										Usability aspects															
	On-chip					Off-chip					Flow control		Integration		Format											
	Immunohistochemistry	Calcium imaging	Migration assay	Angiogenesis	Permeability	TEER	Phase contrast	Light microscopy	ELISA	Colorimetric	Luminescence	ELISA	Luminescence	(LC/GC-MS)	Colorimetric	RNA expression	External pumps	Internal pump	Passive leveling	Sample prep	Sensors	Pumping system	Other actuators	Single-chip	Multi-chip	Microtiter plate format
10.1039/c6an010551e												1						1						1		
10.1039/c6an01282e	1											1					1					1		1		
10.1039/c6lc00229c	1			1	1				1								1				1				1	
10.1039/c6lc00450d	1											1					1							1		
10.1039/c6lc00461j	1					1						1	1					1			1			1		
10.1016/j.talanta.2014.06.020	1						1	1									1						1		1	
10.1016/j.jbiootec.2015.09.038												1			1			1			1				1	
10.1016/j.ejpb.2015.03.002	1					1				1			1	1	1			1			1				1	

Chapter II



DOI	Assays											Usability aspects													
	On-chip					Off-chip						Flow control	Integration		Format										
	Immunohistochemistry	Calcium imaging	Migration assay	Angiogenesis	Permeability	TEER	Phase contrast	Light microscopy	ELISA	Colorimetric	Luminescence	ELISA	Luminescence	(LC/GC-IMS)	Colorimetric	RNA expression	External pumps	Internal pump	Passive leveling	Sample prep	Sensors	Other actuators	Single-chip	Multi-chip	Microtiter plate format
10.1016/j.bio.s.2016.04.028							1	1				1					1			1			1		
10.1016/j.bio.s.2016.07.015	1																1						1		
10.1063/1.4964813	1											1					1						1		
10.2116/analci.32.1217	1						1	1							1	1							1		
10.18632/oncotarget.9382	1		1					1				1					1						1		
10.1021/acsnalchem.6b042028	1																1			1	1	1	1		
10.1021/acsmi.5b053753	1		1												1									1	
10.1038/nmeth.3697	1				1											1	1							1	
10.1007/s10544-013-9821-5	1																1							1	

Chapter II

DOI	Assays										Usability aspects															
	On-chip					Off-chip					Flow control			Integration		Format										
	Immunohistochemistry	Calcium imaging	Migration assay	Angiogenesis	Permeability	TEER	Phase contrast	Light microscopy	ELISA	Colorimetric	Luminescence	ELISA	Luminescence	LC/GC-IMS	Colorimetric	RNA expression	External pumps	Internal pump	Passive leveling	Sample prep	Sensors	Pumping system	Other actuators	Single-chip	Multi-chip	Microtiter plate format
10.1007/s10544-014-9834-8	1			1												1					1		1			
10.1007/s10544-015-9966-9	1			1	1							1	1		1	1								1		
10.1007/s10544-016-0054-0	1								1														1			
10.1007/s10544-016-0117-1	1					1	1	1							1										1	
10.1186/s13287-016-0371-2	1						1							1	1									1		
10.1186/s40478-014-0145-3	1						1	1																1		
10.1063/1.4892894							1	1									1				1			1		



Chapter II



DOI	Assays										Usability aspects															
	On-chip					Off-chip					Flow control		Integration			Format										
	Immunohistochemistry	Calcium imaging	Migration assay	Angiogenesis	Permeability	TEER	Phase contrast	Light microscopy	ELISA	Colorimetric	Luminescence	ELISA	Luminescence	(LC/GC)-MS	Colorimetric	RNA expression	External pumps	Internal pump	Passive leveling	Sample prep	Sensors	Pumping system	Other actuators	Single-chip	Multi-chip	Microtiter plate format
10.1063/1.4920193	1																1			1		1			1	
10.3390/bios5.2.0305							1	1										1		1	1	1	1		1	
10.1002/bit.276087	1												1					1							1	
10.1039/c3lc50819f	1																								1	
10.1039/c4an00541d															1										1	
10.1039/c4ib00144c	1		1				1	1										1							1	
10.1039/c4lc00962b	1																	1							1	
10.1039/c5lc00180c	1	1					1	1			1								1							1

Chapter II



DOI	Assays											Usability aspects														
	On-chip						Off-chip					Flow control			Integration		Format									
	Immunohistochemistry	Calcium imaging	Migration assay	Angiogenesis	Permeability	TEER	Phase contrast	Light microscopy	ELISA	Colorimetric	Luminescence	ELISA	Luminescence	LC/GC-IMS	Colorimetric	RNA expression	External pumps	Internal pump	Passive leveling	Sample prep	Sensors	Pumping system	Other actuators	Single-chip	Multi-chip	Microtiter plate format
10.1371/journal.pone.0153036		1			1												1							1		
10.3791/52526		1										1	1					1			1				1	
10.1002/adm.201600893		1											1		1										1	
10.1002/bit.25659							1	1						1	1	1									1	
10.1002/jbm.a.34772		1															1							1		
10.14348/molcells.2014.0137		1	1					1																1		
10.1177/153537021453928		1		1	1	1	1	1									1							1		
10.1039/c4lc00371c		1			1												1							1		
10.1038/nmat4570		1			1														1						1	

Chapter II

DOI	Assays										Usability aspects						
	Immunohistochemistry	Calcium imaging	Migration assay	Angiogenesis	Permeability	TEER	Phase contrast	Light microscopy	ELISA	Colorimetric	Luminescence	Off-chip	Flow control	Integration	Format		
10.103 5 2																	
10.310 9/1476 7058.2																	
5 3	1				1												
10.107 3/pnas. 5 4																	
5 4	1												1	1	1		
10.103 5 5																	
5 6	1												1	1	1		
10.103 5 7																	
5 7	1			1			1	1							1		
10.100 5 8																	
5 8	1				1	1								1	1		
10.100 5 9																	
5 9	1				1	1					1				1		
10.100 201503 6 0																	
6 0	1						1	1							1		
10.103 6 1																	
6 1	1	1								1			1		1		
10.103 6 2																	
6 2	1		1				1	1			1	1			1		



Chapter II



DOI	Assays										Usability aspects															
	On-chip					Off-chip					Flow control	Integration		Format												
	Immunohistochemistry	Calcium imaging	Migration assay	Angiogenesis	Permeability	TEER	Phase contrast	Light microscopy	ELISA	Colorimetric	Luminescence	ELISA	Luminescence	LC/GC-IMS	Colorimetric	RNA expression	External pumps	Internal pump	Passive leveling	Sample prep	Sensors	Pumping system	Other actuators	Single-chip	Multi-chip	Microtiter plate format
10.33 90/mi 6 70701 3 20		1																		1	1		1			
10.10 38/n 6 mat47 4 82		1																		1	1			1		
10.10 16/j.bi os.20 6 16.06. 5 014						1														1				1		
10.11 26/sci adv.1 6 50142 6 9		1					1	1							1							1		1		
10.10 21/ac 6 50370 7 0f		1		1								1						1							1	
10.10 38/sre 6 p2157 8 9		1												1	1	1									1	
10.10 38/sre 6 p3158 9 9		1		1	1					1								1							1	
10.10 39/c5l 7 c0105 0 0k		1		1	1			1										1							1	
10.10 38/sre 7 p2003 1 0		1						1				1		1											1	

Chapter II

	Assays											Usability aspects														
	On-chip						Off-chip					Flow control			Integration			Format								
DOI	Immunohistochemistry	Calcium imaging	Migration assay	Angiogenesis	Permeability	TEER	Phase contrast	Light microscopy	ELISA	Colorimetric	Luminescence	ELISA	Luminescence	Colorimetric	RNA expression	External pumps	Internal pump	Passive leveling	Sample prep	Sensors	Pumping system	Other actuators	Single-chip	Multi-chip	Microtiter plate format	
10.10379/c4lc021252f	1				1							1		1							1		1			
10.10379/c6lc030910g	1			1													1						1			
10.10379/c5lc041000d																	1				1				1	
10.1021/acs.analchem.5b053513								1					1		1							1		1		
10.1038/micronano.2016.262																1				1				1		
10.1038/ncomms11535	1					1						1	1	1	1				1					1		
Total:	6	5	2	7	6	1	4	9	9	8	2	3	2	1	4	7	5	6	7	1	3	8	9	1	1	3



Chapter II



Chapter III

Microengineered human blood vessel to study microvascular
destabilization *in vivo*

Abidemi Junaid, Wendy Stam, Sophie Dólleman, Vincent van Duinen, Hetty de
Boer, Cees van Kooten, Alireza Mashaghi, Janine van Gils, Thomas Hankemeier,
Anton Jan van Zonneveld

Manuscript to be submitted (2020)

Abstract

Vascular diseases are one of the main causes of mortality in the world. The development of models that effectively recapitulate the human vasculature is essential for studying the pathogenesis and therapeutic approaches for vascular diseases. Here we describe the development of a perfusable microvessel-on-a-chip featuring the human endothelium that is partly surrounded with extracellular matrix (ECM). The system is high-throughput, which allows parallel analysis of organ-level microvessel pathophysiology *in vitro*. Exposure of the microvessels to VEGF, histamine and TNF α led to albumin leakage, reconstituting the vascular leakage seen *in vivo*. Moreover, we demonstrated that this process involves changes in cellular mechanics. Finally, we developed a method to screen blood samples with our platform. Plasma samples were prepared from whole blood and treated with hirudin, corn trypsin inhibitor (CTI) and compstatin. Subsequently, this plasma cocktail was spiked with VEGF, histamine and TNF α and perfused in the microvessels-on-chips, which showed increase in vessel permeability. Our study confirms the effect of destabilizing factors in blood to induce vascular leakage in a physiological relevant *in vitro* setting. We anticipate our assay to serve as a unique tool for microvascular destabilization studies as well as for the development of novel therapeutic strategies to combat vascular diseases.



Introduction

For centuries, vascular diseases produced massive health and economic burdens globally [1]. One of the most crucial functional units of the vascular system are the endothelial cells. They are involved in coagulation of blood, inflammation, hemodynamic, signal transduction and semi-selective barrier. Endothelial dysfunction is a key factor for vascular diseases [2].

As current human 2D models with cultured endothelial cells lack sufficient complexity to assess the functionality of the microvascular system, research on microvascular loss largely depends on pre-clinical animal models for ischemia and reperfusion injury. However, animal models occasionally show an inexact representation of vascular diseases and disorders, because the anatomy, immune systems and inflammatory responses of animal microvessels differ considerably from those in humans [3]. This imperfection leads to failure in predicting efficacy, safety and toxicity of chemicals in humans, which then causes a devastating blow in clinical trial failures [4, 5].

Organs-on-Chips have recently emerged as a new research method to mimic the activities, mechanics and physiological responses of human organ systems. These microsystems can be embedded with a particular disease [6-8]. Moreover, they offer new possibilities for increasing the speed and accuracy of drug testing [9]. Extensive research has shown positive feasibility in using these 3D microfluidic models to create perfusable microvessels for investigating endothelial barrier function [10-12]. Although there are many organs-on-chips on the market that model microvessels, most of these models unfortunately depend on using cell culture media to investigate vascular permeability [13]. To better mimic vascular diseases and disorders, a more reasonable option is to perfuse 3D modelled microvessels with human blood plasma. This is of great importance because plasma contains plethora of circulating markers that regulate cell viability. For example, circulating markers in chronic kidney disease, such as tumor necrosis factor alpha (TNF α) and Interleukin 6 (IL-6) induce systemic inflammatory state and endothelial activation. This results in endothelial cell activation associated with the shedding of components of the glycocalyx, adhesion molecules and endothelial microparticles into the systemic circulation. The process ends with the detachment of endothelial cells accompanied with vascular leakage and heart failure [2, 14, 15].

To investigate the aspects of endothelial function in vascular disease models, we micro-engineered a microfluidics-based, 3D microvessel-on-a-chip platform that mimics human microvessels. Our system allows quantitative and parallel testing of microvascular leakage. Moreover, we developed an approach to screen human blood plasma in the microvessel-on-a-chip for the presence of circulating markers of endothelial activation.

Materials and Methods

Chip design

We designed a novel chip structure (T-design) based on the MIMETAS OrganoPlate platform. This new design involves a T-junction shown in Figure 1 in which the channels are separated by a phaseguide. The design, due to its geometry, enables easy generation of leak tight vessels and quantification of vascular leakage. Fabrication of the glass chipsets was carried out by MIMETAS using a previously established protocol [36].

Cell culture

Human umbilical vein endothelial cells (HUVECs) were cultured in Endothelial Cell Growth Medium 2 (EGM2; C-39216, PromoCell). We used the T-design OrganoPlate for all microfluidic cell culture. Thus, the microvascular and extracellular matrix (ECM) channels were separated by phaseguides. Before seeding the cells, 4 mg/ml rat tail collagen type 1 (3440-005-01, Trevigen) neutralized with 10% 37 g/L Na₂CO₃ (S5761, Sigma) and 10% 1 M HEPES buffer (15630-056, Gibco) was added in the ECM channels. Subsequently, the collagen was let to polymerize by incubating the device for 10 minutes in the incubator at 37°C and 5% CO₂. The observation windows were filled with 50 µl Hank's Balanced Salt Solution with calcium and magnesium buffers (HBSS+; 24020117, Life Technologies) for optical clarity. The ECM inlets were filled with 20 µl HBSS+ to prevent gel dehydration. Cells were seeded with a density of 20·10⁶ cells/ml in gelatin-coated microvascular channels of the OrganoPlate. Afterwards, the cells were incubated at 37°C and 5% CO₂ for one hour to allow microvascular formation. After incubation, 50 µl of medium with 50% EGM2 and 50% Pericyte Growth Medium (cAP-09B,

Angio-Proteomie) was added to the inlets and outlets of the microvascular channels. The device was placed on a rocker platform with a 7° angle of motion and an eight-minute timed operation to allow continuous flow of medium in the microvessels. After 24 h, the medium was refreshed, and the HUVECs were cultured for an additional 3-4 days.

Coagulation Tests

The prothrombin time (PT) assays and the activated partial thrombin time (aPTT) assays were performed in the STart® Line: STart Max® (Diagnostica Stago) and 25 µM compastatin (supplied by our collaborators) was used in both assays. Ethylenediaminetetraacetic acid (EDTA) platelet poor plasma (PPP) was diluted to 50% plasma in dilution media of 50% EGM2 and 50% Pericyte Growth Medium. For the PT assay, 10 µM hirudin (94581-1EA, Sigma-Aldrich) was serially diluted in 50% plasma, 50 µl of each plasma dilution was incubated at 37°C for one minute. Coagulation was initiated with 50 µl of Neoplastine Ci Plus 10 (Diagnostica Stago), 1:10 diluted with dilution medium at 37°C and clotting time was measured. For the aPTT assay, Corn Trypsin Inhibitor (CTI) 500 µg/ml (CTI-01, Haematologic Technologies, Inc.) was serially diluted in 50% plasma and 50 µl of each plasma dilution was incubated at 37°C for three minutes with 50 µl of aPTT reagent (TriniClot). Coagulation was initiated with 50 µl of 25 mM CaCl₂ at 37°C.

Complement assay

The complement activation product C3 was measured by classical pathway activity enzyme-linked immunosorbent assay (ELISA). Wells were coated with 2 µg/ml human IgM in coating buffer (0.1 M NaHCO₃, 0.1 M Na₂CO₃, pH 9.6). Plasma samples were diluted in GVB++ (Gelatin Veronal Buffer, with 1 mM MgCl₂, 2 mM CaCl₂, 0.05% Tween). The in house made monoclonal antibody RfK22, labeled with digoxigenin (DIG) in incubation buffer (PTB; PBS, 0.05% Tween, 1% BSA) was used as a capture antibody. C3 was measured by using anti-DIG-horseradish peroxidase antibody in incubation buffer (PTB; PBS, 0.05% Tween, 1% BSA). Subsequently, the samples were developed with 3,3',5,5'-Tetramethylbenzidine (TMB) substrate solution. After 15 minutes, the reaction was stopped with H₂SO₄ and the optical density (OD) was measured at 450 nm.



Plasma assay

EDTA-plasma samples were treated with 1 μM hirudin (94581-1EA, Sigma-Aldrich), 50 $\mu\text{g}/\text{ml}$ CTI (CTI-01, Haematologic Technologies), 25 μM compstatin and finally recalcified with 3.1 mM CaCl_2 . These treated plasma samples were mixed with 50% EGM2 and 50% Pericyte Growth Medium. Finally, we perfused this cocktail mix in the microvessels-on-chips.

Vascular leakage assay

Endothelial cell culture media and plasma samples of healthy controls were spiked with vascular endothelial growth factor (VEGF; 450-32, PeproTech), histamine (H7125 SIGMA, Sigma-Aldrich) and tumor necrosis factor- α (TNF- α ; H8916 SIGMA, Sigma-Aldrich). To measure vessel permeability, the ECM channel inlets were refreshed with 20 μl HBSS+ buffers (Life Technologies; Bleiswijk; The Netherlands). Then, the media in the inlets and outlets of the microvascular channels were replaced with 40 μl and 30 μl of 125 $\mu\text{g}/\text{ml}$ Albumin-Alexa 555 (A34786, Life Technologies). Following this, the OrganoPlate was placed in the environmental chamber (37°C; 5% CO_2) of a fluorescence microscope system (Nikon Eclipse Ti) and time-lapse images were captured.

We calculated the permeability coefficient by determining the fluorescent intensities in the microvascular channel of captured images. At the same time, the fluorescent intensities in the ECM channel of the capture images was obtained and normalized with the fluorescent intensities in the microvascular channel of each measured time point. This showed the change in intensity ratio inside the gel channel as a function of time. The scatter plot was fitted with a linear trend line to determine the slope. Finally, using Fick's First Law the apparent permeability was determined as [37, 38]:

$$P_{app} (\cdot 10^{-6} \text{ cm/s}) = \frac{d\left(\frac{I_g}{I_p}\right)}{dt} \cdot \frac{A_g}{l_w}$$

where I_p is the intensity in the microvascular channel, I_g is the intensity in the ECM channel, A_g ($480 \cdot 10^{-6} \text{ cm}^2$) is the area of the ECM channel and l_w ($400 \cdot 10^{-4} \text{ cm}$) is the length of the vessel wall that separates between ECM and microvascular region. All data analysis was done with ImageJ and Matlab (2016a, MathWorks).

Transendothelial electrical resistance (TEER) measurements

Cell barrier function was assessed by measuring transendothelial electrical resistance (TEER) in real time using the Electric Cell-substrate Impedance Sensing (ECIS Z θ , Applied BioPhysics) system. HUVECs at a density of $15 \cdot 10^3$ cells per well were dispensed and grown to a confluent monolayer on 1% gelatin-coated 96W20idf electrodes (Applied BioPhysics) in 200 μl EGM2 in a 5% CO₂ incubator at 37°C for 48 hours. For the coating, gelatin was dissolved in water. Monolayer resistance was recorded at 4 kHz over 15 minutes intervals for baseline measurement. Subsequently, 75 μl medium was taken out and 75 μl recalcified 50% EDTA-plasma with 1 μM hirudin, 50 $\mu\text{g/ml}$ CTI and 25 μM compstatin was added for 6 hours before treatment. After 6 hours, 75 μl of the EDTA-plasma cocktail and medium were replaced by 75 μl of the plasma cocktail and medium spiked with VEGF, histamine and TNF α .

For analysis of changes in barrier function, TEER measurements were averaged over the last 10 stable pre-treatment time points as baseline. For the percentage resistance, TEER values were corrected for the base line.

Immunocytochemistry

The medium was aspirated from the medium inlets and outlets of the chips and cells were fixed using 4% paraformaldehyde (PFA) in HBSS+ for 10 minutes at room temperature. The fixative was aspirated and cells were rinsed once with HBSS+. Next, cells were permeabilized for two minutes with 0.2% Triton X-100 in HBSS+ and washed once with HBSS+. The cells were blocked with 5% BSA in HBSS+ for 30 minutes and incubated with primary antibody solution overnight at 4°C. Mouse anti-human CD144 (1:100; 555661, BD Biosciences) and 10H10 (supplied by our collaborators) were used as the primary antibodies. The wells were washed



with HBSS+, followed by the addition of Hoechst (1:2000; H3569, Invitrogen), rhodamine phalloidin (1:200; P1951 SIGMA, Sigma-Aldrich) and secondary antibody solution containing goat-anti-mouse Alexa Fluor 488 (1:250; R37120, Waltham). After one hour of incubation in the dark at room temperature, wells were washed three times with HBSS+. High quality Z-stack images of the stained cells were obtained using a high-content confocal microscope (ImageXpress Micro Confocal, Molecular Devices).



Statistical analysis

For statistical analyses, we used IBM SPSS Statistics 23. Values are given as mean \pm SEM. Multiple comparisons were made by one-way ANOVA followed by Dunnett's t-test. Results were considered significant at *P < 0.05, **P < 0.01, ***P < 0.001.

Results

Development of a functional microvessel-on-a-chip

To construct the human microvessel-on-a-chip, we used the fabricated OrganoPlates (T-design). It is based on a 384-well microtiter plate format and employs coverslip-thickness glass (175 μm) for optical access [7]. A plate comprises microfluidic tissue chips, that can be used to establish 96 microvessels with heights of 120 μm and widths of 400 μm (Figure 1a). Each chip contains phaseguides for adjusting the capillary pressure to pattern type 1 collagen in the ECM channel (Figure 1b). The ECM channel enables diffusion-based solute flux across the endothelial monolayer that was used to measure the endothelial permeability (Figure 1e). After seeding the collagen, we cultured primary HUVECs in the perfusion channel. For easier operation of the chips, gravity-induced flow was used. Immunofluorescence confocal microscopic analysis showed that these cells formed leak-tight microvessel after five days in culture. Cell shape was maintained by F-actin. Moreover, the HUVECs were joined by adherence junctions containing VE-cadherin (Figure 1c and d). This enabled the formation of a robust endothelial barrier or leak-tight microvessel that restricted the passage of fluorescent albumin (67 kDa) between the endothelial monolayer and the ECM channel for 10 minutes

(Figure 1f and h). The endothelial barrier was disturbed with 10 nM thrombin for 20 minutes, which enabled an increase in endothelial permeability and represented vascular leakage (Figure 1g and h). Thus, our human microvessel-on-a-chip effectively recapitulated many of the structures and functions of microvessels under healthy and stressed conditions.

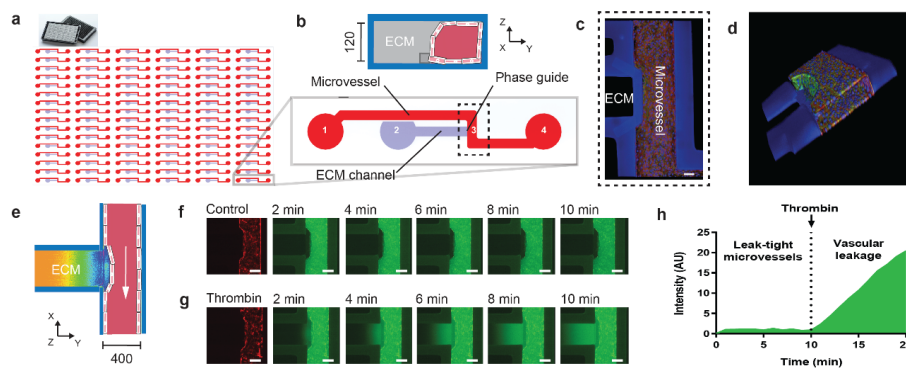


Figure 1 | The human microvessel-on-a-chip. (a) Schematic diagram of 96 microfluidic tissue chips that comprise a gradient design (T-design) in the OrganoPlate. The highlighted rectangular box shows the area depicted in b. (b) Diagram of a single chip; 1 = medium inlet, 2 = gel inlet, 3 = observation window, 4 = medium outlet. The inlay shows the compartments of the microvessel and the ECM. The dashed rectangular box highlights the region shown in c. (c) Cultured HUVECs formed (red, F-actin) a microvessel that exhibited continuous intercellular junctions on-chip, as demonstrated by VE-cadherin staining (green). Scale bar, 100 μm . (d) A 3D reconstruction showing the human microvessel-on-a-chip. (e) Fluorescent intensity profile illustrating the distribution of albumin in a 3D collagen ECM region under experimental conditions. Bluish colors indicate higher fluorescent intensities. (f) Time-lapse fluorescent images of albumin (green) diffusing from the microvessel (red) to the ECM channel. Scale bar, 200 μm . (g) Time-lapse fluorescent images of albumin (green) diffusing from the microvessel (red) to the ECM channel after treatment with 10 nM thrombin for 20 minutes. Scale bar, 200 μm . (h) Fluorescent intensity profile of f and g, illustrating leak-tight microvessels and vascular leakage after treatment with 10 nM thrombin. There was a sharp increase in albumin concentration across the endothelial monolayer and a steady diffusive flux inside the 3D ECM.

Modeling microvascular dysfunction on-chip

Vascular endothelial growth factor (VEGF) is known to increase leakage of plasma components by perturbing endothelial barrier integrity. VEGF activates endothelial cells by inducing phosphorylation and internalization of VE-cadherin [16, 17]. Perfusion of VEGF in our human microvessel-on-a-chip led to a dramatic increase in vessel permeability, as shown in Figure 2a and also in line with TEER measurement and other *in vitro* findings (Figure 2d) [16]. VEGF induced stress fiber formation and VE-cadherin distribution was in a zig-zag pattern with visible gaps between the cells, indicating internalization of VE-cadherin (Figure 2g).



Chapter III

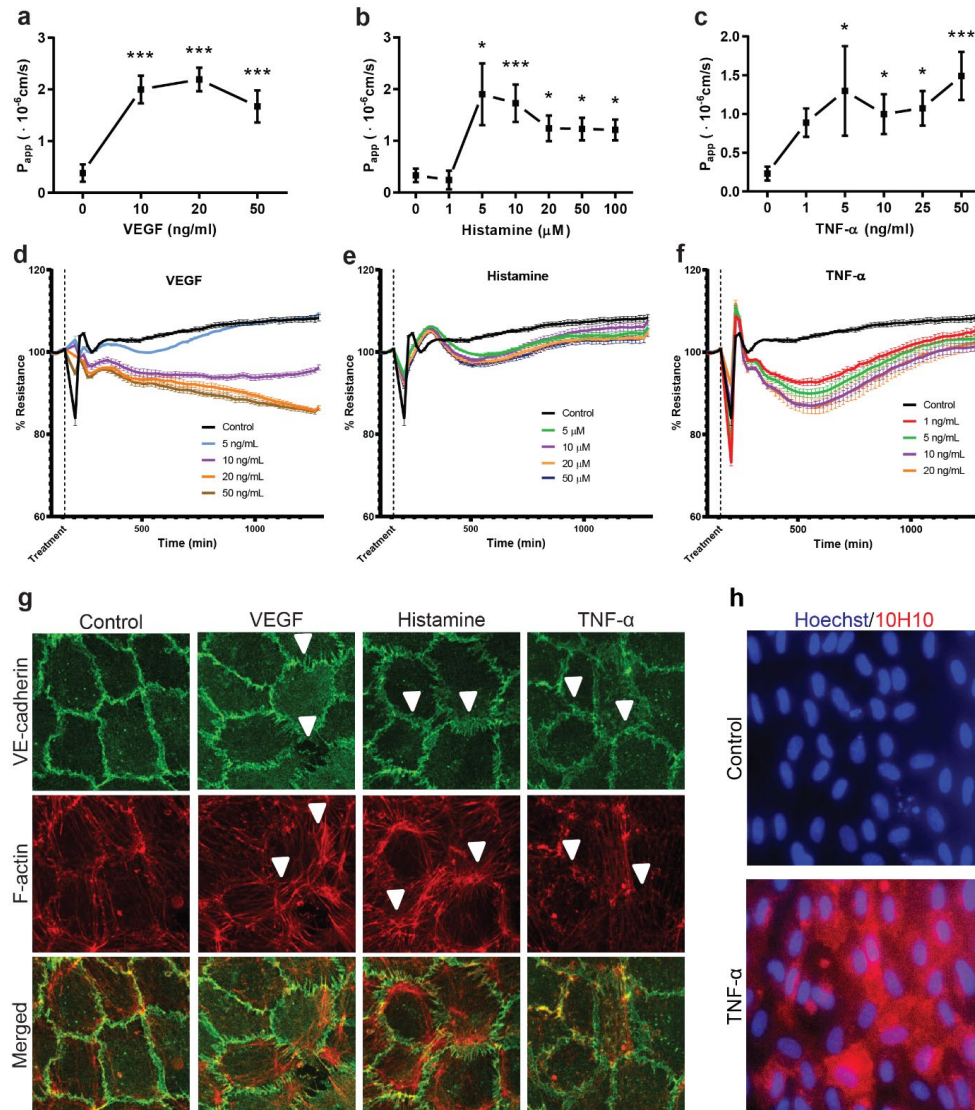


Figure 2 | Modeling microvascular dysfunction in microvessel-on-a-chip. (a) Dose response to VEGF in microvessels. Microvessels were treated for 1.5h at 37°C with several concentrations of VEGF, followed by vascular leakage assay. **(b)** Dose response to histamine in microvessels. Microvessels were treated for 1h at 37°C with several concentrations of histamine, followed by vascular leakage assay. **(c)** Concentration dependence of TNF α effect. Microvessels were treated overnight at 37°C with several concentrations of TNF α , to measure vascular leakage. Data are presented as mean and s.e.m of 3-6 biological replicates; n = 6-19 (chips). Significance determined by ANOVA and Dunnett's t-test; *P < 0.05, **P < 0.01, ***P < 0.001. **(d-f)** The effects of VEGF, histamine and TNF α on endothelial barrier function were measured in the Electric Cell-substrate Impedance Sensing (ECIS) at different doses. Data are represented as mean and s.e.m of 3-4 technical replicates. **(g)**

Chapter III

Microarchitecture of endothelial cells in response to 10 ng/ml VEGF (1.5h), 10 μ M histamine (1h) and 10 ng/ml TNF α (overnight) showing the nucleus (blue), VE-cadherin (green) and F-actin (red). These permeability factors induced morphological rearrangement of VE-cadherin and F-actin (arrow). **(h)** Representative pictures of immunostaining of the nucleus (blue) and tissue factor (red) after treatment with 10 ng/ml TNF α (overnight).

In vivo, histamine is known as inflammatory response factor. It is a mediator of allergic inflammation that increases vascular permeability by changing VE-cadherin localization at endothelial cell junction [18]. To mimic this aspect, we modulated endothelial permeability by stimulation of the microvessels with histamine. Treatment of the microvessels with histamine increased permeability significantly (Figure 2b). The effect was further validated in the impedimetric assay, showing a drop in TEER after administration of histamine (Figure 2e). This organic compound caused increase in stress fiber formation and low distribution of VE-cadherin (Figure 2g).

Endothelial cell activation often involves the exposure of NADPH oxidase (NOX) to cytokines, such as tumor necrosis factor alpha (TNF α), which then induces oxidative stress and at the end vascular leakage of plasma fractions [2, 10]. Stimulation of the microvessels-on-chips with TNF α increased the barrier permeability progressively as we increased the concentration of the cytokine (Figure 2c). The perturbation of the endothelial barrier by TNF α was also confirmed in the ECIS system (Figure 2f). Immunostaining showed changes in VE-cadherin arrangement, actin filaments and tissue factor (TF) expression. These effects are typically seen in vascular diseases (Figure 2g and h) [19].

These results are consistent with the findings from past studies that VEGF, histamine and TNF α induce vascular leakage *in vivo* [18, 20]. They show the importance of adherens junctions in maintaining leak-tight microvessels. Moreover, our findings confirm that the human microvessel-on-a-chip can be used to investigate vascular diseases.

Perfusing human blood plasma in microvessels *in vitro*

Being able to perfuse the microvessel-on-a-chip and measure vascular leakage, our next goal was to introduce human blood plasma in the model. As recalcified EDTA-plasma is known to coagulate, we used a combination of the anticoagulants hirudin and CTI to prevent this.

Hirudin specifically binds and inhibits the activity of thrombin to convert fibrinogen into fibrin. In plasma, hirudin extended the clotting time effectively (Figure 3a). The intrinsic coagulation pathway is activated in our microfluidic system, because of the negative charge property of the glass surface. CTI is a specific human factor XIIa inhibitor and when added to plasma, it prolonged the activated partial thromboplastin time (aPTT) (Figure 3b). Besides coagulation, we suspected the appearance of complement activation in blood plasma collected from humans. To confirm this, we performed a complement activation assay for C3 deposition. Incubation of the plasma cocktail provides exceedingly high levels of C3 deposition, proving complement activation in our system. To inhibit complement activation, we used compstatin, a C3-targeted complement inhibitor [21, 22]. We observed a strong decrease of C3 deposition (Figure 3c). This result confirms that compstatin abrogates complement dysregulation in collected EDTA-plasma. By inhibiting complement activation, we can focus on biomarkers that are unique for various vascular diseases in our microvessel-on-a-chip. Immunofluorescence microscopic analysis showed that these culture conditions resulted in the formation of endothelial cells linked by VE-cadherin. The morphology of these cells was comparable to those cultured with endothelial cell culture media (Figure 3d). Perfusing the microvessels with EDTA-plasma cocktail of healthy donors maintained leak-tight vessels (Supplementary Figure 1). These results show the efficacy of the microvessel-on-a-chip with perfused human blood plasma for (pre-)clinical studies. Altogether, we have developed a high-throughput method that can be used to screen blood for markers that have impact on microvascular physiology and pathology. The first step in the process is to collect blood samples in EDTA-tubes. Subsequently, plasma samples are separated by centrifugation and treated with hirudin, CTI and compstatin. The plasma samples are perfused in the microvessels-on-chips and the permeability of these microvessels are visualized with a high-content confocal microscope and analyzed.



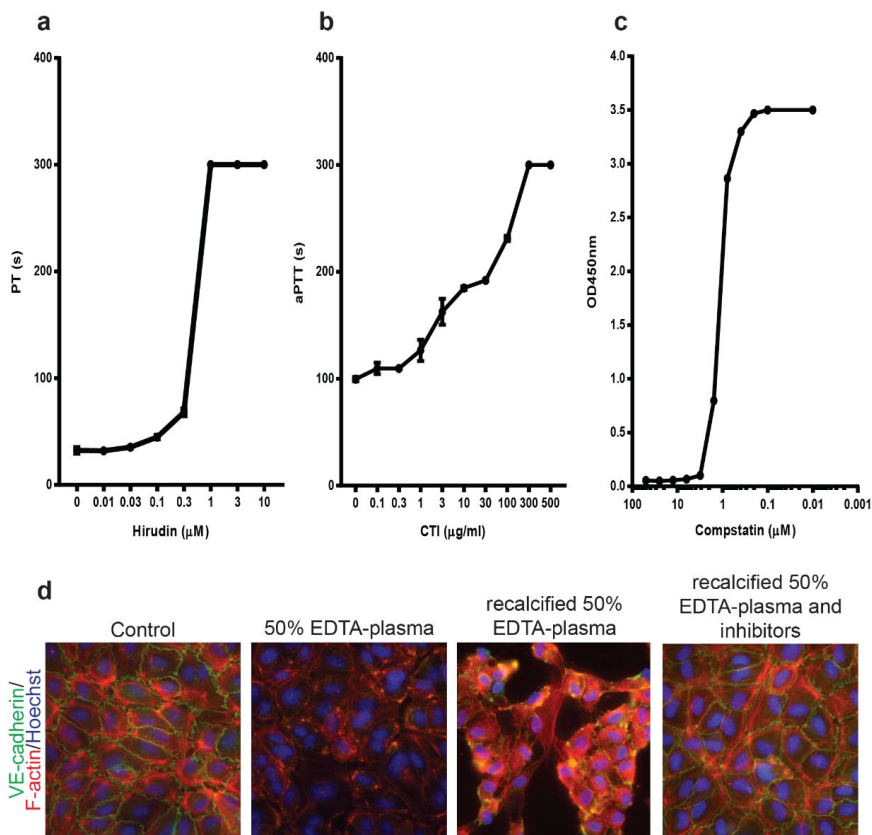


Figure 3 | Coagulation and complement inhibitors for use in EDTA-plasma *in vitro* biocompatibility models. (a) The graph illustrates the effect of added hirudin on the prothrombin time (PT) of re-calcified EDTA-plasma. **(b)** Data represents the effect of CTI on the activated partial thrombin time (aPTT) of recalcified EDTA-plasma. **(c)** Summary of the efficacy of compstatin in selectively inhibiting complement activation in recalcified EDTA-plasma. Data are presented as mean and s.e.m; $n = 2$ **(d)** Immunostaining of HUVECs under endothelial cell culture media (control), 50% EDTA-plasma, recalcified 50% EDTA-plasma and recalcified 50% EDTA-plasma with 1 μM hirudin, 50 $\mu\text{g/ml}$ CTI and 25 μM compstatin.

As human blood plasma contains large number of factors that are major cause of vascular leakage, we next established our microfluidic model for clinical relevancy by spiking the plasma samples with dosage of VEGF, histamine and $\text{TNF}\alpha$. After incubation with these permeability factors, the microvessels lost their leak-tightness (Figure 4a-c). Although the effect was weak due to protective factors in plasma that maintain the hemostasis conditions of the microvessels, the barrier permeability progressively increased as the concentrations of

Chapter III

VEGF, histamine and TNF α increased. Our findings were also validated with the ECIS system. In this system, VEGF, histamine and TNF α spiked in EDTA-plasma effectively decreased the endothelial barrier function (Figure 4d-f). This corroborates with the increased vessel permeability seen in the microvessels-on-chips. Importantly, the increased barrier permeability was associated with the formation of stress fibers and rearrangement of VE-cadherin (Figure 4g). Incubation with TNF α also induced the expression of tissue factor (Figure 4h).



Chapter III

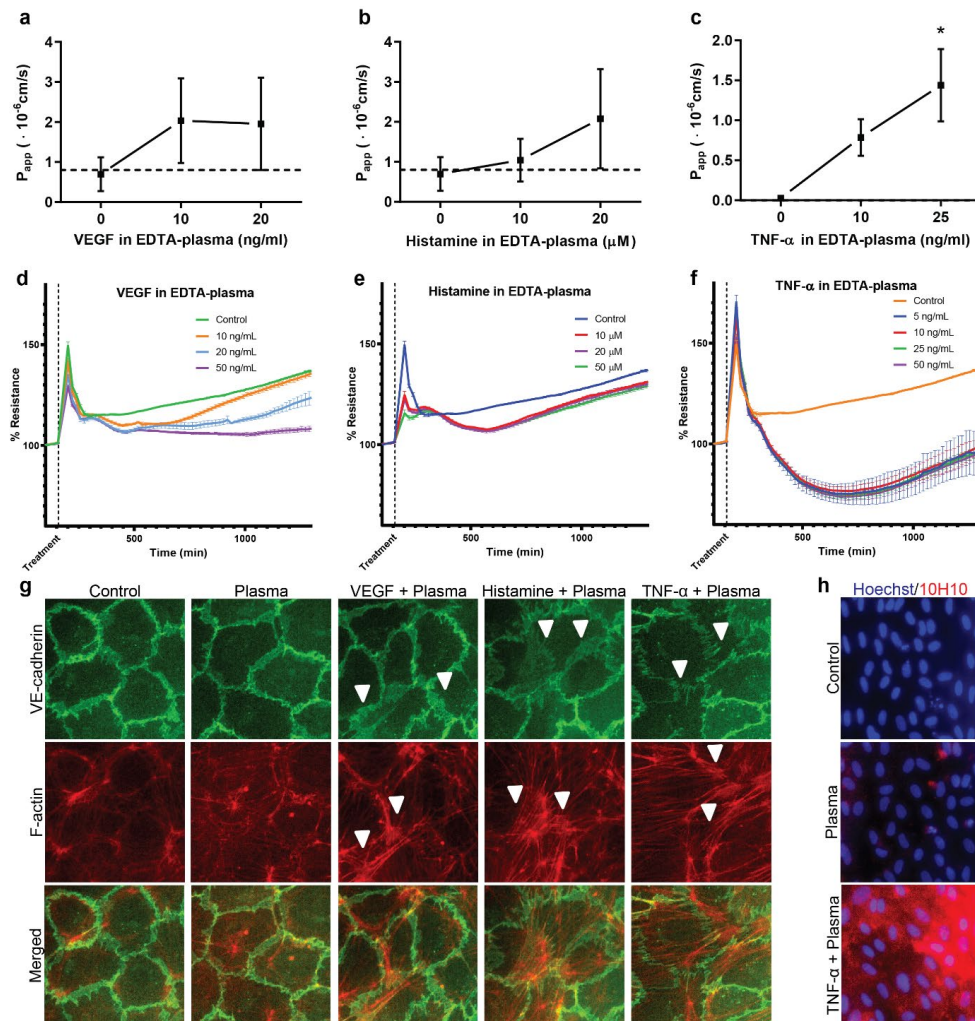


Figure 4 | Permeability effect of perfusing blood plasma in microvessel-on-a-chip. Dose response to (a) VEGF (1.5h), (b) histamine (1h) and (c) TNF α (overnight) spiked at several concentrations in recalcified EDTA-plasma treated with 1 μ M hirudin, 50 μ g/ml CTI and 25 μ M compstatin. Data are presented as mean and s.e.m of two biological replicates; n = 6 (chips). Significance determined by ANOVA and Dunnett's t-test; *P < 0.05. (d-f) The effects of VEGF, histamine and TNF α spiked in recalcified EDTA-plasma on endothelial barrier function were measured in the Electric Cell-substrate Impedance Sensing (ECIS) at different doses. Data are represented as mean and s.e.m of 3-4 technical replicates. (g) Immunostaining of endothelial cells for nucleus (blue), VE-cadherin (green) and F-actin (red) after treatment with 10 ng/ml VEGF (1.5h), 10 μ M histamine (1h) and 10 ng/ml TNF α (overnight) spiked in recalcified EDTA-plasma treated with hirudin, CTI and compstatin. In both conditions an increase in actin stress fiber formation (arrowheads) and morphological arrangement of VE-cadherin were

Chapter III

observed. **(h)** Immunofluorescence for nucleus (blue) and tissue factor expression (red) after treatment with 10 ng/ml TNF α spiked in recalcified EDTA-plasma containing hirudin, CTI and compstatin (overnight).

Discussion

Despite progress in identifying critical regulators of endothelial permeability, it is not fully clear how certain factors in blood induce an impaired endothelial barrier. In this work, we introduced a unique approach using a microfluidic-based *in vitro* assay, microvessel-on-a-chip, that enabled parallel culture, real-time visualization and parallel quantification of endothelial permeability. We showed that VEGF, histamine and TNF α modulate the endothelial barrier. This is also consistent with *in vivo* observations, highlighting the potential of the microvessels-on-chips to study vessel permeability factors in blood [23-25].

Compared to traditional 2D-based assays, the microvessels-on-chips allows us to add physiological relevant cues to the vasculature *in vitro* with several advantages. For example, cell-cell and cell-ECM interaction and perfusion are considerably reduced in 2D cell culture, which in turn significantly limits their ability to mimic the appropriate level of *in vivo* cellular responses. With the microvessels-on-chips we could breach the gap between *in vitro* 2D cell culture and *in vivo* models, enabling us to accurately predict *in vivo* permeability. Furthermore, in our high-throughput platform we are dealing with low volume samples. This gives the possibility to do multiple experiments in a cost effective manner.

Previous studies of endothelial permeability with microfluidic-based approaches were largely done by perfusing cell culture media in the system [26-28]. However, we developed a novel method to directly screen vascular diseases by using primary endothelial cells and blood. In this procedure, we extracted plasma from blood, treated it and perfused it in the cultured human microvessels. To prevent blood plasma from clotting, we primarily inhibited thrombin. This was not only to prevent coagulation induced by recalcification, but also to block the expression of tissue factor that turns on procoagulant activity at the cell surface during vascular diseases [29]. Next to that, due to the negative charge surface of the microchannels of the OrganoPlate, we inhibited the intrinsic pathway of coagulation. This also inhibits the classical pathway of complement activation, since Factor XIIa and kallikrein are known to cleave C1s [30]. Besides preventing clotting, the release of bradykinin, a proinflammatory

peptide that increase endothelial permeability, is suppressed [31]. Considering these factors, there might be crosstalk between the coagulation and complement systems in vascular diseases that can further be intercepted with anti-coagulants and complement inhibitors [32].

The microvessels-on-chips permitted high-throughput stimulation of the vascular permeability induced by our EDTA-plasma cocktail when spiked with VEGF, histamine and TNF α . This vessel permeability was confirmed with TEER measurements by using the ECIS system. However, TEER values vary significantly due to biological and environmental factors, thereby making endothelial cells very sensitive to cytokines and growth factors. On the other hand, the microvessels-on-chips, as a 3D culture system, is a closed system with excellent control and standardization of prepared microvessels with stable endothelial cells [33, 34]. This might have resulted in the reduced permeability effect seen in our platform with greater resemblance to *in vivo* tissue-like physiological responses [35]. Therefore our findings can be applied to disease treatment, where early diagnosis is necessary to properly manage the disease and develop the pharmacokinetic modelling of drug treatments, as initiation of rapid therapy is key to reducing deaths.

Overall, the microengineered human microvessels-on-chips faithfully recapitulated the physiology and pathology of microvessels *in vivo* that can aid as a sensing platform in clinical trials. This offers the possibility to be used as a “disease-on-a-chip” for carrying out cardiovascular studies on drug toxicity *in vitro* as well as dissecting the molecular mechanisms that mediate this process.

Conflict of interest

Authors declare no conflict of interest related to the content of this manuscript.

Acknowledgments

AJ, JvG, TH and AJvZ were financially supported by the RECONNECT CVON Groot consortium, which is funded by the Dutch Heart Foundation.

References

1. Mozaffarian, D., et al., *Executive Summary: Heart Disease and Stroke Statistics-2016 Update A Report From the American Heart Association*. *Circulation*, 2016. **133**(4): p. 447-454.
2. Rabelink, T.J., H.C. de Boer, and A.J. van Zonneveld, *Endothelial activation and circulating markers of endothelial activation in kidney disease*. *Nature Reviews Nephrology*, 2010. **6**(7): p. 404-414.
3. Mestas, J. and C.C.W. Hughes, *Of mice and not men: Differences between mouse and human immunology*. *Journal of Immunology*, 2004. **172**(5): p. 2731-2738.
4. McGonigle, P. and B. Ruggeri, *Animal models of human disease: Challenges in enabling translation*. *Biochemical Pharmacology*, 2014. **87**(1): p. 162-171.
5. van Esbroeck, A.C.M., et al., *Activity-based protein profiling reveals off-target proteins of the FAAH inhibitor BIA 10-2474*. *Science*, 2017. **356**(6342): p. 1084-1087.
6. Benam, K.H., et al., *Small airway-on-a-chip enables analysis of human lung inflammation and drug responses in vitro*. *Nature Methods*, 2016. **13**(2): p. 151-+.
7. Wevers, N.R., et al., *High-throughput compound evaluation on 3D networks of neurons and glia in a microfluidic platform*. *Scientific Reports*, 2016. **6**.
8. Ramadan, Q. and F.C.W. Ting, *In vitro micro-physiological immune-competent model of the human skin*. *Lab on a Chip*, 2016. **16**(10): p. 1899-1908.
9. Trietsch, S.J., et al., *Membrane-free culture and real-time barrier integrity assessment of perfused intestinal epithelium tubes*. *Nature Communications*, 2017. **8**.
10. Zervantonakis, I.K., et al., *Three-dimensional microfluidic model for tumor cell intravasation and endothelial barrier function*. *Proceedings of the National Academy of Sciences of the United States of America*, 2012. **109**(34): p. 13515-13520.
11. Zhang, B., et al., *Biodegradable scaffold with built-in vasculature for organ-on-a-chip engineering and direct surgical anastomosis*. *Nat Mater*, 2016. **15**(6): p. 669-78.
12. Deosarkar, S.P., et al., *A Novel Dynamic Neonatal Blood-Brain Barrier on a Chip*. *PLoS One*, 2015. **10**(11): p. e0142725.
13. Junaid, A., et al., *An end-user perspective on Organ-on-a-Chip: Assays and usability aspects*. *Current Opinion in Biomedical Engineering*, 2017. **1**: p. 15-22.
14. Paulus, W.J. and C. Tschope, *A Novel Paradigm for Heart Failure With Preserved Ejection Fraction Comorbidities Drive Myocardial Dysfunction and Remodeling Through Coronary Microvascular Endothelial Inflammation*. *Journal of the American College of Cardiology*, 2013. **62**(4): p. 263-271.

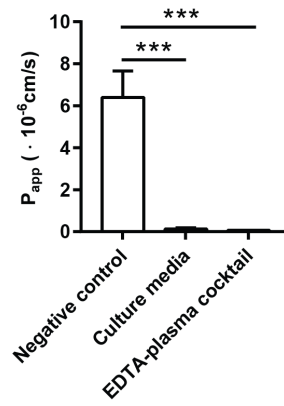
15. Briet, M. and K.D. Burns, *Chronic kidney disease and vascular remodelling: molecular mechanisms and clinical implications*. Clinical Science, 2012. **123**(7-8): p. 399-416.
16. Ulker, E., et al., *Ascorbic acid prevents VEGF-induced increases in endothelial barrier permeability*. Molecular and Cellular Biochemistry, 2016. **412**(1-2): p. 73-79.
17. Park-Windhol, C. and P.A. D'Amore, *Disorders of Vascular Permeability*. Annual Review of Pathology: Mechanisms of Disease, Vol 11, 2016. **11**: p. 251-281.
18. Ashina, K., et al., *Histamine Induces Vascular Hyperpermeability by Increasing Blood Flow and Endothelial Barrier Disruption In Vivo*. Plos One, 2015. **10**(7).
19. Schaefer, A., et al., *Endothelial CD2AP Binds the Receptor ICAM-1 To Control Mechanosignaling, Leukocyte Adhesion, and the Route of Leukocyte Diapedesis In Vitro*. Journal of Immunology, 2017. **198**(12): p. 4823-4836.
20. Kidoya, H., H. Naito, and N. Takakura, *Apelin induces enlarged and nonleaky blood vessels for functional recovery from ischemia*. Blood, 2010. **115**(15): p. 3166-3174.
21. Lindorfer, M.A., et al., *Compstatin Cp40 blocks hematin-mediated deposition of C3b fragments on erythrocytes: Implications for treatment of malarial anemia*. Clinical Immunology, 2016. **171**: p. 32-35.
22. Zhang, Y.Z., et al., *Compstatin analog Cp40 inhibits complement dysregulation in vitro in C3 glomerulopathy*. Immunobiology, 2015. **220**(8): p. 993-998.
23. Kobayashi, K., et al., *Thromboxane A2 exacerbates acute lung injury via promoting edema formation*. Sci Rep, 2016. **6**: p. 32109.
24. Jiang, S., et al., *Vascular endothelial growth factors enhance the permeability of the mouse blood-brain barrier*. PLoS One, 2014. **9**(2): p. e86407.
25. Lundeberg, E., et al., *Assessing Large-Vessel Endothelial Permeability Using Near-Infrared Fluorescence Imaging-Brief Report*. Arteriosclerosis Thrombosis and Vascular Biology, 2015. **35**(4): p. 783-786.
26. Phan, D.T.T., et al., *A vascularized and perfused organ-on-a-chip platform for large-scale drug screening applications*. Lab Chip, 2017. **17**(3): p. 511-520.
27. Ryu, H., et al., *Engineering a Blood Vessel Network Module for Body-on-a-Chip Applications*. J Lab Autom, 2015. **20**(3): p. 296-301.
28. Maoz, B.M., et al., *A linked organ-on-chip model of the human neurovascular unit reveals the metabolic coupling of endothelial and neuronal cells*. Nat Biotechnol, 2018. **36**(9): p. 865-874.
29. Rao, L.V.M. and U.R. Pendurthi, *Regulation of tissue factor coagulant activity on cell surfaces*. Journal of Thrombosis and Haemostasis, 2012. **10**(11): p. 2242-2253.

Chapter III

30. Gorbet, M.B. and M.V. Sefton, *Biomaterial-associated thrombosis: roles of coagulation factors, complement, platelets and leukocytes*. *Biomaterials*, 2004. **25**(26): p. 5681-703.
31. Ehringer, W.D., M.J. Edwards, and F.N. Miller, *Mechanisms of alpha-thrombin, histamine, and bradykinin induced endothelial permeability*. *Journal of Cellular Physiology*, 1996. **167**(3): p. 562-569.
32. Lupu, F., et al., *Crosstalk between the coagulation and complement systems in sepsis*. *Thrombosis Research*, 2014. **133**: p. S28-S31.
33. Ghaffarian, R. and S. Muro, *Models and methods to evaluate transport of drug delivery systems across cellular barriers*. *J Vis Exp*, 2013(80): p. e50638.
34. van Duinen, V., et al., *96 perfusable blood vessels to study vascular permeability in vitro*. *Scientific Reports*, 2017. **7**(1): p. 18071.
35. Lee, J., et al., *In vitro Toxicity Testing of Nanoparticles in 3D Cell Culture*. *Small*, 2009. **5**(10): p. 1213-1221.
36. Vulto, P., et al., *Phaseguides: a paradigm shift in microfluidic priming and emptying*. *Lab on a Chip*, 2011. **11**(9): p. 1596-1602.
37. Huxley, V.H., F.E. Curry, and R.H. Adamson, *Quantitative Fluorescence Microscopy on Single Capillaries - Alpha-Lactalbumin Transport*. *American Journal of Physiology*, 1987. **252**(1): p. H188-H197.
38. van Duinen, V., et al., *96 perfusable blood vessels to study vascular permeability in vitro*. *Scientific Reports*, 2017. **7**.



Supplementary Figures



Supplementary Figure 1 | Permeability of empty microchannels (negative control), microvessels perfused with culture media and EDTA-plasma cocktail (recalcified 50% EDTA-plasma with 1 μM hirudin, 50 $\mu\text{g/ml}$ CTI and 25 μM compstatin). Data are presented as mean and s.e.m; $n = 4-17$ (chips). Significance determined by ANOVA and Dunnett's t-test; *** $P < 0.001$.

Chapter IV

Ebola hemorrhagic shock syndrome-on-a-chip

Abidemi Junaid, Huaqi Tang, Anne van Reeuwijk, Yasmine Abouleila, Petra
Wuelfroth, Vincent van Duinen, Wendy Stam, Anton Jan van Zonneveld, Thomas
Hankemeier, Alireza Mashaghi

iScience (2020) **23**, 100765

Chapter IV

Abstract

Ebola virus, for which we lack effective countermeasures, causes hemorrhagic fever in humans, with significant case fatality rates. Lack of experimental human models for Ebola hemorrhagic fever is a major obstacle that hinders the development of treatment strategies. Here, we model the Ebola hemorrhagic syndrome in a microvessel-on-a-chip system and demonstrate its applicability to drug studies. Luminal infusion of Ebola virus-like particles leads to albumin leakage from the engineered vessels. The process is mediated by the Rho/ROCK pathway and is associated with cytoskeleton remodelling. Infusion of Ebola glycoprotein (GP_{1,2}) generates a similar phenotype, indicating the key role of GP_{1,2} in this process. Finally, we measured the potency of a recently developed experimental drug FX06 and a novel drug candidate, melatonin, in phenotypic rescue. Our study confirms the effects of FX06 and identifies melatonin as an effective, safe, inexpensive therapeutic option that worth investigating in animal models and human trials.

Introduction

Ebola hemorrhagic fever is a rapidly progressive and highly fatal condition for which there is no established treatment [1]. The Ebola epidemic in West Africa (2014-2016) was a health crisis of unprecedented magnitude and impact, causing more than 11,000 deaths and destabilizing three countries [2]. Currently, World Health Organization and African countries are struggling to contain a new large outbreak in Africa, which has led to hundreds of deaths [3]. Vascular integrity impairment with subsequent blood volume loss (the so-called shock syndrome) is the primary cause of death in Ebola patients. Despite supportive care, more than 50% of patients die, with significant interindividual differences in disease outcome reported and attributed to viral loads and host factors [4, 5]. Despite progress, many challenges remain to be addressed, including improving early diagnosis, predicting disease progression, and developing therapeutic and preventive methods.

The lack of experimental models and sensitive detection tools has historically hindered the early detection of Ebola vasculopathy and the development of Ebola drugs. However, rodent models that can mimic certain aspects of Ebola disease in humans have been developed and are now used along with monkey models as *in vivo* models of the disease [6-8]. The use of these models has recently led to the development of experimental therapeutic strategies, including small molecules [9], antibodies [10-13] and nanoparticles [14], as well as glycofullerenes [15]. However, these therapeutics do not directly target hemorrhagic shock syndrome but rather Ebola virus infection. Additionally, animal models are costly and cannot fully recapitulate the physiology and pathology of human organs, making it difficult to predict the efficacy, safety and toxicity of experimental Ebola drugs [16].

In vitro human models for viral hemorrhagic shock syndrome are currently lacking. However, such models would not only be useful for studying the pathogenesis of Ebola in a human-like setting but would also be critical for diagnostics and drug development. Chip-based disease models are becoming important research tools in biology and medicine [17-19]. Examples include the modeling of drug toxicity-induced pulmonary edema in a lung-on-a-chip model [20], the modeling of Alzheimer's disease in a brain-on-a-chip platform [21] and the simulation of diabetic nephropathy in a glomerulus-on-a-chip microdevice [22]. Additionally, there is a growing interest in using *in vitro* engineered models in vascular medicine [23-39], yet no chip-based model of viral hemorrhagic shock syndrome has been introduced. Here, we develop,

for the first time, a microvessel-on-a-chip based model of Ebola (species Zaire ebolavirus) viral hemorrhagic syndrome and demonstrate its usefulness by exploring the signaling and physical processes that underlie the hemorrhagic syndrome and by targeting those processes using drug candidates.

Transparent Methods

Chip design

We designed a novel chip structure (T-design) based on the MIMETAS OrganoPlate platform. This new design involves a T-junction shown in Figure 1 in which the channels are separated by a phaseguide (Vulto et al., 2011). The design, due to its geometry, enables easy generation of leak tight vessels and quantification of vascular leakage. With the T-design there is a small area that has direct contact with the ECM, which makes it easy to create leak tight vessels compared to if a larger area of the microvessel has contact with the ECM. Additionally, this likely increases the duration of the permeability measurement before the system becomes saturated. Fabrication of the glass chipsets was carried out by MIMETAS using a previously established protocol (Vulto et al., 2011).

Cell culture

Human umbilical vein endothelial cells (HUVECs) were cultured in Endothelial Cell Growth Medium 2 (C-39216; PromoCell). We used the T-design OrganoPlate for all microfluidic cell culture. Thus, the microvascular and extracellular matrix (ECM) channels were separated by phaseguides. Before seeding the cells, 4 mg/ml rat tail collagen type 1 (3440-005-01; Trevigen) neutralized with 10% 37 g/L Na₂CO₃ (S5761; Sigma) and 10% 1 M HEPES buffer (15630-056; Gibco) was added in the ECM channels. Subsequently, the collagen was let to polymerize by incubating the device for 10 minutes in the incubator at 37°C and 5% CO₂. The observation windows were filled with 50 µl Hank's Balanced Salt Solution with calcium and magnesium buffers (HBSS+; 24020117; Life Technologies) for optical clarity and to prevent gel dehydration. We trypsinized cells at 80-90% confluency and seeded 20·10⁶ cells/ml in gelatin-coated microvascular channels of the OrganoPlate. Afterwards, the cells were incubated at

37°C and 5% CO₂ for one hour to allow microvascular formation. After incubation, 50 µl of culture medium was added to the inlets and outlets of the microvascular channels. The device was placed on a rocker platform with a 7° angle of motion and an eight-minute timed operation to allow continuous flow of medium in the microvessels. After 24 h, the medium was refreshed, and the HUVECs were cultured for an additional 3-4 days.

Permeability assay

Endothelial cell culture medium was spiked with U46619 (D8174; Sigma), Ebola virus-like particles (VLPs; ZEBO-VLP; The Native Antigen Company) and the Ebola virus envelope glycoprotein (GP_{1,2}; EBOVKW95-ENV; The Native Antigen Company). The Ebola VLPs were diluted in 0.2% Endothelial Cell Growth Medium 2 to the desired experimental concentrations. RevitaCell™ Supplement (A2644501; ThermoFisher), FX06 (F4 Pharma GmbH) and melatonin (M5250; Sigma) were used to treat vessel permeability. To prevent the degradation of FX06 in the microvessels, 100 nM carboxypeptidase inhibitor (C0279; Sigma) was added.

To measure vessel permeability, the ECM channel inlets were refreshed with 20 µl HBSS+. Then, the media in the inlets and outlets of the microvascular channels were replaced with 40 µl and 30 µl, respectively, of 125 µg/ml Alexa Fluor 555-conjugated albumin (A34786; Life Technologies). Next, the OrganoPlate was placed in the environmental chamber (37°C; 5% CO₂) of a fluorescence microscope system (Nikon Eclipse Ti), and time-lapse images were captured.

We calculated the permeability coefficient by determining the fluorescence intensities in the microvascular (I_p) and ECM (I_g) channels of the captured images and normalizing them to each other at each time point. This calculation showed the change in the intensity ratio inside the gel channel as a function of time. The area of the ECM channel (A_g) was $480 \cdot 10^{-6} \text{ cm}^2$, and the length of the vessel wall between the ECM and microvascular regions (l_w) was $400 \cdot 10^{-4} \text{ cm}$. The scatter plot was fitted with a linear trend line to determine the slope, and the apparent permeability was calculated as follows:

$$P_{app} (\cdot 10^{-6} \text{ cm/s}) = \frac{d\left(\frac{I_g}{I_p}\right)}{dt} \cdot \frac{A_g}{l_w}$$

Immunohistochemistry

The medium was aspirated from the medium inlets, and the chip outlets and cells were fixed using 4% paraformaldehyde (PFA) in HBSS+ for 10 minutes at room temperature. The fixative was aspirated, and the cells were rinsed once with HBSS+. Next, the cells were permeabilized for two minutes with 0.2% Triton X-100 in HBSS+ and washed once with HBSS+. The cells were blocked in 5% BSA in HBSS+ for 30 minutes and incubated with the primary antibody solution overnight at 4°C. Mouse anti-human CD144 (1:100; 555661; BD Biosciences) and mouse anti-human CD62E (25µg/ml; BBA26-200; R&D Systems) were used as the primary antibodies. The wells were washed with HBSS+, followed by a one-hour incubation with Hoechst (1:2000; H3569; Invitrogen), rhodamine phalloidin (1:200; P1951; SIGMA) and the secondary antibody solution, containing an Alexa Fluor 488-conjugated goat-anti-mouse antibody (1:250; R37120; Waltham). The wells were washed three times with HBSS+. High-quality Z-stack images of the stained cells were acquired using a high-content confocal microscope (Molecular Devices, ImageXpress Micro Confocal). Quantification of Pearson's correlation coefficient for the co-localization of VE-cadherin and F-actin was performed using Coloc2 (ImageJ). Results are depicted as means ± SEMs (n=2).

Statistical analysis

We used IBM SPSS Statistics 23 for statistical analyses. Outliers in the box plots were identified by SPSS. The plotted data are the means ± SEMs of three or four biological replicates. Multiple comparisons were performed by one-way ANOVA followed by Dunnett's t-test. The results were considered significant at *P < 0.05, **P < 0.01 and ***P < 0.001.

Results

Here, we describe a simple chip-based model of Ebola-induced vascular integrity loss. To provide the proof-of-principle for this approach and to ensure that the platform can be extended to a low-cost, easy-to-use high-throughput platform for diagnostics, we included the minimal components needed to model the process. We first generated microvessels within the fabricated OrganoPlates (T-design) using human endothelial cells (primary HUVECs) at the interface of a collagen type 1 network. The chip design allowed us to culture 96 microvessels with heights of 120 μm and widths of 400 μm (see Figure 1a-d). To develop the model and generate all the data for the current study, we have used approximately a total of 550 independent chips. To ensure that the engineered vessel recapitulated the physiological barrier function of a natural vessel, we measured the transport of albumin across the endothelial wall into the collagen network. In a physiological setting, the vessel is expected to be impermeable but to respond dynamically to physiological stimuli. Permeability experiments were carried out after incubating the microvessels with and without histamine (an endogenous biogenic amine known to induce vascular permeability during inflammatory processes) for 40 or 60 minutes. As shown in Figure 1e, we observed no leakage of albumin from the engineered vessels (control; without stimuli) within a 10-minute interval during the permeability assay. Permeability was, however, induced by the administration of histamine, indicating that the endothelial wall is not passive and responds to stimuli as expected (see Figure 1e-g).

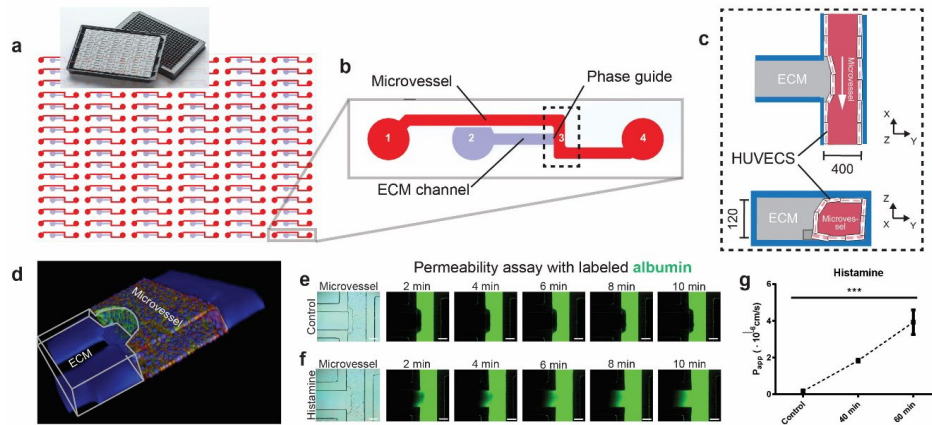


Figure 1 | Viral hemorrhagic syndrome-on-a-chip. (a) Schematic diagram of the 96 microfluidic devices composing the gradient design (T-design) in the OrganoPlate, based on a 384 wells plate interface on top and 96 microfluidic devices integrated in the bottom. (b) Each microfluidic tissue chip consists of a microvessel compartment with medium inlet (1) and outlet (4), gel inlet (2) and observation window (3). The dashed highlighted rectangular box indicates the region depicted in c. (c) Diagram of the monolayers of human umbilical vein endothelial cells (HUVECs) forming a microvessel next to the ECM in the microfluidic system. (d) A 3D reconstruction showing the human microvessel-on-a-chip that was formed by cultured HUVECs (red, F-actin) and demonstrated continuous on-chip junctions (green, VE-cadherin). (e) Time-lapse fluorescence images of albumin (green) perfusion in the microvessel channel. Scale bar, 200 μm . (f) 100 μM histamine was pipetted in the medium inlet and outlet of the microfluidic device and incubated for 60 minutes under perfusion with the Mimetas rocker platform. Subsequently, labeled albumin (green) was added to the medium inlet and outlet and time-lapse fluorescence images of albumin (green) diffusing from the microvessel to the ECM channel were taken. Scale bar, 200 μm . (g) Apparent permeability (P_{app}) of microvessels in the time response to 100 μM histamine. The control is microvessel without histamine treatment. Data are represented as mean \pm SEM.

Next, we infused various concentrations of VLPs to determine whether VLPs alone are sufficient to induce permeability and whether the extent of permeability is viral load-dependent. Infusion of VLPs led to a dramatic increase in the permeability of the engineered microvessels, as shown in Figure 2a and b. The VLPs used in these experiments were non-replicating, indicating that the viral components interact directly with endothelial cells and affect their barrier function, presumably by affecting cellular mechanics and intercellular interactions. Immunostaining of F-actin indicated that Ebola VLPs indeed alter the mechanics and physical interaction of endothelial cells, explaining the induction of permeability (see

Figure 2c). However, treatment with VLPs did not result in an apparent rearrangement of VE-cadherin but instead caused a clear increase in actin stress fiber formation, consistent with the findings in previous reports [40]. Moreover, we observed significant upregulation of E-selectin, a mediator of immune cell recruitment and a biomarker for endothelial dysfunction, clearly indicating the activation of the engineered endothelium (see Supplementary figure 1).

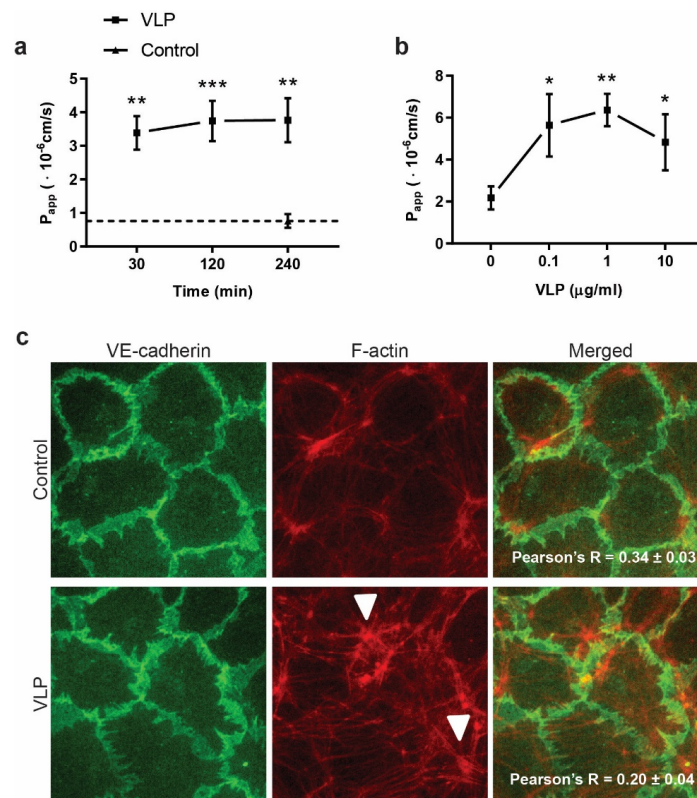


Figure 2 | Microvascular dysfunction in the viral hemorrhagic shock syndrome-on-a-chip platform. (a) Apparent permeability (P_{app}) of microvessels in response to Ebola VLPs at several time points. Microvessels were exposed to 1 $\mu\text{g/ml}$ VLPs, followed by a permeability assay. (b) Concentration dependence of the VLP effect. Microvessels were treated for 2 h with the indicated concentrations of VLPs, followed by a permeability assay. (c) Endothelial cells stained for VE-cadherin (green) and F-actin (red) after exposure to 1 $\mu\text{g/ml}$ VLPs for 2 h. A moderate increase in actin filament stress fiber formation was observed (arrowheads). Pearson's correlation coefficient was lower in microvessels exposed to Ebola VLPs than in the control, showing an increase in stress fiber formation and endothelial cell activation. Data are represented as mean \pm SEM.

Chapter IV

Next, we assessed whether VLPs affect cellular mechanics by modulating the Rho/ROCK pathway. Over-activation of the Rho/ROCK pathway is an underlying mechanism of several vasculopathies, including endotoxin-induced septic vasculopathy [41-43]. Given that some of the major pathophysiological mechanisms of Ebola virus disease resemble those of bacterial septic shock [44, 45], it is conceivable that the Rho/ROCK pathway may also play a critical role in the pathogenesis of the severe vascular leak observed in Ebola disease [46]. To test this hypothesis, we first determined whether we could stimulate the Rho/ROCK pathway in our engineered system and generate a phenotype similar to that observed after the infusion of Ebola VLPs. We used U46619, a small molecule that activates the Rho/ROCK pathway, and measured the time- and concentration-dependent response of the vessels [47]. Treatment of the microvessels with U46619 (10 μ M) increased permeability significantly (see Figure 3a). As the concentration of U46619 increased, the barrier permeability progressively increased (see Figure 3b). Immunostaining of F-actin revealed induced alterations in the cellular cytoskeleton associated with the disruption of the endothelial barrier (see Figure 3c).

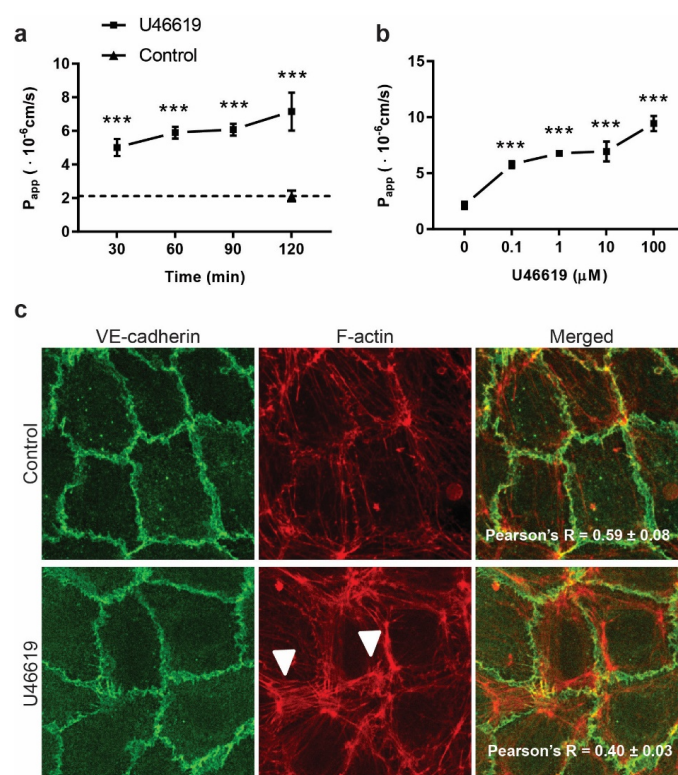


Figure 3 | U46619 induces vascular permeability in the microvessel-on-a-chip platform. (a) Time dependence of U46619-induced barrier opening. Microvessels were exposed to 10 μ M U46619, followed by a permeability assay. **(b)** Dose response to U46619 in microvessels. Microvessels were treated with several concentrations of U46619 for 1 h to measure permeability. **(c)** Immunofluorescence micrographs of on-chip cultured endothelium. After treatment for 1 h with 10 μ M U46619, endothelial cells were stained for VE-cadherin (green) and F-actin (red). An increase in actin stress fiber formation was observed (arrowheads). Pearson's correlation coefficient was lower in microvessels exposed to U46619 than in the control, showing an increase in stress fiber formation and endothelial cell activation. Data are represented as mean \pm SEM.

Subsequently, we investigated whether Rho/ROCK pathway inhibition suppresses the Ebola VLP-induced vascular phenotype. As RevitaCell™ Supplement [48] is known to specifically inhibit ROCK, we investigated whether this compound could reverse the Ebola VLP-induced phenotype. We compared vascular permeability of the microvessels-on-chips exposed to Ebola VLPs only with permeability of microvessels exposed to Ebola VLPs and RevitaCell™ Supplement simultaneously to inhibit the Rho/ROCK pathway. We observed a full suppression

of the VLP-induced permeability upon administration of the inhibitor together with the VLPs (see Figure 4). This result shows that Ebola VLPs critically modulate the Rho/ROCK pathway in hemorrhagic shock syndrome.

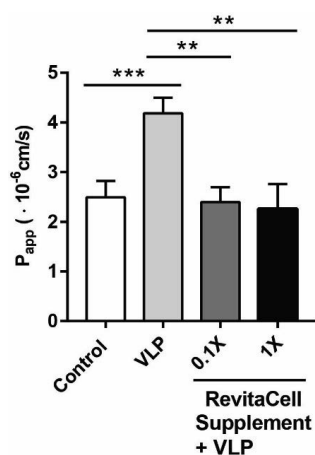


Figure 4 | ROCK-specific inhibitor treatment abolishes VLP-induced vascular permeability. Microvessels were either left untreated, incubated with 1 μ g/ml Ebola VLPs or exposed to both RevitaCell™ Supplement (0.1 and 1 \times) and 1 μ g/ml Ebola VLPs simultaneously, with an incubation time of 2 h. Data are represented as mean \pm SEM.

Existing evidence suggests that Ebola virus envelope glycoprotein GP_{1,2} is a key mediator of viral pathogenesis and a determinant of disease severity [49]. To test whether GP_{1,2} alone could simulate Ebola VLPs effect, we infused purified GP_{1,2} into our engineered vessels and measured the dose and time responses. Figure 5a shows that stimulation with 100 ng/ml GPs_{1,2} for 120 and 240 minutes led to a significant increase in vessel permeability. Moreover, we measured the dose-response curve using the chip platform (see Figure 5b). Importantly, the increased permeability of GPs_{1,2}-treated microvessels was associated with the formation of stress fibers (see Figure 5c). These results directly show the ability of Ebola GP_{1,2} to induce vasculopathy and indicate that our chip-based model can detect both VLP-induced and GPs_{1,2}-induced vascular permeability.

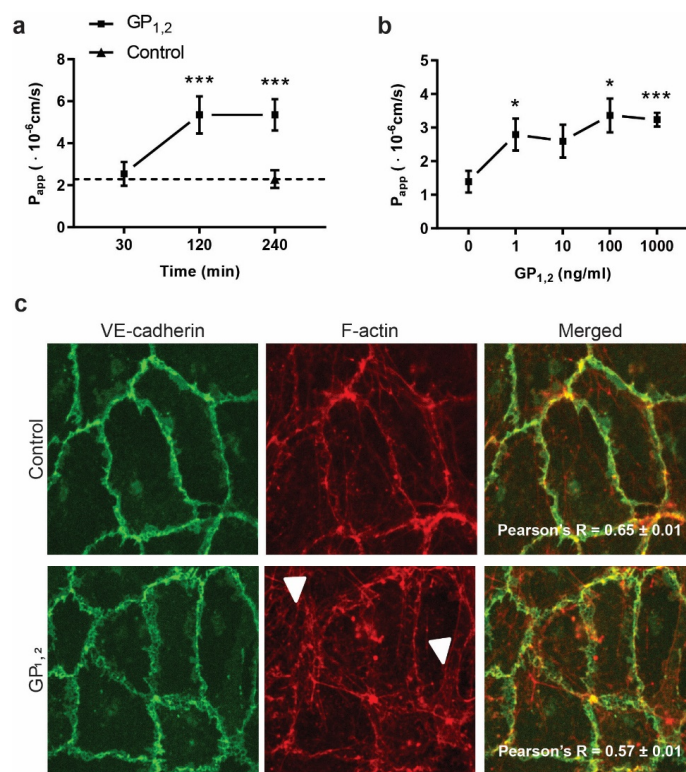


Figure 5 | Endothelial cell activation induced by the Ebola glycoprotein. (a) Permeability assay of microvessels exposed to 100 ng/ml GP_{1,2} at the indicated time points. **(b)** Dose response to GP_{1,2}. Microvessels were incubated with GP_{1,2} at the indicated concentrations for 2 h to measure permeability. **(c)** Immunostaining of endothelial cells for VE-cadherin (green) and F-actin (red) after treatment with 100 ng/ml GP_{1,2}. A moderate increase in actin stress fiber formation was observed (arrowheads). Pearson's correlation coefficient was lower in microvessels exposed to Ebola GPs_{1,2} than in the control, showing an increase in stress fiber formation and endothelial cell activation. Data are represented as mean ± SEM.

To demonstrate the applicability of our chip-based assay to pharmacological studies, we used this platform to study the effect of two potential drugs. According to our simple working model, Ebola virus stimulates the Rho/ROCK pathway, thereby inducing actin bundle formation and a tensile force that loosens the intercellular junctions formed by VE-cadherin. We targeted this process at two levels: (1) Rho/ROCK signaling (intracellular), via melatonin; and (2) VE-cadherin (extracellular) and the associated actin bundles, via FX06 (see Figure 6a) [50-52]. We found that both molecules effectively suppress vasculopathy and further showed

that FX06, which binds to VE-cadherin, thus reducing adhesion, also affects actin bundle formation directly (or indirectly via Fyn-mediated signaling[53]) (Supplementary figure 2). Treatment with FX06 counteracted vascular leakage in VLP-treated vessels, which is consistent with the results of previous animal experiments [54] and the clinical benefit noted in a case report [55] (see Figure 6b). However, vascular integrity was not directly measured in any previous study. Similarly, melatonin reduced vascular permeability in our viral hemorrhagic shock syndrome-on-a-chip model (see Figure 6c and Supplementary figure 3).

IV

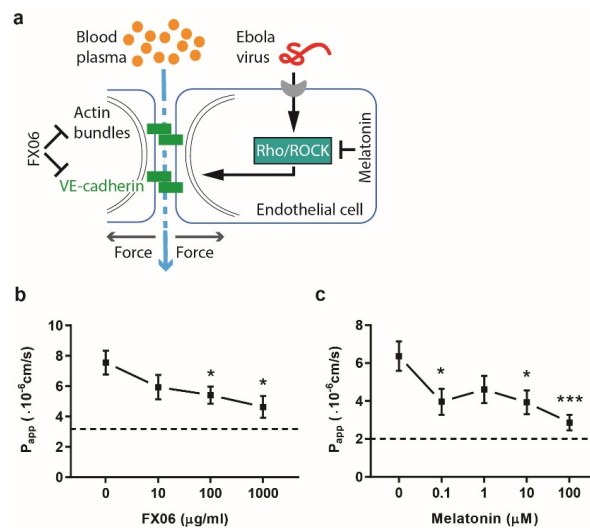


Figure 6 | FX06 and melatonin effectively ameliorate vascular integrity loss in the Ebola hemorrhagic shock syndrome-on-a-chip model. (a) FX06 and melatonin rebalance mechanical forces in endothelial cells to restore vascular integrity in Ebola viral hemorrhagic shock syndrome. **(b)** Microvessels exposed to 1 μg/ml Ebola VLPs were treated with FX06 at the indicated concentrations for 2 h. Subsequently, a permeability assay was carried out. **(c)** Dose response to melatonin in microvessels exposed to 1 μg/ml Ebola VLPs for 2 h, followed by a permeability assay. Data are represented as mean ± SEM.

A similar effect of melatonin was also observed when we stimulated the Rho/ROCK pathway with U46619 (Supplementary figure 4). This observed effect of melatonin is intriguing, as the effect of melatonin on the permeability of vessels has been previously reported in the context of cancer and septic shock, and the function of melatonin has been attributed to Rho/ROCK pathway modulation and subsequent changes to the cytoskeletal elements including actin

stress fibers [56, 57]. Melatonin has been proposed as a potential drug for Ebola hemorrhagic shock [58-60] but has never been tested experimentally. Given that melatonin is a natural molecule in the body and is safe when administered for at least a year [61] and given our observation that melatonin effectively suppresses the Ebola-induced loss of vascular integrity, our study suggests that melatonin is a promising drug for treating Ebola hemorrhagic shock syndrome. However, additional investigations are required to confirm the clinical therapeutic efficacy of melatonin.

Discussion

Vasculopathy is a critical and fatal consequence of Ebola virus infection [62-64]. Despite extended *in vivo* studies, the underlying molecular mechanisms are still elusive, no effective cure is available, and treatment strategies are primarily palliative. To discover and develop new drugs for Ebola in a cost-effective manner with high predictive power, microengineered disease models of human organs are needed. The hemorrhagic shock syndrome-on-a-chip described here is the first of its kind. Despite its simplicity, this model is robust, with significant fidelity in mimicking, at least partly, the structure and functions of human microvessels and Ebola disease-associated vasculopathy. This platform permitted high-throughput simulation of the vascular permeability induced by Ebola VLPs and Ebola GP_{1,2} as well as an increased surface expression of E-selectin which mediates disseminated intravascular coagulation, and death [58, 65].

Our study provides direct evidence for the usefulness of two candidate drugs, FX06 (which directly targets mechanical elements [66]) and melatonin (which directly targets biochemical signaling [67]), for treating Ebola patients. Although melatonin and FX06 are not antiviral molecules, they can be used to reduce the severity of hemorrhagic shock syndrome. Melatonin has not been used clinically to treat Ebola before, however, it was used routinely in other several clinical settings in humans [68]. Intravenous administration of 60 mg melatonin (equivalent to ~100 μ M in blood) is believed to be safe and with no complications [69, 70]. This indicates that the highest concentration of melatonin (100 μ M) used in our study is considered safe and can be translated to future clinical applications. Similarly, the highest

concentration of FX06 in our model is clinically relevant and has been used clinically to treat one Ebola patient [55].

Our *in vitro* model will help in understanding the underlying mechanisms of melatonin and FX06. This will allow the development of new compounds capable of delaying the effect of Ebola-induced vascular leakage. Additionally, the model can be of help in screening for therapeutic monoclonal antibodies[71, 72], in which the effect of antibodies targeting endothelial cells or VLPs to block the interaction between the two can be assayed. Finally, we stress the importance of the dose-response analysis enabled by the proposed platform. Recently, some Ebola drugs such as favipiravir have been abandoned because of problems with dosing [73]. The developed *in vitro* model can aid in the efforts to develop an effective pharmacokinetic model of drug treatments, and therefore, assist in designing the proper dose regimens. This chip-based platform will thus be a valuable tool complementing state-of-the-art technologies for combating current and future Ebola outbreaks.

Limitations of the Study

We note that this study has certain limitations that will be addressed in our future studies. The bidirectionality of the flow in the microvessels is one of the limitations in our system. Currently, we are developing a perfusion pump, which can provide a unidirectional flow for each microvessel channel by covering the whole plate, to solve this problem. We, however, anticipate that the observed vascular permeability remains largely unaffected by the flow directionality, as our preliminary analysis shows (Supplementary figure 5). The proposed approach is high-throughput, yet the analysis time can be further reduced using high content imaging systems.

Our approach allows us to disentangle the direct contribution of VLPs and viral proteins to vascular integrity loss from the contributions of host immunity (indirect mechanism) and the process of infection. The proposed *in vitro* model can be used in future to address the contributions of immune cells and to study endothelial cell infection. Shed glycoproteins from infected macrophages and dendritic cells can be readily assayed using the proposed approach. The engineered vessels can be further improved by including tissue specific ECM and other vascular cells (e.g., pericytes). The pharmacological analysis can be further extended to

Chapter IV

investigate the kinetics of recovery (after titration of the inhibitors) in the proposed in vitro model and to translate the results to nonhuman primate and human settings. Certain control and complementary experiments need to be performed (e.g., testing VP40-only VLPs) before exploring the translatability of the results. The platform can also be adapted to investigate therapeutic antibodies and other drug options. Finally, this study will contribute to understanding and detection of other highly dangerous viral infections that cause hemorrhagic shock including Lassa and Dengue.

Acknowledgments

We are grateful to Cesar Munoz-Fontela, Tom Ottenhoff, Marielle Haks, Beatriz Escudero-Perez, and Viktor Volchkov for discussions. We thank F4 Pharma GmbH for the generous gift of FX06. AM and YA acknowledge the support by the Leiden University Fund (W19340-5-EML) and Netherlands Organization for Scientific Research (NWA.1228.191.329). HT is financially supported by the CSC Scholarship offered by the China Scholarship Council. AJ, TH and AJvZ were financially supported by the RECONNECT CVON Groot consortium, which is funded by the Dutch Heart Foundation and TH, AJvZ and VvD were supported by a ZonMW MKMD grant (114022501). AM, TH and HT acknowledge the support by the Netherlands Organization for Scientific Research (NWO-TTW, grant number 16249).

Author contributions

AM conceived, designed and supervised the research. AJ, HT, AvR, and YA performed the experiments. WS helped with the immunostaining. AJ, HT and AM analysed the data. AM, HT, and AJ wrote the paper. All authors participated in the revisions of the manuscript and read and approved the final version.

Declaration of interests

Authors declare no conflict of interest related to the content of this manuscript. T.H. is shareholder in Mimetas BV, which was involved in the fabrication of the chips used in this study.

References

1. Jameson, J.L., et al., *Harrison's Principles of Internal Medicine (20th Edition)*. 2018: McGraw-Hill Education.
2. Nicholas G. Evans, T.C.S., Maimuna S. Majumder, *Ebola's Message: Public Health and Medicine in the Twenty-First Century*. 2016: The MIT Press.
3. Dyer, O., *Congo's Ebola epidemic is now its worst ever and still spreading*. BMJ, 2019. **364**.
4. de La Vega, M.A., et al., *Ebola viral load at diagnosis associates with patient outcome and outbreak evolution*. Journal of Clinical Investigation, 2015. **125**(12): p. 4421-4428.
5. Hartley, M.A., et al., *Predicting Ebola Severity: A Clinical Prioritization Score for Ebola Virus Disease*. Plos Neglected Tropical Diseases, 2017. **11**(2).
6. Willyard, C., *Advances in marmoset and mouse models buoy Ebola research*. Nature Medicine, 2014. **20**(12): p. 1356-1357.
7. Bennett, R.S., et al., *Nonhuman Primate Models of Ebola Virus Disease*. Marburg- and Ebolaviruses: From Ecosystems to Molecules, 2017. **411**: p. 171-193.
8. de la Vega, M.A., et al., *Modeling Ebola Virus Transmission Using Ferrets*. Msphere, 2018. **3**(5).
9. Warren, T.K., et al., *Therapeutic efficacy of the small molecule GS-5734 against Ebola virus in rhesus monkeys*. Nature, 2016. **531**(7594): p. 381-+.
10. Qiu, X.G., et al., *Characterization of Zaire ebolavirus glycoprotein-specific monoclonal antibodies*. Clinical Immunology, 2011. **141**(2): p. 218-227.
11. Qiu, X.G., et al., *Successful Treatment of Ebola Virus-Infected Cynomolgus Macaques with Monoclonal Antibodies*. Science Translational Medicine, 2012. **4**(138).
12. Olinger, G.G., et al., *Delayed treatment of Ebola virus infection with plant-derived monoclonal antibodies provides protection in rhesus macaques*. Proceedings of the National Academy of Sciences of the United States of America, 2012. **109**(44): p. 18030-18035.

Chapter IV

13. Wilson, J.A., et al., *Epitopes involved in antibody-mediated protection from Ebola virus*. Science, 2000. **287**(5458): p. 1664-1666.
14. Thi, E.P., et al., *Lipid nanoparticle siRNA treatment of Ebola-virus-Makona-infected nonhuman primates*. Nature, 2015. **521**(7552): p. 362-+.
15. Munoz, A., et al., *Synthesis of giant globular multivalent glycofullerenes as potent inhibitors in a model of Ebola virus infection*. Nature Chemistry, 2016. **8**(1): p. 50-57.
16. Mestas, J. and C.C.W. Hughes, *Of mice and not men: Differences between mouse and human immunology*. Journal of Immunology, 2004. **172**(5): p. 2731-2738.
17. Reardon, S., *'Organs-on-chips' go mainstream*. Nature, 2015. **523**(7560): p. 266-266.
18. Junaid, A., et al., *An end-user perspective on Organ-on-a-Chip: Assays and usability aspects*. Current Opinion in Biomedical Engineering, 2017. **1**: p. 15-22.
19. Tejavibulya, N. and S.K. Sia, *Personalized Disease Models on a Chip*. Cell Systems, 2016. **3**(5): p. 416-418.
20. Huh, D., et al., *A Human Disease Model of Drug Toxicity-Induced Pulmonary Edema in a Lung-on-a-Chip Microdevice*. Science Translational Medicine, 2012. **4**(159).
21. Park, J., et al., *Three-dimensional brain-on-a-chip with an interstitial level of flow and its application as an in vitro model of Alzheimer's disease*. Lab on a Chip, 2015. **15**(1): p. 141-150.
22. Wang, L., et al., *A disease model of diabetic nephropathy in a glomerulus-on-a-chip microdevice*. Lab on a Chip, 2017. **17**(10): p. 1749-1760.
23. Jeon, J.S., et al., *Generation of 3D functional microvascular networks with human mesenchymal stem cells in microfluidic systems*. Integrative Biology, 2014. **6**(5): p. 555-563.
24. Qiu, Y.Z., et al., *Microvasculature-on-a-chip for the long-term study of endothelial barrier dysfunction and microvascular obstruction in disease*. Nature Biomedical Engineering, 2018. **2**(6): p. 453-463.
25. van Duinen, V., et al., *96 perfusable blood vessels to study vascular permeability in vitro*. Scientific Reports, 2017. **7**.
26. Kim, S., et al., *Engineering of functional, perfusable 3D microvascular networks on a chip*. Lab on a Chip, 2013. **13**(8): p. 1489-1500.
27. Smith, Q. and S. Gerecht, *Going with the flow: microfluidic platforms in vascular tissue engineering*. Current Opinion in Chemical Engineering, 2014. **3**: p. 42-50.
28. Tien, J., *Microfluidic approaches for engineering vasculature*. Current Opinion in Chemical Engineering, 2014. **3**: p. 36-41.

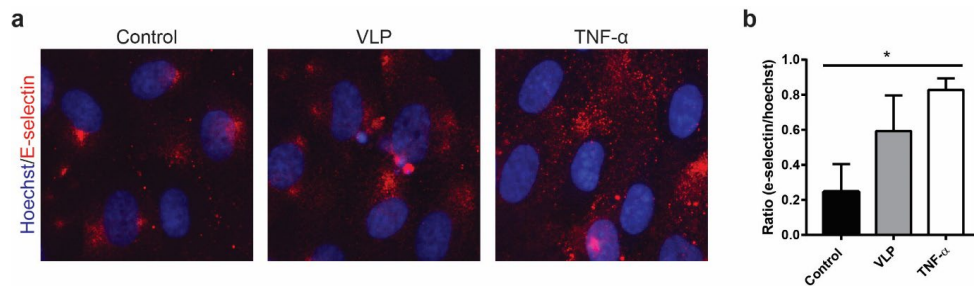
29. Sato, M., et al., *Microcirculation-on-a-Chip: A Microfluidic Platform for Assaying Blood- and Lymphatic-Vessel Permeability*. Plos One, 2015. **10**(9).
30. Bersini, S. and M. Moretti, *3D functional and perfusable microvascular networks for organotypic microfluidic models*. Journal of Materials Science-Materials in Medicine, 2015. **26**(5).
31. Chen, M.B., et al., *On-chip human microvasculature assay for visualization and quantification of tumor cell extravasation dynamics*. Nature Protocols, 2017. **12**(5): p. 865-880.
32. Hovell, C.M., Y.J. Sei, and Y. Kim, *Microengineered Vascular Systems for Drug Development*. Jala, 2015. **20**(3): p. 251-258.
33. Takei, T., S. Sakai, and M. Yoshida, *In vitro formation of vascular-like networks using hydrogels*. Journal of Bioscience and Bioengineering, 2016. **122**(5): p. 519-527.
34. Rayner, S.G. and Y. Zheng, *Engineered Microvessels for the Study of Human Disease*. Journal of Biomechanical Engineering-Transactions of the Asme, 2016. **138**(11).
35. Kim, S., et al., *Vasculature-On-A-Chip for In Vitro Disease Models*. Bioengineering (Basel), 2017. **4**(1).
36. Haase, K. and R.D. Kamm, *Advances in on-chip vascularization*. Regenerative Medicine, 2017. **12**(3): p. 285-302.
37. Akbari, E., G.B. Spychalski, and J.W. Song, *Microfluidic approaches to the study of angiogenesis and the microcirculation*. Microcirculation, 2017. **24**(5).
38. Shin, M., et al., *Endothelialized networks with a vascular geometry in microfabricated poly(dimethyl siloxane)*. Biomedical Microdevices, 2004. **6**(4): p. 269-278.
39. Song, J.W., et al., *Computer-controlled microcirculatory support system for endothelial cell culture and shearing*. Analytical Chemistry, 2005. **77**(13): p. 3993-3999.
40. Wahl-Jensen, V.M., et al., *Effects of Ebola virus glycoproteins on endothelial cell activation and barrier function*. Journal of Virology, 2005. **79**(16): p. 10442-10450.
41. Tasaka, S., et al., *Attenuation of endotoxin-induced acute lung injury by the Rho-associated kinase inhibitor, Y-27632*. American Journal of Respiratory Cell and Molecular Biology, 2005. **32**(6): p. 504-510.
42. Li, Y., et al., *Fasudil attenuates lipopolysaccharide-induced acute lung injury in mice through the Rho/Rho kinase pathway*. Medical Science Monitor, 2010. **16**(4): p. Br112-Br118.
43. Suzuki, K., et al., *Fasudil, a Rho-kinase inhibitor, attenuates lipopolysaccharide-induced vascular hyperpermeability and colonic muscle relaxation in guinea pigs*. Journal of Surgical Research, 2012. **178**(1): p. 352-357.

Chapter IV

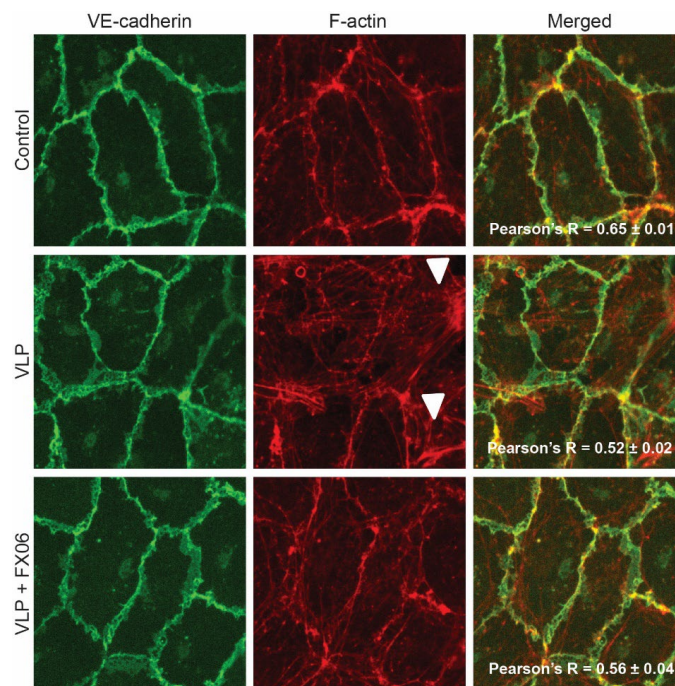
44. Mahanty, S. and M. Bray, *Pathogenesis of filoviral haemorrhagic fevers*. Lancet Infectious Diseases, 2004. **4**(8): p. 487-498.
45. Bray, M. and S. Mahanty, *Ebola hemorrhagic fever and septic shock*. Journal of Infectious Diseases, 2003. **188**(11): p. 1613-1617.
46. Eisa-Beygi, S. and X.Y. Wen, *Could pharmacological curtailment of the RhoA/Rho-kinase pathway reverse the endothelial barrier dysfunction associated with Ebola virus infection?* Antiviral Research, 2015. **114**: p. 53-56.
47. Kobayashi, K., et al., *Thromboxane A(2) exacerbates acute lung injury via promoting edema formation*. Scientific Reports, 2016. **6**.
48. Hansen, M., et al., *Efficient production of erythroid, megakaryocytic and myeloid cells, using single cell-derived iPSC colony differentiation*. Stem Cell Research, 2018. **29**: p. 232-244.
49. Mohan, G.S., et al., *Less Is More: Ebola Virus Surface Glycoprotein Expression Levels Regulate Virus Production and Infectivity*. Journal of Virology, 2015. **89**(2): p. 1205-1217.
50. Bergt, S., et al., *The Fibrin-Derived Peptide B beta(15-42) (FX06) Ameliorates Vascular Leakage and Improves Survival and Neurocognitive Recovery: Implications From Two Animal Models of Cardiopulmonary Resuscitation*. Critical Care Medicine, 2016. **44**(10): p. E988-E995.
51. Uyeki, T.M., et al., *Clinical Management of Ebola Virus Disease in the United States and Europe*. New England Journal of Medicine, 2016. **374**(7): p. 636-646.
52. Petzelbauer, P., et al., *The fibrin-derived peptide Bbeta15-42 protects the myocardium against ischemia-reperfusion injury*. Nat Med, 2005. **11**(3): p. 298-304.
53. Groger, M., et al., *Peptide Bbeta(15-42) preserves endothelial barrier function in shock*. PLoS One, 2009. **4**(4): p. e5391.
54. Roesner, J.P., et al., *Bbeta15-42 (FX06) reduces pulmonary, myocardial, liver, and small intestine damage in a pig model of hemorrhagic shock and reperfusion*. Crit Care Med, 2009. **37**(2): p. 598-605.
55. Wolf, T., et al., *Severe Ebola virus disease with vascular leakage and multiorgan failure: treatment of a patient in intensive care*. Lancet, 2015. **385**(9976): p. 1428-1435.
56. Borin, T.F., et al., *Melatonin decreases breast cancer metastasis by modulating Rho-associated kinase protein-1 expression*. Journal of Pineal Research, 2016. **60**(1): p. 3-15.
57. Tang, S.T., et al., *Melatonin Attenuates Aortic Endothelial Permeability and Arteriosclerosis in Streptozotocin-Induced Diabetic Rats: Possible Role of MLCK- and MLCP-Dependent MLC Phosphorylation*. Journal of Cardiovascular Pharmacology and Therapeutics, 2016. **21**(1): p. 82-92.
58. Tan, D.X., et al., *Ebola virus disease: potential use of melatonin as a treatment*. Journal of Pineal Research, 2014. **57**(4): p. 381-384.

59. Masters, A., et al., *Melatonin, the Hormone of Darkness: From Sleep Promotion to Ebola Treatment*. *Brain Disord Ther*, 2014. **4**(1).
60. Wiwanitkit, V., *Ebola Virus Infection: What Should Be Known?* *North American Journal of Medical Sciences*, 2014. **6**(11): p. 549-552.
61. Chahbouni, M., et al., *Melatonin treatment normalizes plasma pro-inflammatory cytokines and nitrosative/oxidative stress in patients suffering from Duchenne muscular dystrophy*. *Journal of Pineal Research*, 2010. **48**(3): p. 282-289.
62. Escudero-Perez, B., et al., *Shed GP of Ebola Virus Triggers Immune Activation and Increased Vascular Permeability*. *Plos Pathogens*, 2014. **10**(11).
63. Lyon, G.M., et al., *Clinical Care of Two Patients with Ebola Virus Disease in the United States*. *New England Journal of Medicine*, 2014. **371**(25): p. 2402-2409.
64. Bah, E.I., et al., *Clinical Presentation of Patients with Ebola Virus Disease in Conakry, Guinea*. *New England Journal of Medicine*, 2015. **372**(1): p. 40-47.
65. Boral, B.M., D.J. Williams, and L.I. Boral, *Disseminated Intravascular Coagulation*. *American Journal of Clinical Pathology*, 2016. **146**(6): p. 670-680.
66. Urbschat, A., et al., *The Small Fibrinopeptide B beta(15-42) as Renoprotective Agent Preserving the Endothelial and Vascular Integrity in Early Ischemia Reperfusion Injury in the Mouse Kidney*. *Plos One*, 2014. **9**(1).
67. Yang, X.P., et al., *Ameliorative effect of melatonin against increased intestinal permeability in diabetic rats: possible involvement of MLCK-dependent MLC phosphorylation*. *Molecular and Cellular Biochemistry*, 2016. **416**(1-2): p. 23-32.
68. Sanchez-Barcelo, E.J., et al., *Clinical Uses of Melatonin: Evaluation of Human Trials*. *Current Medicinal Chemistry*, 2010. **17**(19): p. 2070-2095.
69. Kucukakin, B., et al., *Utility of melatonin to treat surgical stress after major vascular surgery - a safety study*. *Journal of Pineal Research*, 2008. **44**(4): p. 426-431.
70. Gitto, E., et al., *Melatonin reduces oxidative stress in surgical neonates*. *Journal of Pediatric Surgery*, 2004. **39**(2): p. 184-188.
71. Saphire, E.O., et al., *Antibody-mediated protection against Ebola virus*. *Nat Immunol*, 2018. **19**(11): p. 1169-1178.
72. Saphire, E.O., et al., *Systematic Analysis of Monoclonal Antibodies against Ebola Virus GP Defines Features that Contribute to Protection*. *Cell*, 2018. **174**(4): p. 938-952 e13.
73. Dunning, J. and W. Fischer, *Ebola: the battle plan must include specific treatments*. *Lancet*, 2015. **385**(9976): p. 1373-1375.

Supplementary figures



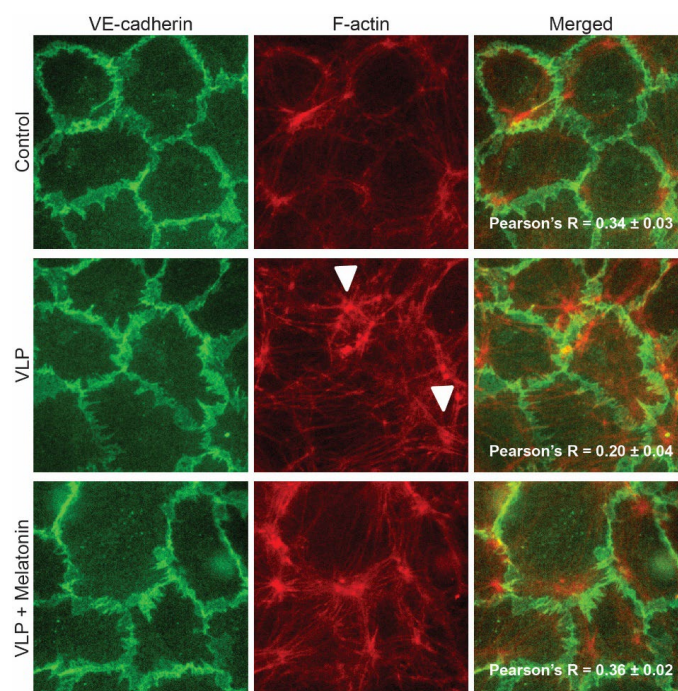
Supplementary figure 1 | Ebola VLPs elevated E-selectin in microvessels. (a) Immunofluorescence for E-selectin expression (red) patterns in an untreated microvessel, 1 $\mu\text{g/ml}$ Ebola VLP-infected microvessels or 10 ng/ml TNF- α -treated microvessels for 18 h. **(b)** Quantitative determination of E-selectin expression in the absence (control) and presence of 1 $\mu\text{g/ml}$ Ebola VLPs or 100 ng/ml TNF- α for 2 h. Data are represented as mean \pm SEM. A marginally significant difference ($*P < 0.1$) between the three conditions was found.



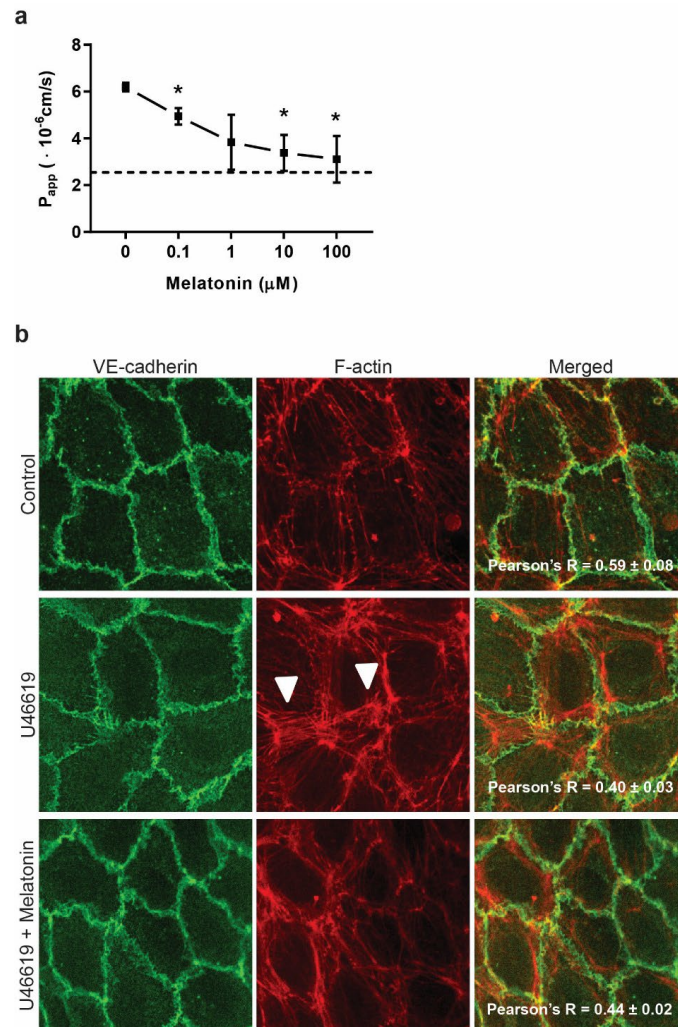
Supplementary figure 2 | Endothelial cells stained for VE-cadherin (green) and F-actin (red) after exposure to 1 $\mu\text{g/ml}$ VLPs with or without 100 ng/ml FX06 for 2 h. A moderate increase in actin stress fiber formation was observed in microvessels exposed to Ebola VLPs (arrowheads). This increase was abrogated by FX06 treatment.

Chapter IV

Pearson's correlation coefficient was used to quantify the co-localization of VE-cadherin and junction-associated actin filaments. Data are represented as mean \pm SEM.

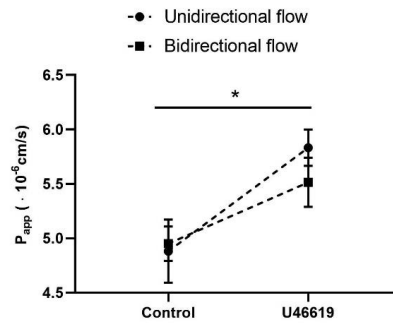


Supplementary figure 3 | Immunostaining of endothelial cells for VE-cadherin (green) and F-actin (red) after exposure to 1 μ g/ml of VLPs with or without 10 μ M melatonin for 2 h. A moderate increase in actin stress fiber formation was observed in microvessels incubated with Ebola VLPs (arrowheads). Treatment with melatonin reduced actin stress fiber formation. Pearson's correlation coefficient was used to quantify the co-localization of VE-cadherin and junction-associated actin filaments. Data are represented as mean \pm SEM.



Supplementary figure 4 | Melatonin reduced vascular permeability in U46619-treated microvessels. (a) Microvessels exposed to 10 μM U46619 were treated with the indicated concentrations of melatonin for 1 h. Subsequently, a permeability assay was carried out. **(b)** Endothelial cells stained for VE-cadherin (green) and F-actin (red) after exposure to 10 μM U46619 with or without 10 μM melatonin for 1 h. A moderate increase in actin stress fiber formation was observed in microvessels incubated with U46619 (arrowheads). This increase was abrogated by melatonin treatment. Pearson's correlation coefficient was used to quantify the co-localization of VE-cadherin and junction-associated actin filaments. Data are represented as mean ± SEM.

Chapter IV



Supplementary figure 5 | U46619 induces leakage irrespective of the directionality of the flow within the microvessels. The microvessels were incubated with 10 μM U46619 and perfused under unidirectional and bidirectional flow for 8 minutes, following a permeability assay. We did not observe a statistically significant difference between the two flow conditions. The data is generated using 42 chips, including 21 control chips and 21 U46619 chips. Data are represented as mean \pm SEM.

IV

Chapter V

Metabolic response of blood vessels to TNF α

Abidemi Junaid, Johannes Schoeman, Wei Yang, Wendy Stam, Alireza Mashaghi,
Anton Jan van Zonneveld, Thomas Hankemeier

eLIFE (2020) **9**, e54754

Chapter V

Abstract

TNF α signaling in the vascular endothelium elicits multiple inflammatory responses that drive vascular destabilization and leakage. Bioactive lipids are main drivers of these processes. *In vitro* mechanistic studies of bioactive lipids have been largely based on two-dimensional endothelial cell cultures that, due to lack of laminar flow and the growth of the cells on non-compliant stiff substrates, often display a pro-inflammatory phenotype. This complicates the assessment of inflammatory processes. Three-dimensional microvessels-on-a-chip models provide a unique opportunity to generate endothelial microvessels in a more physiological environment. Using an optimized targeted liquid chromatography–tandem mass spectrometry measurements of a panel of pro- and anti-inflammatory bioactive lipids, we measure the profile changes upon administration of TNF α . We demonstrate that bioactive lipid profiles can be readily detected from three-dimensional microvessels-on-a-chip and display a more dynamic, less inflammatory response to TNF α , that resembles more the human situation, compared to classical two-dimensional endothelial cell cultures.

V

Introduction

Tumor necrosis factor- α (TNF α) is a central mediator of the inflammatory response[1]. TNF α can be generated by monocytes or macrophages and activates endothelial cells at sites of tissue injury or infection through TNF receptor-1 (TNFR1)[2-4]. Following activation, the endothelium elicits a multitude of local responses such as vascular leakage, leukocyte adhesion and coagulation that together are essential to the physiological homeostatic responses to anti-microbial immunity.

However, chronic exposure to adverse metabolic and hemostatic risk factors[5], obesity[6], or disease states such as kidney disease[7] or rheumatoid arthritis[8] are all associated with a systemic inflammatory condition and elevated circulating levels of TNF α . As a consequence, TNF α signaling induces the generation of high levels of free radicals in the vascular endothelium that, when excessive, can deplete the cellular anti-oxidant defense systems and lead to a state of oxidative stress and vascular dysfunction [9].

Mechanistically, TNF α signaling in endothelial cells involves the activation of NF κ B and results in the increased synthesis of reactive oxygen species (ROS) from a number of sources such as mitochondria, NADPH oxidase, uncoupled eNOS, xanthine oxidase, and peroxidases[10, 11]. On its turn, elevated ROS can lead to the generation of bioactive lipids directly or indirectly, such as prostaglandins, isoprostanes, lysophosphatidic acid classes, sphingolipids and platelet activating factor (PAF). Under physiologic conditions, in concert with the transcriptional regulation of a plethora of inflammatory genes[12], these bioactive lipids are critically involved in the first response of endothelial cells to environmental changes, controlling vascular permeability and platelet- and leukocyte adhesion. Also, in fore mentioned patients, isoprostanoids such as 8-epiPGF 2α are generated by peroxidation during conditions of oxidative stress[13] and serve as gold standard oxidative stress plasma markers[14] associating with an increased risk for cardiovascular disease and its underlying causes[15, 16].

The central role of TNF α in many disease states has identified this cytokine as an important therapeutic target to counteract vascular inflammation[1, 17] and several TNF α blockers have been approved by the FDA and have been effective for the suppression of immune-system diseases, such as Crohn's disease, ulcerative colitis, rheumatoid arthritis, ankylosing spondylitis, psoriatic arthritis and plaque psoriasis[18].

Following the success of the TNF α antagonists, a deeper understanding of the impact of oxidative stress on the homeostasis of the human vascular endothelium may yield more specific targets for inflammatory diseases affecting the vasculature. To that end, many *in vitro* mechanistic studies have relied on static, two-dimensional (2D) cultures of primary endothelial cells such as those derived from human umbilical veins (HUVECs)[19]. However, in recent years it has become increasingly apparent that these cultures reflect a ‘stressed’ endothelial phenotype due to the lack of their native environmental cues. *In vitro*, endothelial cells are usually cultured on surfaces such as plastics and glass that are much stiffer than natural substrates such as the extracellular matrix. Recent studies demonstrated that primary endothelial cells on a hard substrate adopt a pro-inflammatory phenotype[20, 21]. Vascular stiffness is strongly associated with vascular disorders such as arterial hypertension, kidney disease and atherosclerosis[22]. Likewise, native microvessels need laminar shear to maintain a quiescent phenotype and the lack of laminar shear stress in static cultures converts endothelial cells to a pro-inflammatory “diseased” phenotype[23].

V

Novel microfluidics-based perfused three-dimensional (3D) microvessels-on-a-chip models provide a unique opportunity to generate endothelial microvessels in a more physiological environment. We employed a gelatin coated 3D microvessels-on-a-chip model in which endothelial cells are organized in a tube-like architecture, with densities of cells and area to volume ratios that are closer to a physiological condition than those in typical 2D culture.

To assess whether these 3D microvessels display a more anti-inflammatory phenotype, we used an optimized targeted liquid chromatography–tandem mass spectrometry measurements of a panel of pro- and anti-inflammatory bioactive lipids and generated expression profiles both in TNF α treated microvessels under flow as well as in 2D endothelial cell cultures under static condition. We demonstrate bioactive lipid profiles can be readily detected from single microvessels and display a more dynamic, less inflammatory response to TNF α , that resembles more the human situation, compared to classical 2D endothelial cell cultures.

Methods

Key resources table

Reagent type (species) or resource	Designation	Source or reference	Identifiers	Additional information
biological sample (include species here)	primary human umbilical vein endothelial cells	Leiden University Medical Center (LUMC)		freshly isolated from umbilical cord of male newborns
chemical compound, drug	phorbol 12-myristate 13-acetate	Sigma-Aldrich	Cat#:P8139	
peptide, recombinant protein	tumor necrosis factor- α	Sigma-Aldrich	Cat#:H8916	
biological sample (include species here)	rat tail collagen type 1	Trevigen	Cat#:3440-005-01	
antibody	mouse anti-human CD144	BD Biosciences	Cat#:555661; RRID:AB_396015	IF(1:150)
antibody	sheep anti-human CD31	R&D Systems	Cat#:AF806; RRID:AB_355617	IF(1:150)
antibody	rabbit anti-human vWF	Agilent Dako	Cat#:A0082; RRID:AB_2315602	IF(1:1000)
antibody	alexa fluor 488-conjugated goat anti-mouse	ThermoFisher	Cat#:R37120; RRID:AB_2556548	IF(1:250)
antibody	alexa fluor 488-conjugated donkey anti-sheep	ThermoFisher	Cat#:A11015; RRID:AB_141362	IF(1:250)



Reagent type (species) or resource	Designation	Source or reference	Identifiers	Additional information
antibody	alexa fluor 647-conjugated goat anti-rabbit	ThermoFisher	Cat#:A27040; RRID:AB_2536101	IF(1:250)
other	rhodamine phalloidin	Sigma-Aldrich	Cat#:P1951; RRID:AB_2315148	IF(1:200)
other	hoechst	Invitrogen	Cat#:H3569; RRID:AB_2651133	IF(1:2000)
software, algorithm	LabSolutions	Shimadzu	RRID:SCR_018241	
software, algorithm	SPSS	SPSS	RRID:SCR_002865	
software, algorithm	GraphPad Prism	GraphPad	RRID:SCR_002798	

Cell culture

Human umbilical vein endothelial cells (HUVECs) were isolated from umbilical cord of newborns, collected with informed consent, by an adaption of the method developed by Jaffe et al. in 1973 [19]. Although denoted as veins, umbilical veins carry oxygenated blood and thus the phenotype of their endothelium is similar to arterial endothelial cells.

The umbilical cord was severed from the placenta soon after birth and placed in a sterile container filled with phosphate-buffered saline (PBS; Fresenius Kabi, The Netherlands) and held at 4°C until processing. The cord was inspected and at both ends a piece of 1 cm was cut off to remove damaged tissue from clamping. Subsequently, the umbilical vein was cannulated and perfused with PBS to wash out the blood and allowed to drain. When clear fluid flow was observed, the vein was filled with trypsin/EDTA solution (CC-5012, Lonza, USA), placed in the container filled with PBS and incubated at 37°C for 20 min. After incubation, the trypsin-EDTA solution containing the endothelial cells was flushed from the cord with air and afterwards PBS. The effluent was collected in a sterile 50 ml tube containing 20 ml Endothelial Cell Growth Medium 2 (EGM2; C-39216, PromoCell, Germany) supplemented with antibiotics and the cell suspension was centrifuged at 1200 rpm for 7 min. The cell pellet was

Chapter V

resuspended in 10 ml EGM2 and cultured on 1% gelatin-coated T75 flasks. Cells were maintained in a 37°C incubator with 5% CO₂ and the medium was refreshed every other day. After 80% confluency, cells were split at 1:3 ratio and cultured in new 1% gelatin-coated T75 flasks. The isolated cells were positive for the endothelial cell markers, including platelet endothelial cell adhesion molecule (PECAM-1) and von Willebrand factor (vWF) (Figure 1). All experiments using HUVECs were repeated 6 times using cells from 3 different male donors at passage 3.

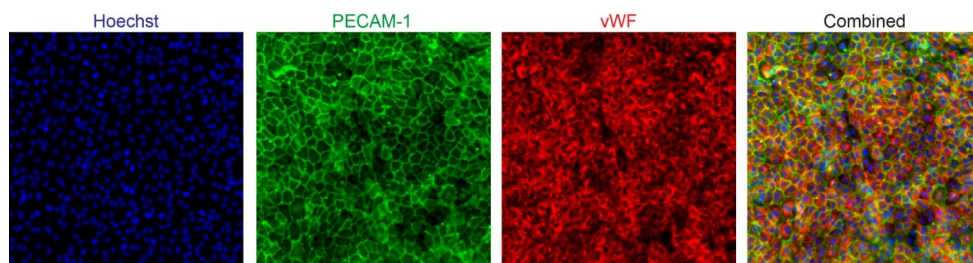


Figure 1 | Expression of platelet endothelial cell adhesion molecule (PECAM-1) and von Willebrand factor (vWF) in isolated human umbilical vein endothelial cells (HUVECs).

For 2D experiments, we cultured $50 \cdot 10^3$ cells/ml in 24-well plates overnight at 37 °C in humidified air containing 5% CO₂. The following day, the cells were incubated with 15 and 50 ng/ml TNF α (H8916, Sigma-Aldrich, The Netherlands) and 20 ng/ml phorbol 12-myristate 13-acetate (PMA; P8139, Sigma-Aldrich, The Netherlands) for 18 hours. The medium was collected and stored in -80°C.

We used the OrganoPlate (9603-400-B, MIMETAS, The Netherlands) for all microfluidic cell culture experiments. The microvascular and extracellular matrix (ECM) channels were separated by phaseguides [53]. Before seeding the cells, 4 mg/ml rat tail collagen type 1 (3440-005-01, Trevigen, USA) neutralized with 10% 37 g/L Na₂CO₃ (S5761, Sigma-Aldrich, The Netherlands) and 10% 1 M HEPES buffer (15630-056, Gibco, The Netherlands) was added in the ECM channels. Subsequently, the collagen was let to polymerize by incubating the device for 10 min in the incubator at 37°C and 5% CO₂. The observation windows were filled with 50 μ l Hank's Balanced Salt Solution with calcium and magnesium buffers (HBSS+; 24020117, Life

Technologies, The Netherlands) for optical clarity and to prevent gel dehydration. Using a repeater pipette, 2 μl of 1% gelatin was added into the inlet of each microvascular channel and the device was put in the incubator at 37°C for 30 min. We trypsinized cells at 80-90% confluency and seeded $15 \cdot 10^6$ cells/ml in the outlet of the microvascular channels of the OrganoPlate. Afterwards, the cells were incubated at 37°C and 5% CO₂ for one hour to allow microvascular formation. After incubation, 50 μl of culture medium was added to the inlets and outlets of the microvascular channels. The device was placed on a rocker platform with a 7° angle of motion and an eight-minute timed operation to allow continuous flow of minor volumes of medium in the microvessels. The microvascular channels typically contain volumes of < 1 μl . After 24 hours, the medium was refreshed, and the HUVECs were cultured for an additional 3-4 days. The microvessels were treated with TNF α (0.4, 15 and 50 ng/ml) and PMA (20 ng/ml) for 18 hours. Subsequently, medium of four microvessels were pooled to form one sample to allow analyses of metabolites at low concentrations due to low cell numbers. This still allowed us to create three biological replicates with 4 – 6 technical replicates data per experimental condition for metabolomics analyses. The samples were stored in -80°C.

V

Immunofluorescence staining

For immunofluorescence staining, HUVECs were fixed using 4% paraformaldehyde (PFA) in HBSS+ for 10 min at room temperature. The fixative was aspirated, and the cells were rinsed once with HBSS+. Next, the cells were permeabilized for 2 min with 0.2% Triton X-100 in HBSS+ and washed once with HBSS+. The cells were blocked in 5% BSA in HBSS+ for 30 min and incubated with the primary antibody solution overnight at 4°C. Mouse anti-human CD144 (1:150; 555661, BD Biosciences, USA), sheep anti-human CD31 (1:150; AF806, R&D Systems, The Netherlands) and rabbit anti-human vWF (1:1000; A0082, Agilent Dako, USA) were used as the primary antibodies. The cells were washed with HBSS+, followed by an one-hour incubation with Hoechst (1:2000; H3569, Invitrogen, USA), rhodamine phalloidin (1:200; P1951, Sigma-Aldrich, The Netherlands) and the secondary antibody solution, containing Alexa Fluor 488-conjugated goat anti-mouse (1:250; R37120, ThermoFisher, USA), Alexa Fluor 488-conjugated donkey anti-sheep (1:250; A11015, ThermoFisher, USA) and Alexa Fluor 647-conjugated goat anti-rabbit (1:250; A27040, ThermoFisher, USA) antibodies. The cells were

washed three times with HBSS+. High-quality Z-stack images of the stained cells were acquired using a high-content confocal microscope (Molecular Devices, ImageXpress Micro Confocal).

Metabolic profiling

All samples were measured using an oxidative and nitrosative stress profiling platform which has been developed and validated in our lab [28]. This platform covers various isoprostane classes, signaling lipids from the sphingosine and sphinganine classes and their phosphorylated forms, as well as three classes of lysophosphatidic acids: lysophosphatidic acids, alkyl-lysophosphatidic acids and cyclic-lysophosphatidic acids (all ranging from C14 to C22 chain length species). For metabolite extraction, sample preparation procedure was according to the in-house experimental protocol which has been standardized and published; extra samples were pooled for internal quality control (QC) [28]. Briefly, cell media (150 μ l) were thawed on ice and added with 5 μ l antioxidant solution and 10 μ l internal standards (ISTDs). Acidified with citric acid/phosphate buffer (pH 4.5), all samples were then dealt with liquid-liquid extraction (LLE) with 1 mL of butanol and ethyl acetate (1:1 v/v). Samples were vortexed and centrifuged and then the organic phase was collected and dried. After reconstitution with ice-cold 70% MeOH injection solution, each sample was again vortexed and centrifuged and the supernatant was transferred to the insert in a glass vial. Ultra-performance liquid chromatography tandem mass spectrometry (UPLC-MS/MS) based analysis was then applied for low-pH measurement (Shimadzu LCMS-8060, Japan) and high-pH measurement (Shimadzu LCMS-8050, Japan) respectively.

Calibration curve preparation

Standard stock solutions were prepared in MeOH containing butylated hydroxytoluene (0.4 mg/ml). A calibration stock was made with concentrations found in Supplementary Table 1 for the prostaglandins, isoprostanes, LPAs, sphingolipids and PAF available base standards and was labeled "C9". This solution was diluted to levels C8 to C1 and from these mixes, 20 μ l was added to 150 μ l sample to construct the calibration curves.

Data pre-processing

LabSolutions (Shimadzu, Version 5.91) was applied to accomplish all the peak determination and integration. For each metabolite, the response ratio was obtained by calculating the ratio of peak area of the target compound to the peak area of the assigned internal standard. After QC evaluation, metabolites of which QC samples had an RSD less than 30% were used for further statistical analysis. Finally, the absolute concentration of the targets was determined using the calibration curves.

Statistical analysis

Heatmaps and bar plots were created with GraphPad Prism 7 (GraphPad Software). The fold change was calculated by normalizing the conditions to the control group. Subsequently, the data was log₂ transformed and used for the heatmaps. The absolute concentration of those compounds were visualized in the bar plots. We used IBM SPSS Statistics 23 (IBM) for statistical analyses. Bar plots were plotted as mean ± s.e.m. of three biological replicates per condition; n = 4 – 6 technical replicates. Significance levels were set at *P<0.1, **P<0.05, ***P < 0.01, ****P < 0.001 using the unpaired Student's t-test.

Results and discussion

Bioactive lipids generated by 3D microvessels-on-a-chip can be measured by UPLC-MS/MS

In this paper, we present a novel set-up to measure the metabolic response of 3D endothelial microvessels to TNF α , including pro- and anti-inflammatory markers. We cultured 96 perfused microvessels against extracellular matrix (ECM) using the microvessels-on-a-chip platform technology recently developed by using the OrganoPlate platform of MIMETAS[24, 25]. The microchannels in the OrganoPlate were coated with gelatin, preventing endothelial cells from growing on glass and enabling them to form stable microvessels. The shear stress in the microvessels, calculated based on a previous work, ranges from 1-5 dyne/cm² [26]. *In vivo*, the shear stress ranges from 95.5 dyne/cm² at the smallest capillaries to 2.8 dyne/cm² at the

postcapillary venules[27]. Conditioned medium perfused through TNF α treated and control (untreated) microvessels was sampled, pooled and measured with a UPLC-MS/MS metabolomics method developed recently by us to study inflammation and oxidative stress (Figure 2)[28].

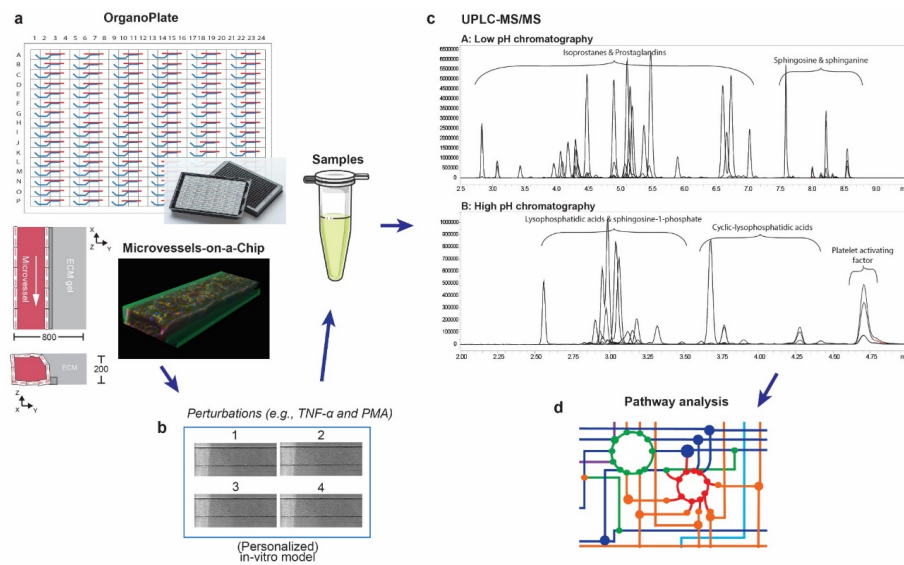


Figure 2 | Metabolomics workflow. (a) Schematic diagram of the OrganoPlate 2-lane design and 3D reconstruction of the microvessels-on-a-chip formed by cultured HUVECs (blue: Hoechst, red: F-actin and green: VE-cadherin). All dimensions are in μm . (b) Collection of culture media after perfusion. The medium of four microvessels were pooled to form one sample. (c) Identification and quantification of prostaglandins, isoprostanes, lysophosphatidic acid (LPA) classes, sphingolipids and platelet activating factor (PAF) in microvessels-on-a-chip by UPLC-MS/MS using two different solvent gradients. (d) Pathway analysis.

As a metabolic read-out for TNF α signaling, we measured prostaglandins, isoprostanes, LPAs, lysosphingolipids and PAF and first assessed the concentrations of these metabolites in the basic EGM2 medium and compared their concentrations after 18 hours incubation to condition the medium in the microvessels-on-a-chip cultures. As shown in Table 1, the peaks detected demonstrated that, while members of the prostaglandins and isoprostanes clearly increased after conditioning of the medium, most of the LPA metabolites were readily

Chapter V

detectable in the medium and actually displayed a significant decreased concentration. When the EGM2 medium was incubated for 18 hours without exposure to the microvessels no significant changes in the concentrations of these metabolites was observed. Therefore, we conclude that during the conditioning of the medium, prostaglandins and isoprostanoids are excreted from the endothelial cells and that the LPA metabolites are consumed or actively degraded by the cells.

Table 1 | The peak area ratio of metabolites in the culture medium (EGM2) normalized with the peak area ratio of metabolites found in the culture medium after perfusion in the microvessels-on-a-chip for 18 hours (EGM2 HUVECs). The peak area ratio is the peak area of the metabolites divided by the appropriate peak area of the internal standards. Fold changes below the 1 (blue) and above the 1 (red) indicates that low and high concentrations of fatty acids were present in medium before exposure to the microvessels. The data represents one biological replicate; n = 3 technical replicates.

Bioactive lipid*	EGM2/EGM2 HUVECs	Bioactive lipid*	EGM2/EGM2 HUVECs
PGF2 α	0.1	LPA C22:5	18.2
PGF3 α	2.1	LPA C16:0	21.3
8-iso-13, 14-dihydro-PGF2 α	0.0	LPA C18:1	48.4
8-iso-PGF2 α	0.2	LPA C22:4	5.9
5-iPF2 α	0.4	cLPA C20:4	78.6
8, 12-iPF2 α IV	0.5	LPA C18:0	0.0
LPA C14:0	6.2	cLPA C18:2	0.0
LPA C16:1	25.4	cLPA C16:0	14.8
LPA C22:6	17.7	cLPA C18:1	25.8
LPA C18:2	77.2	cLPA C18:0	11.1
LPA C20:4	31.0	S-1-P C18:1	0.9

*The rest of the metabolites shown in Figure 4 are not displayed, because they were not detected in the EGM2.

When we assessed the biolipid composition of the conditioned medium of TNF α stimulated microvessels, 33 measured metabolites passed the quality control (QC) thresholds. Figure 3 shows examples of the chromatograms of prostaglandin E2 and different isoprostanoid isomers that were secreted by the microvessels after exposure to TNF α for 18 hours compared to the control samples showing a marked increase in abundance of a number of these metabolites. The control samples are microvessels without exposure to TNF α .

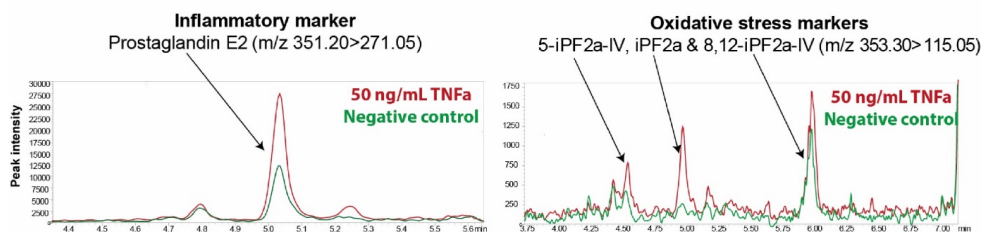


Figure 3 | Inflammatory and oxidative stress markers in microvessels-on-a-chip. Reconstructed LC-MS/MS ion chromatograms of PGE2, 5-iPF2 α IV, iPF2 α and 8, 12-iPF2 α IV in microvessels treated with 50 ng/ml TNF α for 18 hours.

Bar plots of the absolute concentrations of prostaglandins are presented in Figure 4a, showing a significant difference between untreated and TNF α treated microvessels. While at physiological concentration of TNF α (0.4 ng/ml) there was an increase in the excretion of PGF1 α , PGF2 α , PGF3 α , PGE2, PGD2 and 13, 14-dihydro-PGF2 α , however, no significant difference between the untreated and TNF α treated microvessels was evident, except for PGF1 α . At 15 ng/ml a stronger differential response was observed for selected isoprostanes, several LPAs, sphingolipids and PAF (Figure 4b-e). The relative concentrations of the bioactive lipids found in the microvessels-on-a-chip are strikingly similar with those found in normal human blood vessels (Table 2).

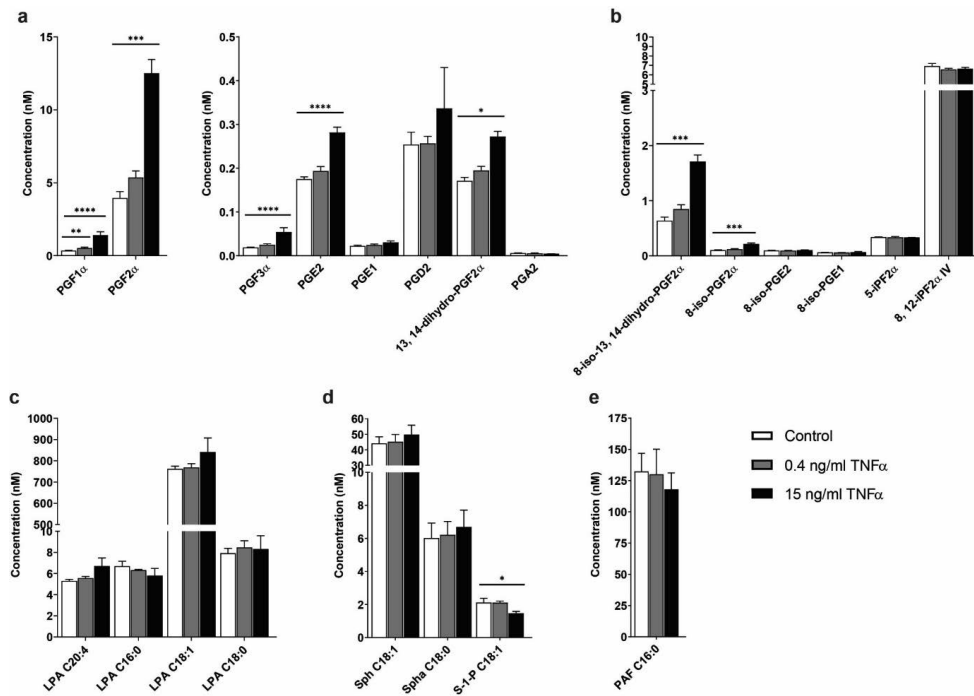


Figure 4 | TNF α -induced concentration profile changes of the signaling lipids in the microvessels-on-a-chip. Concentrations of (a) prostaglandins, (b) isoprostanes, (c) lysophosphatidic acid (LPA) classes, (d) sphingolipids and (e) platelet activating factor (PAF) with available standards detected in the microvessels without TNF α exposure (control) and after exposure to 0.4 and 15 ng/ml TNF α for 18 hours. Data represent mean and s.e.m. of three biological replicates per condition; n = 4 – 6 technical replicates. Significance determined by unpaired Student's t-test; *P<0.1, **P<0.05, ***P < 0.01, ****P < 0.001

Chapter V

Table 2 | Comparison of the concentration of bioactive lipids between living human blood vessel and human microvessels-on-a-chip. The concentrations in human blood vessel were obtained from HMDB[54-57].

Bioactive lipid	Human blood vessel		Microvessels-on-a-chip	
	Healthy	Diseased	Healthy	Diseased
PGF1 α	-0.0317 - 0.376 nM	-	-0.350 nM	-0.527 - 1.412 nM
PGF2 α	-0.144 - 0.371 nM	- 0.4 - 1.6 nM	-3.96 nM	-5.36 - 12.5 nM
PGE2*	-0.13 - 0.172 nM	-	-0.175 nM	-0.194 - 0.281 nM
PGE1	< 0.1 nM	-	-0.0225 nM	-0.0246 - 0.0308 nM
PGD2	-0.065 - 0.2 nM	-	-0.254 nM	-0.257 - 0.336 nM
PGA2	-0.0448 - 0.496 nM	-	-0.006 nM	-0.0048 - 0.0058 nM
8-iso-PGF2 α	-0.057 - 0.57 nM	-	-0.103 nM	-0.122 - 0.216 nM
S-1-P C18:1	-0.5 - 3.0 nM	-	-2.12 nM	-1.47 - 2.11 nM
Sph C18:1	-1.3 - 50 nM	-	-44.2 nM	-45.2 - 49.8 nM
Spha C18:0	-1.3 - 50 nM	-	-6.0 nM	-6.2 - 6.7 nM

Phorbol 12-myristate 13-acetate (PMA) is an activator of protein kinase C (PKC), hence of NF κ B, that relates to TNF α signaling and causes a wide range of effects in cells. As it is a known and potent up-regulator of cyclooxygenase-2 (COX-2) [29], we next measured the effect of PMA on the secretion of the biolipids to compare the TNF α response to a condition of maximal stimulation. When our combined results were plotted in a heatmap, marked differences are observed between control- and TNF α or PMA-treated microvessels (Table 3).



Chapter V

Table 3 | Heatmap of prostaglandins, isoprostanes, lysophosphatidic acid (LPA) classes, sphingolipids and platelet activating factor (PAF) detected in the microvessels-on-a-chip.

	Bioactive lipid	Fold change of concentration			Inflammatory action	Platelet activation	Vascular tone	Angiogenic action
		15 ng/ml TNF	50 ng/ml TNF	20 ng/ml PMA				
Prostaglandins	PGF1 α	2.0	1.8	5.0	anti	no	con	
	PGF2 α	1.7	1.5	5.0	pro	no	con	pro
	PGF3 α	1.5	1.1	4.4	anti			
	PGE2*	0.7	0.7	3.7	pro	anti	dil	pro
	PGE1	0.5	0.4	2.7	anti	anti	dil	pro
	PGD2	0.4	3.4	3.5	anti	anti	con	anti
	13, 14-dihydro-PGF2 α	0.7	0.5	2.3	pro			
	PGA2	-0.3	0.0	2.6	anti	no		
Isoprostanes	8-iso-13, 14-dihydro-PGF2 α	1.4	1.3	4.6				anti
	8-iso-PGF2 α *	1.1	0.9	4.2	pro	anti	con	anti
	8-iso-PGE2	0.1	0.0	2.1	pro	anti	con	anti
	8-iso-PGE1	0.1	0.0	0.7		anti	con	anti
	5-iPF2 α	0.0	0.0	0.0				
	8, 12-iPF2 α IV	-0.1	0.0	0.2				
Lysophosphatidic acids	LPA C14:0	-0.2	-0.2	-0.4	pro	pro	con	pro
	LPA C16:1	-0.4	-0.3	-0.6	pro	pro	con	pro
	LPA C22:6*	0.4	0.5	0.2	pro	pro	con	pro
	LPA C18:2	0.1	0.0	-0.1	pro	pro	con	pro
	LPA C20:4	0.3	0.4	0.3	pro	pro	con	pro
	LPA C22:5*	0.5	0.6	0.3	pro	pro	con	pro
	LPA C16:0	-0.2	-0.3	-0.3	pro	pro	con	pro
	LPA C18:1	0.1	0.2	-0.1	pro	pro	con	pro
	cLPA C20:4	-0.1	-0.2	-0.1	anti	anti	no	
	LPA C18:0	0.1	0.0	-0.2	pro	pro	con	pro
	cLPA C16:0	-0.2	0.0	0.0	anti	anti	no	
	cLPA C18:0	-0.2	-0.1	-0.2	anti	anti	no	
Sphingolipids	S-1-P C18:1	-0.5	-0.6	-0.9	anti	anti	con	pro
	Sph C18:1	0.2	0.1	0.0	anti	anti	con	pro
	Spha C18:0	0.2	0.0	-0.1				
	PAF C16:0	-0.2	-0.2	-0.4	pro	pro	con	pro

The fold changes were measured with respect to the controls and log2 transformed. The controls are microvessels unexposed to TNF α and PMA. The metabolites are characterized by their inflammatory action (anti- or pro-inflammatory), platelet activation (anti- or pro-platelet activation), vascular tone (constriction or dilation) and angiogenic action (anti- or pro-angiogenic). The data was obtained from the experiments done in Figure 4

with three biological replicates per condition; n = 4 – 6 technical replicates. *Validated markers of oxidative stress.

Impact of TNF α on prostaglandin levels

As shown in Table 3, overnight exposure to TNF α and PMA shows increase in the release of the prostaglandins PGF1 α , PGF2 α , PGF3 α , PGE2, PGD2 and 13, 14-dihydro-PGF2 α from the TNF α treated microvessels (Figure 4a and Table 3). During inflammation, ROS contributes to the increased PGE2, PGF2 α , PGD2 and 13, 14-dihydro-PGF2 α production through the release of arachidonic acid and COX-2 activation, having a pro-inflammatory effect in the endothelium[30, 31]. At the same time, anti-inflammatory prostaglandins PGF1 α , PGF3 α , PGE1, and PGA2 are also secreted by the endothelium[32, 33]. PGE1 and PGA2 are known to suppress TNF α induced NF κ B activation and production of ROS[34]. Relating to these two prostaglandins, no differences were detected in our system between untreated and TNF α treated microvessels for 18 hours.

Impact of TNF α on isoprostane levels

When we focus on the compounds produced by the reaction of free radicals with arachidonic acid, the isoprostanes, high levels of 8-iso-13, 14-dihydro-PGF2 α and 8-iso-PGF2 α were detected in the supernatant of TNF α treated microvessels (Figure 4b and Table 3). These metabolites inhibit platelet aggregation and induce monocyte adhesion to endothelial cells [35, 36]. We also detected 8-iso-PGE2, 5-iPF2 α , 8, 12-iPF2 α IV and 8-iso-PGE1 in the control sample and TNF α induced microvessels. 8-iso-PGE1 is recognized as vasoconstrictor with a similar effect as PGF2 α [37]. However, no significant difference between the two groups was evident after incubating the microvessels for 18 hours with TNF α .

Impact of TNF α on lysophosphatidic acids, sphingolipids and platelet activating factor

Looking at lipids that mediate diverse biological actions, the LPA classes, sphingosine and PAF are appropriate markers to take along in our metabolic read-out, because of their diverse

biological actions. The LPA classes consist of LPAs and cyclic-lysophosphatidic acids (cLPAs). They are formed by activated platelets and oxidation of low-density lipoproteins (LDLs) [38]. Once an inflammatory response is triggered, LPAs can activate platelets [39] and lead to endothelial dysfunction by activating NF κ B [40-43]. On the other hand, cLPAs inhibit pro-inflammatory cytokine expression in the endothelium [44]. In our data, we saw high concentrations of several LPAs in the control sample compared to TNF α treated microvessels. Similar results were seen in the levels of sphingosine-1-phosphate (S-1-P) and PAF (Table 3 and Figure 4c-e). In TNF α signaling, S-1-P binds to TNF receptor-associated factor 2 (TRAF2) to activate NF κ B, while PAF induces vascular permeability [45, 46].

TNF α induced bioactive lipid profiles from endothelial cells in 3D configuration are less inflammatory compared to 2D monolayers

To assess whether these three-dimensional microvessels display a more anti-inflammatory phenotype, we compared the bioactive lipid response of the 3D microvessels-on-a-chip to TNF α to that of 2D endothelial cell monolayers. In addition, we made a detailed inventory of the reported action of the individual lipids on inflammation, platelet activation, vascular tone and angiogenesis (for references see Supplementary Table 2). When the TNF α -induced biolipids profiles are listed in relation to their biological activities (Table 4) we conclude that the 3D microvessels-on-a-chip display a more dynamic, less inflammatory response to TNF α , that resembles more the human situation, compared to classical 2D endothelial cell cultures. In particular, the anti-inflammatory prostaglandins PGF1 α , PGF3 α , and PGD2 are increased to a larger extent and the anti-inflammatory lysophosphatidic acids are maintained or decreased to a lesser extent. In concert, the pro-inflammatory lipids PGE2, 8-iso-PGE2 and 8-iso-PGF2 α are present at higher levels in the medium of the TNF α exposed 2D endothelial monolayer culture. The elevated levels of the oxidative stress markers PGE2, 8-iso-PGF2 α [14], LPA C22:5 and LPA C22:6[18] confirm the increased inflammatory status of the 2D cultures making it tempting to speculate that an increased production of ROS in these cells may underlie these responses. The response of the microvasculature to inflammatory cytokines such as TNF α is often directly associated with inhibition of platelet activation (to maintain patency of the microvessel), a vasoconstrictive response and a pro-angiogenic response characterized by the

Chapter V

loss of endothelial cell-cell contacts and microvascular leakage. Many of these activities are also driven by the bioactive lipids in our panel (Supplementary Table 2) and it is interesting to note that concomitantly to the less inflammatory nature of the profiles of the conditioned media derived from the 3D microvessel the profile also suggests to be more restrictive of platelet activation, less vasoconstrictive and less angiogenic. It should be noted that we did not compare the excretion of bioactive of unstimulated 2D cell cultures and 3D vessels as the normalization on the number of endothelial cells would not have been straightforward.

V

Chapter V

Table 4 | Heatmap of pro- and anti- inflammatory and oxidative stress markers measured in 3D microvessels-on-a-chip and 2D endothelial cell monolayers.

Bioactive lipid	Fold change of concentration		Inflammatory action	Platelet activation	Vascular tone	Angiogenic action
	2D TNF	3D TNF				
PGF1 α	1.9	3.4	anti	no	con	
PGF3 α	1.0	6.6	anti			
PGE1	2.1	1.9	anti	anti	dil	pro
PGD2	2.3	6.5	anti	anti	con	anti
PGA2	0.7	0.0	anti	no		
cLPA C20:4	-0.7	-0.5	anti	anti	no	
cLPA C18:2	-0.5	0.0	anti	anti	no	
cLPA C16:0	-0.6	-0.3	anti	anti	no	
cLPA C18:1	-0.9	-0.2	anti	anti	no	
cLPA C18:0	-0.6	-0.2	anti	anti	no	
S-1-P C18:1	-2.0	-0.9	anti	anti	con	pro
8-iso-PGE1	1.8	1.9		anti	con	anti
5-iPF2 α	0.3	-0.1				
PGF2 α	1.9	2.2	pro	no	con	pro
PGE2*	2.4	1.0	pro	anti	dil	pro
13, 14-dihydro-PGF2 α	0.9	1.1	pro			
8-iso-13, 14-dihydro-PGF2 α	1.9	1.9				anti
8-iso-PGF2 α *	2.0	1.3	pro	anti	con	anti
8-iso-PGE2	0.6	-0.3	pro	anti	con	anti
LPA C14:0	0.0	-0.8	pro	pro	con	pro
LPA C16:1	-1.0	-1.0	pro	pro	con	pro
LPA C22:6*	0.0	-0.3	pro	pro	con	pro
LPA C18:2	-1.0	-1.2	pro	pro	con	pro
LPA C20:4	-0.2	-0.4	pro	pro	con	pro
LPA C22:5*	1.0	-0.1	pro	pro	con	pro
LPA C16:0	-0.6	-0.6	pro	pro	con	pro
LPA C18:1	-0.5	-1.0	pro	pro	con	pro
LPA C18:0	0.1	-0.9	pro	pro	con	pro
PAF C16:0	-0.5	-0.8	pro	pro	con	pro

The cells were treated with 15 ng/ml TNF α in the same experiment as Figure 4. The fold changes were measured with respect to the controls and log2 transformed. The controls are microvessels unexposed to TNF α and PMA. The metabolites are characterized by their inflammatory action (anti- or pro-inflammatory), platelet activation (anti- or pro-platelet activation), vascular tone (constriction or dilation) and angiogenic action (anti- or pro-

Chapter V

angiogenic). The data represents one biological replicate; n = 2 – 3 technical replicates. *Validated markers of oxidative stress.

The observed differences between the 2D and the 3D chip-based platforms may be attributed to the mechanical properties of the two systems[47]. The microvessels-on-a-chip are surrounded by an ECM layer and the 3D configuration allows intensified cell-cell interactions, resembling the *in vivo* situation. Moreover, vascular endothelial cells *in vivo* are influenced by distinct hemodynamic forces and this applies also to the endothelial cells in our microvessels-on-a-chip. Evidence suggest that shear stress activates phospholipids turnover that is involved in the production of free arachidonic acid [48]. This might also explain the differences we see between the increase/decrease of fatty acids in the microvessels-on-a-chip and the 2D cell culture. As shear stress influences RhoA activity and stress fiber formation, the regulation of fatty acids, RhoA might be important in this process [49]. In addition, the environmental changes in the 3D configuration could impact on the expression of the TNF receptors.

Several reports showed that oxidative stress induces endothelial dysfunction, which plays a central role in vascular diseases. It can promote the expression of pro-inflammatory and pro-coagulant factors, apoptosis and impair the release of nitric oxide [50, 51]. This study set out with the aim of using metabolomics as a readout of endothelial function in microvessels-on-a-chip exposed to TNF α to trigger inflammatory responses seen in vasculopathy. For the first time we show that the regulation of prostaglandins, isoprostanes, LPAs, sphingolipids and PAF can be measured in our microfluidic system, even though they cause profound physiological effects at very dilute concentrations that serve as early-stage markers of oxidative stress and inflammation [52]. The findings support the model that TNF α signaling induces ROS production that causes changes in signal transduction and gene expression, which leads to release of oxidative stress and inflammatory markers (Figure 5). Further research should be undertaken to confirm the results in gene and protein levels.

V

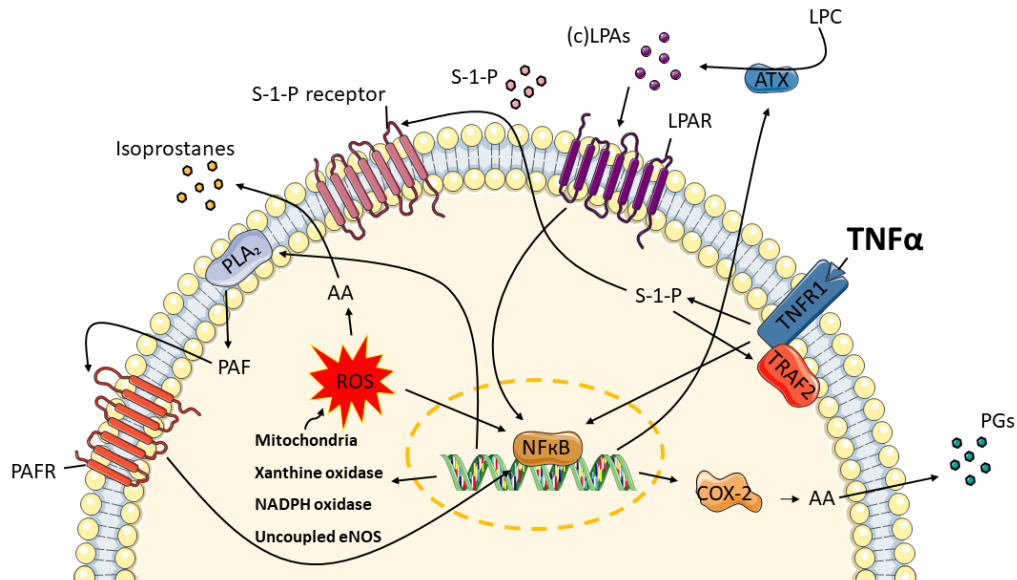


Figure 5 | TNF α induces the release of oxidative stress and inflammatory markers in endothelial cells. Exposure to TNF α , causes TNF signaling in the microvessels to produce ROS from endogenous sources: mitochondria, xanthine oxidase, NADPH oxidase and uncoupled eNOS. Sphingosine-1-phosphate (S-1-P) is needed in order for TNF receptor-associated factor 2 (TRAF2) to form a complex with the TNF receptor 1 (TNFR1). These lead to the conversion of arachidonic acid (AA) to isoprostanes and NF κ B activation. Moreover, AA is enzymatically converted by cyclooxygenase-2 (COX-2) to prostaglandins (PGs). At the same time, autotaxin (ATX) and phospholipase A₂ (PLA₂) are upregulated, resulting in the syntheses of lysophosphatidic acid (LPA) classes and platelet activating factor (PAF). Through their receptors, LPAs and PAF further promote the activation of COX-2.

Conclusions

We demonstrate bioactive lipid profiles can be readily detected from minor volumes of < 1 μ l of conditioned medium from microvessels-on-a-chip and display a more dynamic, less inflammatory response to TNF α compared to classical two-dimensional endothelial cell cultures. We can conclude that the response to TNF α resembles for the microvessels-on-a-chip more the human situation as described in the literature than the 2D endothelial cell culture. As the physiological readout of endothelial function is a critical aspect in using microvessels-on-a-chip for disease and drug research, the results suggest that the metabolic readout using metabolomics is more informative compared to morphological changes studied with imaging analyses of phenotypic changes. But it is the combination of both techniques,

Chapter V

metabolic readout using metabolomics and imaging analysis that may facilitate mechanistic studies and the detection and validation of biomarkers for microvascular disease at the systemic level. Furthermore, it will provide the information needed to understand microvascular destabilization and will generate a knowledge base for developing and testing personalized therapeutic interventions.

Data availability

All data generated or analysed during this study are included in this published article (and its Supplementary Information files).

Conflict of interest

TH is co-founder of MIMETAS and has some shares in MIMETAS. All other authors declare no conflict of interest related to the content of this manuscript.

Acknowledgements

This study was financially supported by the RECONNECT CVON Groot consortium, which is funded by the Dutch Heart Foundation. AJ and TH, AJvZ were supported by a ZonMW MKMD grant (114022501). AM and TH acknowledge the support by the NWO-TTW (IMMUNMET, grant number 16249). TH acknowledge the support by the TKI METABOCHIP project.

Author Contributions

Conceptualization: Abidemi Junaid, Anton Jan van Zonneveld and Thomas Hankemeier. Investigation: Abidemi Junaid, Johannes Schoeman, Wei Yang and Wendy Stam. Writing – original draft: Abidemi Junaid. Writing – review & editing: All authors. Supervision: Alireza Mashaghi, Anton Jan van Zonneveld and Thomas Hankemeier. Funding acquisition: Anton Jan van Zonneveld and Thomas Hankemeier.

References

1. Sedger, L.M. and M.F. McDermott, *TNF and TNF-receptors: From mediators of cell death and inflammation to therapeutic giants - past, present and future*. Cytokine Growth Factor Rev, 2014. **25**(4): p. 453-72.
2. Chimen, M., et al., *Monocyte Subsets Coregulate Inflammatory Responses by Integrated Signaling through TNF and IL-6 at the Endothelial Cell Interface*. Journal of Immunology, 2017. **198**(7): p. 2834-2843.
3. Torres-Castro, I., et al., *Human monocytes and macrophages undergo M1-type inflammatory polarization in response to high levels of glucose*. Immunology Letters, 2016. **176**: p. 81-89.
4. Green, L.A., et al., *Endogenous Transmembrane TNF-Alpha Protects Against Premature Senescence in Endothelial Colony Forming Cells*. Circ Res, 2016. **118**(10): p. 1512-24.
5. Masi, S., et al., *Mitochondrial oxidative stress, endothelial function and metabolic control in patients with type II diabetes and periodontitis: A randomised controlled clinical trial*. Int J Cardiol, 2018. **271**: p. 263-268.
6. Engin, A., *Endothelial Dysfunction in Obesity*. Adv Exp Med Biol, 2017. **960**: p. 345-379.
7. Rabelink, T.J., H.C. de Boer, and A.J. van Zonneveld, *Endothelial activation and circulating markers of endothelial activation in kidney disease*. Nat Rev Nephrol, 2010. **6**(7): p. 404-14.
8. van Zonneveld, A.J., et al., *Inflammation, vascular injury and repair in rheumatoid arthritis*. Ann Rheum Dis, 2010. **69 Suppl 1**: p. i57-60.
9. Pisoschi, A.M. and A. Pop, *The role of antioxidants in the chemistry of oxidative stress: A review*. Eur J Med Chem, 2015. **97**: p. 55-74.
10. Cai, H. and D.G. Harrison, *Endothelial dysfunction in cardiovascular diseases: the role of oxidant stress*. Circ Res, 2000. **87**(10): p. 840-4.
11. Blaser, H., et al., *TNF and ROS Crosstalk in Inflammation*. Trends Cell Biol, 2016. **26**(4): p. 249-261.
12. Poussin, C., et al., *3D human microvessel-on-a-chip model for studying monocyte-to-endothelium adhesion under flow - application in systems toxicology*. ALTEX, 2019.
13. Morrow, J.D., et al., *A series of prostaglandin F2-like compounds are produced in vivo in humans by a non-cyclooxygenase, free radical-catalyzed mechanism*. Proc Natl Acad Sci U S A, 1990. **87**(23): p. 9383-7.
14. Ridker, P.M., et al., *Established and emerging plasma biomarkers in the prediction of first atherothrombotic events*. Circulation, 2004. **109**(25 Suppl 1): p. IV6-19.

Chapter V

15. Moutzouri, E., et al., *Comparison of the effect of simvastatin versus simvastatin/ezetimibe versus rosuvastatin on markers of inflammation and oxidative stress in subjects with hypercholesterolemia*. *Atherosclerosis*, 2013. **231**(1): p. 8-14.
16. Vassalle, C., et al., *Oxidative stress and its association with coronary artery disease and different atherogenic risk factors*. *J Intern Med*, 2004. **256**(4): p. 308-15.
17. Esposito, E. and S. Cuzzocrea, *TNF-Alpha as a Therapeutic Target in Inflammatory Diseases, Ischemia-Reperfusion Injury and Trauma*. *Current Medicinal Chemistry*, 2009. **16**(24): p. 3152-3167.
18. Ackerman, S.J., et al., *Polyunsaturated lysophosphatidic acid as a potential asthma biomarker*. *Biomark Med*, 2016. **10**(2): p. 123-35.
19. Jaffe, E.A., et al., *Culture of human endothelial cells derived from umbilical veins. Identification by morphologic and immunologic criteria*. *J Clin Invest*, 1973. **52**(11): p. 2745-56.
20. Stroka, K.M. and H. Aranda-Espinoza, *Endothelial cell substrate stiffness influences neutrophil transmigration via myosin light chain kinase-dependent cell contraction*. *Blood*, 2011. **118**(6): p. 1632-1640.
21. Huveneers, S., M.J.A.P. Daemen, and P.L. Hordijk, *Between Rho(k) and a Hard Place The Relation Between Vessel Wall Stiffness, Endothelial Contractility, and Cardiovascular Disease*. *Circulation Research*, 2015. **116**(5): p. 895-908.
22. Huveneers, S., M.J. Daemen, and P.L. Hordijk, *Between Rho(k) and a hard place: the relation between vessel wall stiffness, endothelial contractility, and cardiovascular disease*. *Circ Res*, 2015. **116**(5): p. 895-908.
23. Baeyens, N., et al., *Endothelial fluid shear stress sensing in vascular health and disease*. *J Clin Invest*, 2016. **126**(3): p. 821-8.
24. Wevers, N.R., et al., *A perfused human blood-brain barrier on-a-chip for high-throughput assessment of barrier function and antibody transport*. *Fluids Barriers CNS*, 2018. **15**(1): p. 23.
25. van Duinen, V., et al., *96 perfusable blood vessels to study vascular permeability in vitro*. *Sci Rep*, 2017. **7**(1): p. 18071.
26. van Duinen, V., et al., *96 perfusable blood vessels to study vascular permeability in vitro*. *Scientific Reports*, 2017. **7**.
27. Koutsiaris, A.G., et al., *Volume flow and wall shear stress quantification in the human conjunctival capillaries and post-capillary venules in vivo*. *Biorheology*, 2007. **44**(5-6): p. 375-386.

28. Schoeman, J.C., et al., *Development and application of a UHPLC-MS/MS metabolomics based comprehensive systemic and tissue-specific screening method for inflammatory, oxidative and nitrosative stress*. Anal Bioanal Chem, 2018. **410**(10): p. 2551-2568.
29. Chang, M.S., et al., *Phorbol 12-myristate 13-acetate upregulates cyclooxygenase-2 expression in human pulmonary epithelial cells via Ras, Raf-1, ERK, and NF-kappa B, but not p38 MAPK, pathways*. Cellular Signalling, 2005. **17**(3): p. 299-310.
30. Wong, M.S.K. and P.M. Vanhoutte, *COX-mediated endothelium-dependent contractions: from the past to recent discoveries*. Acta Pharmacologica Sinica, 2010. **31**(9): p. 1095-1102.
31. Dworski, R., et al., *Assessment of oxidant stress in allergic asthma by measurement of the major urinary metabolite of F2-isoprostane, 15-F2t-IsoP (8-iso-PGF2alpha)*. Clin Exp Allergy, 2001. **31**(3): p. 387-90.
32. Trebaticka, J., et al., *Cardiovascular Diseases, Depression Disorders and Potential Effects of Omega-3 Fatty Acids*. Physiological Research, 2017. **66**(3): p. 363-382.
33. Gezginci-Oktayoglu, S., N. Orhan, and S. Bolkent, *Prostaglandin-E-1 has a protective effect on renal ischemia/reperfusion-induced oxidative stress and inflammation mediated gastric damage in rats*. International Immunopharmacology, 2016. **36**: p. 142-150.
34. Ohmura, T., et al., *Regulation of lung endothelial permeability and inflammatory responses by prostaglandin A2: role of EP4 receptor*. Molecular Biology of the Cell, 2017. **28**(12): p. 1622-1635.
35. Rokach, J., et al., *The isoprostanes: A perspective*. Prostaglandins & Other Lipid Mediators, 1997. **54**(6): p. 823-851.
36. Durackova, Z., *Some Current Insights into Oxidative Stress*. Physiological Research, 2010. **59**(4): p. 459-469.
37. Nakano, J. and J.M. Kessinger, *Effects of 8-isoprostaglandin E1 on the systemic and pulmonary circulations in dogs*. Proc Soc Exp Biol Med, 1970. **133**(4): p. 1314-7.
38. Karshovska, E., et al., *Endothelial specific autotaxin in atherosclerosis*. European Heart Journal, 2018. **39**: p. 1404-1405.
39. Khandoga, A.L., et al., *Lysophosphatidic acid-induced platelet shape change revealed through LPA(1-5) receptor-selective probes and albumin*. Platelets, 2008. **19**(6): p. 415-27.
40. Biermann, D., et al., *Impact of AT2 receptor deficiency on postnatal cardiovascular development*. PLoS One, 2012. **7**(10): p. e47916.
41. Yang, B., et al., *The effect of lysophosphatidic acid on Toll-like receptor 4 expression and the nuclear factor-kappa B signaling pathway in THP-1 cells*. Molecular and Cellular Biochemistry, 2016. **422**(1-2): p. 41-49.

Chapter V

42. Ninou, J., C. Magkrioti, and V. Aidinis, *Autotaxin in Pathophysiology and Pulmonary Fibrosis*. *Frontiers in Medicine*, 2018. **5**.
43. Palmetshofer, A., S.C. Robson, and V. Nehls, *Lysophosphatidic acid activates nuclear factor kappa B and induces proinflammatory gene expression in endothelial cells*. *Thrombosis and Haemostasis*, 1999. **82**(5): p. 1532-1537.
44. Tsukahara, T., H. Haniu, and Y. Matsuda, *Cyclic Phosphatidic Acid Inhibits Alkyl-Glycerophosphate-Induced Downregulation of Histone Deacetylase 2 Expression and Suppresses the Inflammatory Response in Human Coronary Artery Endothelial Cells*. *International Journal of Medical Sciences*, 2014. **11**(9): p. 955-961.
45. Alvarez, S.E., et al., *Sphingosine-1-phosphate is a missing cofactor for the E3 ubiquitin ligase TRAF2*. *Nature*, 2010. **465**(7301): p. 1084-U149.
46. Ramakrishnan, A.V.K.P., et al., *Platelet activating factor: A potential biomarker in acute coronary syndrome?* *Cardiovascular Therapeutics*, 2017. **35**(1): p. 64-70.
47. Lee, J., et al., *In vitro Toxicity Testing of Nanoparticles in 3D Cell Culture*. *Small*, 2009. **5**(10): p. 1213-1221.
48. Bhagyalakshmi, A., et al., *Fluid Shear-Stress Stimulates Membrane Phospholipid-Metabolism in Cultured Human Endothelial-Cells*. *Journal of Vascular Research*, 1992. **29**(6): p. 443-449.
49. Liu, B., et al., *RhoA and Membrane Fluidity Mediates the Spatially Polarized Src/FAK Activation in Response to Shear Stress*. *Scientific Reports*, 2014. **4**.
50. Schulz, E., T. Gori, and T. Munzel, *Oxidative stress and endothelial dysfunction in hypertension*. *Hypertens Res*, 2011. **34**(6): p. 665-73.
51. Shiraki, A., et al., *The glucagon-like peptide 1 analog liraglutide reduces TNF-alpha-induced oxidative stress and inflammation in endothelial cells*. *Atherosclerosis*, 2012. **221**(2): p. 375-82.
52. Ryu, Y., M.J. Reid, and K.V. Thomas, *Liquid chromatography-high resolution mass spectrometry with immunoaffinity clean-up for the determination of the oxidative stress biomarker 8-iso-prostaglandin F2alpha in wastewater*. *J Chromatogr A*, 2015. **1409**: p. 146-51.
53. Vulto, P., et al., *Phaseguides: a paradigm shift in microfluidic priming and emptying*. *Lab on a Chip*, 2011. **11**(9): p. 1596-1602.
54. Wishart, D.S., et al., *HMDB 4.0: the human metabolome database for 2018*. *Nucleic Acids Research*, 2018. **46**(D1): p. D608-D617.
55. Wishart, D.S., et al., *HMDB 3.0-The Human Metabolome Database in 2013*. *Nucleic Acids Research*, 2013. **41**(D1): p. D801-D807.

Chapter V

56. Wishart, D.S., et al., *HMDB: the human metabolome database*. Nucleic Acids Research, 2007. **35**: p. D521-D526.

57. Wishart, D.S., et al., *HMDB: a knowledgebase for the human metabolome*. Nucleic Acids Research, 2009. **37**: p. D603-D610.

Supplementary Tables

Supplementary Table 1 | An overview of the concentrations of the calibration solution.

Bioactive lipid	Stock concentration (nM)								
	C9	C8	C7	C6	C5	C4	C3	C2	C1
PGF1 α	53.3	26.7	13.3	6.7	3.3	1.7	0.8	0.4	0.2
PGF2 α	53.3	26.7	13.3	6.7	3.3	1.7	0.8	0.4	0.2
PGF3 α	53.3	26.7	13.3	6.7	3.3	1.7	0.8	0.4	0.2
PGE2	53.3	26.7	13.3	6.7	3.3	1.7	0.8	0.4	0.2
PGE1	53.3	26.7	13.3	6.7	3.3	1.7	0.8	0.4	0.2
PGD2	53.3	26.7	13.3	6.7	3.3	1.7	0.8	0.4	0.2
13, 14-dihydro-PGF2 α	41.9	21.0	10.5	5.2	2.6	1.3	0.7	0.3	0.2
PGA2	53.3	26.7	13.3	6.7	3.3	1.7	0.8	0.4	0.2
8-iso-13, 14-dihydro-PGF2 α	53.3	26.7	13.3	6.7	3.3	1.7	0.8	0.4	0.2
8-iso-PGF2 α	53.3	26.7	13.3	6.7	3.3	1.7	0.8	0.4	0.2
8-iso-PGE2	53.3	26.7	13.3	6.7	3.3	1.7	0.8	0.4	0.2
8-iso-PGE1	53.3	26.7	13.3	6.7	3.3	1.7	0.8	0.4	0.2
5-iPF2 α	53.3	26.7	13.3	6.7	3.3	1.7	0.8	0.4	0.2
8, 12-iPF2 α IV	53.3	26.7	13.3	6.7	3.3	1.7	0.8	0.4	0.2
LPA C20:4	2400.0	1200.0	600.0	300.0	150.0	75.0	37.5	18.8	9.4
LPA C16:0	2400.0	1200.0	600.0	300.0	150.0	75.0	37.5	18.8	9.4
LPA C18:1	3200.0	1600.0	800.0	400.0	200.0	100.0	50.0	25.0	12.5
LPA C18:0	2666.7	1333.3	666.7	333.3	166.7	83.3	41.7	20.8	10.4
cLPA C18:1	2400.0	1200.0	600.0	300.0	150.0	75.0	37.5	18.8	9.4
S-1-P C18:1	8000.0	4000.0	2000.0	1000.0	500.0	250.0	125.0	62.5	31.3
Spha C18:1	9600.0	4800.0	2400.0	1200.0	600.0	300.0	150.0	75.0	37.5
Spha C18:0	9600.0	4800.0	2400.0	1200.0	600.0	300.0	150.0	75.0	37.5
PAF C16:0	1333.3	666.7	333.3	166.7	83.3	41.7	20.8	10.4	5.2

Chapter V

Supplementary Table 2 | References regarding the action of bioactive lipids on inflammation, platelets, vascular tone and angiogenesis.

Bioactive lipid	PMID
PGF1 α	3110148
PGF2 α	11438482 6999547 1415588
PGF3 α	16297610
PGE2*	30112590
PGE1	6999547 24431002 12494264
PGD2	6999547 30734298 29671869
13, 14-dihydro-PGF2 α	
PGA2	6999547 15723383
8-iso-13, 14-dihydro-PGF2 α	
8-iso-PGF2 α *	11344105 15640282 18802021 10711349
8-iso-PGE2	12716476 10711349 24646155
8-iso-PGE1	10711349
5-iPF2 α	
8, 12-iPF2 α IV	
LPA C14:0	25825155 30928673
LPA C16:1	25825155 30928673
LPA C22:6*	25825155 30928673
LPA C18:2	25825155 30928673
LPA C20:4	25825155 30928673
LPA C22:5*	25825155 30928673
LPA C16:0	25825155 30928673
LPA C18:1	25825155 30928673
LPA C22:4	25825155 30928673
cLPA C20:4	25013374 18554524
LPA C18:0	25825155 30928673
cLPA C18:2	25013374 18554524
cLPA C16:0	25013374 18554524
cLPA C18:1	25013374 18554524
cLPA C18:0	25013374 18554524
S-1-P C18:1	28609704 31049553 20577214 27565080
Sph C18:1	28609704 31049553 20577214 27565080
Spha C18:0	
PAF C16:0	17588613 12038971

*Validated markers of oxidative stress.



Chapter V

V

Chapter VI

An integrated microvessels-on-a-chip platform for automated multi-channel perfusion and continual *in situ* oxygen monitoring

Abidemi Junaid, Raphaël Zwier, Ankur Kislaya, Wendy Stam, Bas Trietsch, Jerry Westerweel, Alireza Mashaghi, Janine van Gils, Anton Jan van Zonneveld, Thomas Hankemeier

Manuscript to be submitted (2020)

Abstract

Organs-on-Chips have recently emerged as a viable system for modelling microvascular diseases and drug screening. These *in vitro* microvascular disease models, featuring biomimetic compositions, architectures and functions found in the human microvessel, are expected to replace the traditional models based on two-dimensional (2D) static cell culture. Since blood flow and shear stress play a significant role in modulating the physiological responses of endothelial cells in the microvessels, incorporation of flow is often essential for microvessels-on-chips to serve as biologically relevant models. Here, we describe the development of a multi-channel microfluidic pumping and *in situ* oxygen monitoring system for the microvessels-on-chips. We performed biochemical assays in the microvessels-on-chips under shear stress and oxygen measurement to validate our system. The morphology and gene expression of the microvessels-on-chips under shear stress were similar to what is found *in vivo* and deviate significantly from shearless models. We believe that our integrated microvessels-on-a-chip platform has paved the way to promote high-throughput perfusion and real-time oxygen measurement in an automated manner for modeling the microvascular system.

Introduction

Heart failure (HF) is the number one cause of death worldwide [1]. In recent years it has become clear that as much as 50% of HF patients show symptoms of HF in the presence of preserved ejection fraction (HFpEF) [2]. Recent studies have identified causal relation between HFpEF and microvascular dysfunction [3, 4]. Therefore, finding ways to treat microvascular dysfunction has become very important in drug discovery. To address this issue, new approaches are required to fill the technology gap needed for effective drug discovery and screening [5].

For decades now, conventional cell culture models have been used to study microvascular diseases. Conventional cell culture models require two-dimensional (2D) cell culturing, static conditions, large working volumes, and recurrent system disturbance. Hence, they fail to reconstitute the *in vivo* cellular dynamic environment and are not suitable for monitoring the microenvironment that can be translated to *in vivo* situation. Organs-on-Chips have recently been proposed to mimic the physiological conditions of the microvessels. These miniaturized human microvessel models have several advantages over conventional models, such as three-dimensional (3D) structure, cell-cell interactions and extracellular matrix (ECM) [6, 7]. Therefore, they have been successfully used to model diseases and study the effects of drugs [8]. Although, many in the field focus on the construction of biomimetic microvessel models, it is now firmly acknowledged that incorporating perfusion and sensors would allow the exertion of mechanical forces on the surface of endothelial cells and *in situ* monitoring the status of the microvessels [9, 10]. Such a need originates from the fact that perfusion trigger the production of proteins and transcription factors that are able to suppress pro-inflammatory signaling pathways and this can be measured online with biosensors [11].

One of the challenges of organs-on-chips is to fabricate functional microvessels that can be integrated with other systems, can withstand continuous perfusion after cell seeding and run in fully automated manner over extended periods of time. This is because commercially available perfusion systems together with sensors are often incompatible with microfluidic systems. However, several efforts have been initiated toward the accomplishment of this goal. For example, prototype organs-on-chips under shear force and with *in situ* sensing capabilities were developed to perfuse endothelial cells with real time monitoring of mechanical microenvironment, record field potential and measure transepithelial electrical resistance

(TEER) [12, 13]. However, these organs-on-chips were built upon a single chip, limited to monitoring of a single microenvironment and with no automation [14].

Here, we report the development of an integrated organ-on-a-chip modular platform that includes a multi-channel micropump for high-throughput perfusion of fluids and a physical sensor for monitoring oxygen in extracellular microenvironment. The oxygen monitoring could be performed *in situ* without interrupting the system. The micropump and oxygen sensor were controlled by LabView in an automated manner. We analyzed the performance of the platform by adapting it to the microvessels-on-chips and carrying out biochemical assays to correlate the phenotype of endothelial cells to the *in vivo* situation. We anticipate that in the future, our platform technology will enable organ-on-a-chip models to achieve automation and *in situ* monitoring of biochemical parameters while being perfused.

Methods

μ PIV

PIV is a quantitative method which is commonly used for measuring velocity field in experimental fluid mechanics. This technique measures the velocity of a fluid element indirectly by measuring the displacement of tracer particles within the fluid which must be added prior to the start of the experiment. A high-power light source for the illumination of the tiny tracer particles is required to expose the image sensor of the camera to sufficient scattered light. In micro-scale application, it is generally referred to as μ PIV [24, 25]. This measurement was carried out on the rerouted 2-lane in order to calibrate the shear stress of our microfluidic pump. The microfluidic channel has a height of 200 μ m and is 400 μ m wide. The working fluid is a solution of 2% blood serum (viscosity and density are 1.25 mPa·s and 1.0242 g/mL respectively) dissolved in water. The viscosity of the prepared solution was checked at 37°C using a viscometer (Contraves Low shear 40). The dynamic viscosity was determined for different deflections varying from 80 rad/s to -80 rad/s in steps of 20 rad/s and averaged to get the mean dynamic viscosity of 0.87 mPa·s. The solution was seeded with

monodispersed polystyrene particles with a diameter of $1.046 \pm 0.016 \mu\text{m}$ (Microparticles GmbH).

Images were recorded from LaVision's Imager Intense camera (CCD, 12-bit 1376×1050pixels, pixel pitch 6.4 μm). The camera was mounted on the Nikon eclipse Ti2 inverted microscope equipped with 10x objective lens (Nikon CFI Plan Fluor). The camera exposure time was set at 4000 μs to allow enough light to enter the image sensor for clear identification of the particle images. The acquisition frequency of 9.5 Hz was used to capture the in-plane displacement of 2 pixel between two consecutive recordings. For statistical averaging to reduce the random noise, 3000 images were acquired for each data set. Images were acquired for flow behavior at different pulsatile pump rotational speed between 10 to 100 RPM. Image acquisition and PIV processing are performed with the LaVision DaVis 8.3 software. In PIV processing, for reducing the background image, a time filter is used to subtract the minimum intensity from all images. Followed by taking sequential time-series of the single-pass FFT cross-correlation for all the images. For the velocity field reconstruction, the interrogation windows of 64×64 pixels with 50% overlap was chosen. The microfluidic pump shear stress was derived from the equations:

$$\bar{v} (m/s) = \frac{s}{t}$$

$$Q(m^3/s) = A \cdot \bar{v}$$

$$\tau(\text{dyne}/\text{cm}^2) = \frac{6 \cdot Q \cdot \eta}{w \cdot h^2} \cdot 10$$

where \bar{v} is particle velocity; s is the distance the particle traveled in time t ; Q is the volume flow rate, A is the cross-section area of the microfluidic channel; τ is the calculated shear stress; η is the measured viscosity of the media; w and h are the width and height of the channel.

Cell culture

Human umbilical vein endothelial cells (HUVECs) were cultured in Endothelial Cell Growth Medium 2 (C-39216; PromoCell). For all microfluidic cell culture, we used a modified 2-lane

OrganoPlate, rerouted 2-lane, made by MIMETAS with inlets and outlets that are compatible with our microfluidic pump. The microvascular and extracellular matrix (ECM) channels were separated by phaseguides [16]. Before seeding the cells, 4 mg/ml rat tail collagen type 1 (3440-005-01; Trevigen) neutralized with 10% 37 g/L Na₂CO₃ (S5761; Sigma) and 10% 1 M HEPES buffer (15630-056; Gibco) was added in the ECM channels. Subsequently, the collagen was let to polymerize by incubating the device for 10 minutes in the incubator at 37°C and 5% CO₂. The observation windows were filled with 50 µl Hank's Balanced Salt Solution with calcium and magnesium buffers (HBSS+; 24020117; Life Technologies) for optical clarity and to prevent gel dehydration. Using a repeater pipette, 20 µl of 1% gelatin was added into the inlet of each microvascular channel and the device was put in the incubator at 37°C for 30 minutes. Subsequently, the gelatin was replaced with 20 µl of culture media. We trypsinized cells at 80-90% confluency and seeded 15·10⁶ cells/ml in the outlet of the microvascular channels of the OrganoPlate. Afterwards, the cells were incubated at 37°C and 5% CO₂ for one hour to allow microvascular formation. After incubation, 50 µl of culture medium was added to the inlets and outlets of the microvascular channels. The device was placed on an interval rocker platform (Perfusion rocker, MIMETAS) with a 7° angle of motion and an eight-minute timed operation to allow continuous bidirectional flow of medium in the microvessels. After 48h, the medium was refreshed, and the microvessels were perfused for 24, 48 and 96h with the microfluidic pump for unidirectional flow.

Quantitative RT-PCR

RNA isolation was performed using Buffer RLT lysis buffer (Qiagen) and isolated using Qiagen's RNAeasy kit according to manufactures instructions. Subsequently, lysate of eight microvessels were pooled to form one sample to allow analyses of gene expressions at low concentrations due to low cell numbers. 250 ng of total RNA was used for reverse transcription mediated cDNA synthesis using random and oligo(dT) primers (Bio-Rad) according to the manufacturer's protocols. SYBR Select (Invitrogen) and a Biorad CFX384 were used for qRT-PCR analysis. The primer sequences of target genes used were as follows: *Klf2* (sense), CTACACCAAGAGTTCGCATCTG; *Klf2* (antisense), CCGTGTGCTTTCGGTAGTG; *Klf4* (sense), TCAACCTGGCGGACATCAAC; *Klf4* (antisense), AGCACGAACTGCCATCA; *18S rRNA* (sense), GGATGTAAAGGATGGAAAATACA; *18S rRNA* (antisense), TCCAGGTCTTCACGGAGCTTGTT.

Levels of expression were normalized to *18S rRNA* and quantified using the comparative cycle threshold ($\Delta\Delta\text{Ct}$) method.

Cell morphology assessment

The medium was aspirated from the medium inlets, and the chip outlets and cells were fixed using 4% paraformaldehyde (PFA) in HBSS+ for 10 minutes at room temperature. The fixative was aspirated, and the cells were rinsed once with HBSS+. Next, the cells were permeabilized for two minutes with 0.2% Triton X-100 in HBSS+ and washed once with HBSS+. The cells were blocked in 5% BSA in HBSS+ for 30 minutes and incubated with the primary antibody solution overnight at 4°C. Mouse anti-human CD144 (1:100; 555661; BD Biosciences) was used as the primary antibodies. The wells were washed with HBSS+, followed by a one-hour incubation with Hoechst (1:2000; H3569; Invitrogen), rhodamine phalloidin (1:200; P1951; SIGMA) and the secondary antibody solution, containing an Alexa Fluor 488-conjugated goat-anti-mouse antibody (1:250; R37120; Waltham). The wells were washed three times with HBSS+. High-quality Z-stack images of the stained cells were acquired using a high-content confocal microscope (Molecular Devices, ImageXpress Micro Confocal). The orientation of the cells was determined using OrientationJ, an ImageJ plug-in, and plotted in a Rose diagram using Matlab R2015a (Mathworks).

Statistical analysis

For statistical analyses, we used IBM SPSS Statistics 23. Values are given as mean \pm SEM. Multiple comparisons were made by one-way ANOVA followed by Dunnett's t-test. Results were considered significant at * $P < 0.1$, ** $P < 0.05$, *** $P < 0.01$.

Results

Our integrated microvessel-on-a-chip platform was designed to be modular in hypoxia incubator. The platform is compatible with microfluidic culture plate, a physical sensor suite for measurement of oxygen in the microenvironment and microfluidic pump for perfusing 16

Chapter VI

microchannels simultaneously (Figure 1a and b). The platform was contained within a custom designed XY and Z stages of Zaber Technologies (Figure 1c). The XY stage was fixed at a height of 133 mm. The Z stage was integrated with an optical fiber and probe to measure the oxygen concentration in the OrganoPlate with PyroScience Piccolo2 oxygen sensor [15]. The probe acted as a feedback to set the height of the optical fiber with the Z stage in order for the oxygen sensor to have a strong signal strength (Figure 1d). The XY and Z stages were connected to Zaber Technologies integrated controllers that could be operated together with the probe, using a set of LabView codes. The XY stage was calibrated to move to the coordinates of the desired microchannel in the microfluidic culture plate while the Z stage is automated to position the optical fiber of the oxygen sensor in correct height with our feedback control system.

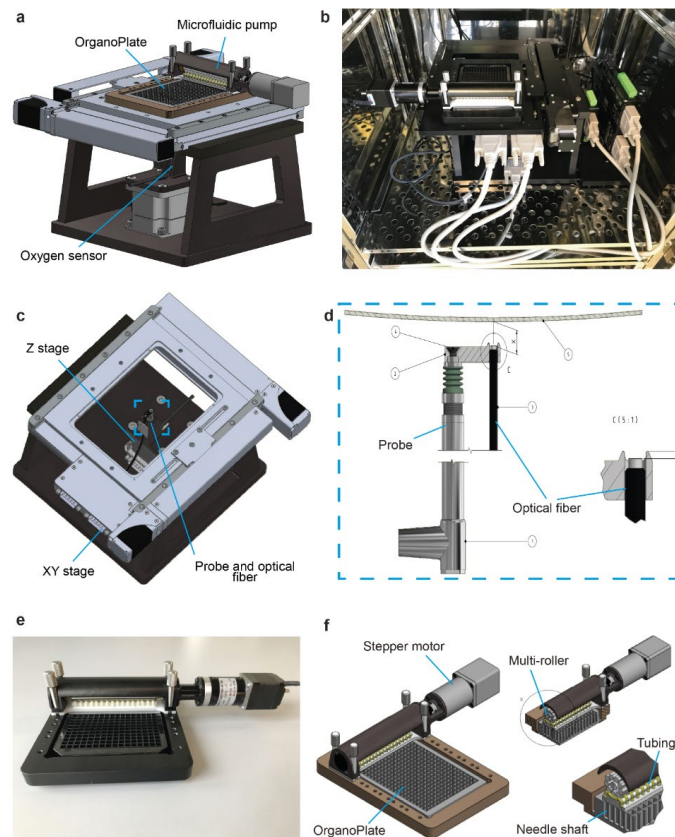


Figure 1 | Integrated automated microvessels-on-a-chip and oxygen monitoring platform. (a) Schematic of a full system where the OrganoPlate is placed on XY and Z stages with the microfluidic pump and oxygen sensor. **(b)** A photograph of the integrated platform placed in an incubator. **(c)** Top view of the integrated platform showing the oxygen sensor. The dashed rectangular box highlights the region shown in **d**. **(d)** The probe and optical fibre of the oxygen sensor. **(e)** A photograph of the microfluidic pump connected to 16 microchannels in the OrganoPlate. **(f)** Schematic diagram of the pumping system.

On top of the XY stage, the microfluidic pump was placed. This is a miniaturized, mechanically-actuated 16-channel peristaltic pump (Figure 1e and f). The small footprint of the micropump renders it portable, and allows its use on microscope stages adjacent to microfluidic devices with a 384 wells plate interface. The microfluidic pump has three core components: a multi-roller, silicon tubings (OD=2.05 mm and ID=0.25 mm) and needle shafts (OD=0.72 mm and ID=0.41 mm). A stepper motor (NEMA-11 Bipolar Stepper 28STH32), controlled with LabView,

drives the pump. As the multi-roller rotates, it compresses the tubings and pushes fluid in the direction of rotation. The number of rotations per minute (RPM) determines the flow rate.

To provide the proof-of-principle for our integrated microvessels-on-chips, we designed a novel chip structure, the rerouted 2-lane, based on the MIMETAS OrganoPlate platform. The rerouted 2-lane consists of a stratified array of 96 microfluidic chips embedded in a customized 384-well microtiter plate format that is compatible with the microfluidic pump (Figure 1e, f and 2a). Each chip contains a single microfluidic chip fixed between two layers of glass: a top plate with inlets that corresponds to the underside of selected microtiter plate wells and a bottom plate. Each chip is connected through four neighboring wells and two lanes. The flow of media is driven by the microfluidic pump from the first inlet well connected to the fourth medium outlet well through a culture lane. The second well is connected to the gel inlet for loading of extracellular matrix (ECM) lane and the fourth well is used as an observation window for monitoring the cells (Figure 2b). In the chip, microvessels were generated in the culture lane using HUVECs at the interface of collagen type 1 ECM (Figure 2c and d). The culture and ECM lanes are separated by a phaseguide, preventing the collagen from flowing into the culture lane [16].

Chapter VI

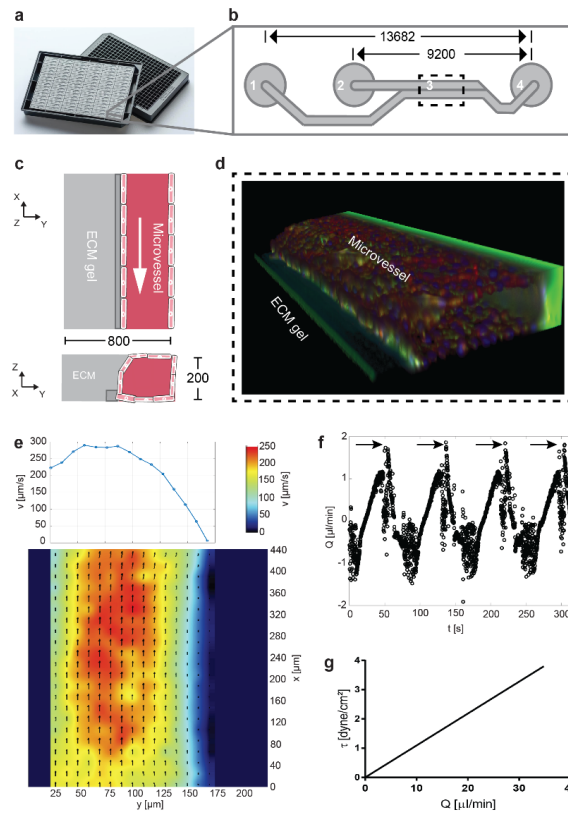


Figure 2 | Microfluidic cell culture device and operations. (a) A photograph of the rerouted 2-lane OrganoPlate. (b) Schematic of a single rerouted 2-lane chip; 1 = Medium inlet, 2 = Gel inlet, 3 = Observation window, 4 = Medium outlet; The dashed rectangular box highlights the region shown in d. (c) Top and side view of a microchannel interfacing with a phaseguide, ECM and culture lanes. All dimensions are in μm . (d) A 3D reconstruction showing the human microvessel-on-a-chip. (e) Measured channel cross section velocity profile. The flow regime shows some variation in velocity with parabolic trend across the channel width. (f) Representative flow pattern for a single microchannel. Arrows indicate point of roller release. (g) The channel shear stress, τ , at varying measured flow rates, Q .

To investigate the flow characteristics of the ex vivo flow chamber, micro-particle image velocimetry (μPIV) experiments were conducted at several rotational speed of the microfluidic pump. We could see that the velocity distributions on the median plane of the microchannel are in accordance to theoretical velocity distribution of laminar flow in square sectional ducts except for the region near the ECM and wall [17]. This is because of the ECM and wall

roughness and the impact of particles on the surfaces (Figure 2e). The velocity was averaged on cross section, \bar{v} , which was then used to determine the flow rate, Q . Sudden flow rate changes occurred at the point of release of roller pins leading to slight pulsation, indicated with arrows in Figure 2f. Based on the flow rate, the shear stress, τ , in our system was determined (Figure 2g).

Shear stress controls different endothelial phenotypic characteristics [18]. To verify the use of our multi-channel microfluidic pump in 3D cell culture applications, we studied the morphology, cytoskeleton remodeling and gene expression of the microvessels-on-chips under unidirectional flow. Endothelial cells cultured in 12-well plate representing the static condition and microvessels perfused with an interval rocker platform (Perfusion rocker, MIMETAS) were taken along as controls. The interval rocker platform introduces gravitational and bidirectional flow in the microvessels-on-chips and it has been demonstrated to create functional microvessels at a 7° angle of motion and an eight-minute timed operation [19]. HUVECs were cultured in the microvessels-on-chips overnight with the interval rocker platform and this continued for additional 24h or they were put under flow for 24h with our integrated microfluidic platform set at physiological umbilical vein shear stress of 3 dyne/cm² and 20% oxygen. At the same time, cells were cultured in the 12-well plate to observe their morphology under static condition. At this condition, the orientation of the cells did not follow any specific trend (having the orientation angles of 0 – 90°) and there was lots of actin stress fiber formation. In comparison, with the interval rocker platform, the cells started following the direction of the flow (corresponding to the orientation angles of 0 – 60°), however, actin stress fiber formation was still visible. In contrary, in the presence of the microfluidic pump, the endothelial cells were highly orientated to the direction of flow with orientation angles of 0 – 30° and there was a decrease in stress fiber formation (Figure 3a and b). To further validate the functionality of our microfluidic pump, we looked at the impact of shear stress on regulating the shear dependent genes *Klf2* and *Klf4*. Shear stress at 0.38 dyne/cm² with the microfluidic pump was introduced for 24, 48 and 96h in the microvessels-on-chips. Microvessels perfused with the microfluidic pump compared with those perfused with the interval rocker and cells cultured in the 12-well plate, show significant upregulation of *Klf2* and *Klf4* (Figure 3c). In relation to the results of 0.38 dyne/cm², at physiological umbilical vein shear stress of 3 dyne/cm², we also saw an upregulation of *Klf2* and *Klf4* with the microfluidic

pump for 24h compared to cells in 12-well plate and microvessels perfused with interval rocker platform (Figure 3d). Longer time periods with 3 dyne/cm² could not be measured, due to an increase in endothelial cell death.

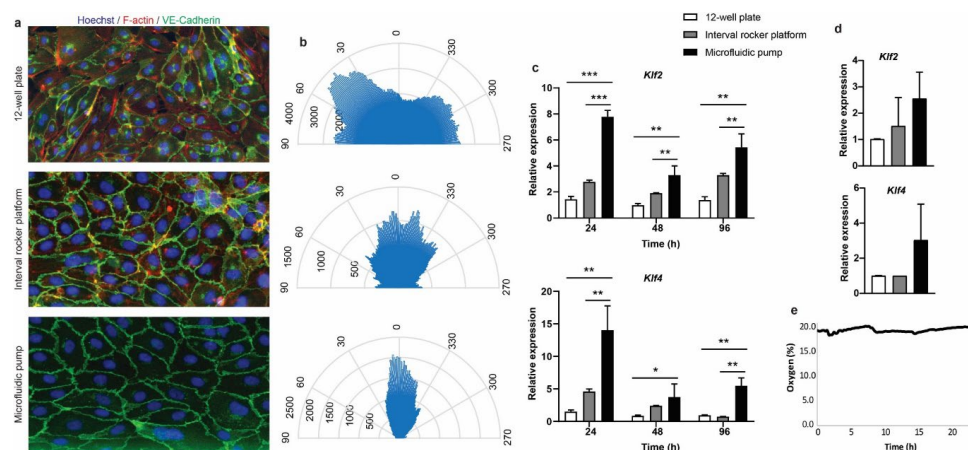


Figure 3 | Effects of flow on remodelling of the cytoskeleton in endothelial cells. HUVECs were cultured in 12-well plate representing the static condition, microvessels-on-chips were perfused with an interval rocker platform (Perfusion rocker, MIMETAS) and microfluidic pump. The interval rocker platform was set at a 7° angle of motion and an eight-minute timed operation to allow continuous bidirectional flow of medium in the microvessels. The microfluidic pump allowed unidirectional flow of medium in the microvessels. **(a-b)** Fluorescent images of cells with corresponding Rose plot of HUVEC alignment suggest that endothelial cells cultured in 12-well plate and microvessels-on-chips perfused with the interval rocker platform are more randomly orientated, whereas microvessels-on-chips perfused with the microfluidic pump with a shear stress of 3.0 dyne/cm² are uniformly orientated and aligned in one direction. **(c)** Shear stress of 0.38 dyne/cm² introduced with microfluidic pump in the microvessels for 24, 48 and 96h resulted in increased *Klf2* and *Klf4* expression. **(d)** Shear stress of 3.0 dyne/cm² introduced with the microfluidic pump in the microvessels for 24h resulted in increased *Klf2* and *Klf4* expression. Data are presented as mean and s.e.m; n = 2. **(e)** Continual measurement of oxygen within the integrated microvessels-on-chips.

Since, the integrated microvessels-on-chips platform is a fully closed system, the oxygen concentration was constantly monitored in order to be sure of gas permeability. The relatively stable oxygen levels observed in Figure 3e could be attributed to the gas permeability of the silicon tubings of the microfluidic pump. Interestingly, it takes the oxygen level in the

microfluidic device about 17h to reach steady state after the incubator has been set to 3.4% O₂ (Supplementary Figure 1). This has important implications for carrying out hypoxia studies in the future. Taken together, these results suggest that the integrated microvessels-on-a-chip platform induces flow dynamics that has an effect on the morphology of the endothelial cells. This is connected to the change in the mechanically induced signaling related to change in gene expression.

Discussion

In this article, we describe the design, fabrication and performance of a 16-channel peristaltic micropump for timed routing of fluids to interface physical sensor for monitoring oxygen. We used microvessels in the OrganoPlate as a working example to test the micropump. The sensing was performed *in situ* in an uninterrupted and automated manner, allowing for long-term monitoring of oxygen.

Various pumps have been developed to induce flow for microfluidic applications, but only very few are multi-channel pumps [20]. Multi-channel pumping can save time and resources to carry out large scale drug screening. Recent reports have addressed the need to create microfluidic pumping systems that are portable and can be integrated with other devices [10, 14]. Our system is rendered suitable since the pump approaches dimensions of microfluidic devices.

In this study, we show that flow has an effect on the morphology and cytoskeleton of the endothelial cells. The *in vivo* umbilical vein shear stress has been characterized to be as low as 3 dyne/cm² [21]. Considering this shear stress value under unidirectional flow, induced by our microfluidic pump, endothelial cells were more aligned to the direction flow in comparison to bidirectional flow with the interval rocker platform and cells cultured in 12-well plate [18]. Furthermore, the microvessels exhibited a change in the expression of proteins that are known to play significant roles in regulating shear-sensitive endothelial functions, such as inflammation, oxidative stress and angiogenesis [11]. These observations demonstrated the suitability of the presented microfluidic pumping system for studying the effect of flow on the biology of endothelial cells *in vivo*.

Meanwhile, we acknowledge several limitations of our current integrated microfluidic multi-channel pumping system. We could introduce shear stress of 3 dyne/cm² with our microfluidic pump for 24h, longer periods lead to increased cell death and instability of the microvessels. This observation may be explained by the fact that there is some degree of back pressure and pulsation in the system, which can effect cell viability after a long period of time [22]. Moreover, the channel wall is rigid and this condition is not met in reality, because the microvessels *in vivo* are distensible and their diameter changes with fluidic pressure [23]. Although flow characteristics are not superior to syringe pumps, the microfluidic pump design offers many advantages. The interface of liquids to and from the pump is completed without requiring excessive tubings, but via needle shafts in the inlets and outlets of the OrganoPlate. This miniaturizes the whole set-up of the system and reduces pump dead volumes. Furthermore, the microfluidic pump with the OrganoPlate fits on microscope stages, allowing unobstructed microscopic observation during perfusion.

The microfluidic pump can only perfuse 16 microvessels in parallel. Effort is being made to perfuse 96 microvessels, thereby covering the whole OrganoPlate and further improving the microfluidic pump for high-throughput perfusion [19]. Additionally, it is realized that the current platform requires manual sampling in the microvessels-on-chips. Further work is required to integrate an automated sampling system in order to achieve a long-lasting, self-assembled microvascular network without temporal exposure to the out-side environment.

Conflict of interest

Authors declare no conflict of interest related to the content of this manuscript. T.H. is shareholder in Mimetas BV, which was involved in the fabrication of the chips used in this study.

Acknowledgements

This study was financially supported by the RECONNECT CVON Groot consortium, which is funded by the Dutch Heart Foundation. AJ and TH, AJvZ were supported by a ZonMW MKMD

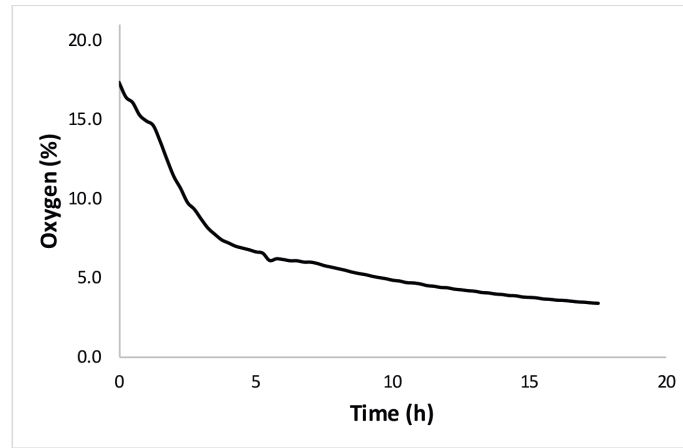
grant (114022501). AM and TH acknowledge the support by the NWO-TTW (IMMUNMET, grant number 16249). TH acknowledged the support by the TKI METABOCHIP project.

References

1. Organization, W.H. *Cardiovascular Diseases*. [cited 2019 19-08-2019]; Available from: <https://www.who.int/health-topics/cardiovascular-diseases/>.
2. Owan, T.E., et al., *Trends in prevalence and outcome of heart failure with preserved ejection fraction*. *N Engl J Med*, 2006. **355**(3): p. 251-9.
3. Paulus, W.J. and C. Tschope, *A novel paradigm for heart failure with preserved ejection fraction: comorbidities drive myocardial dysfunction and remodeling through coronary microvascular endothelial inflammation*. *J Am Coll Cardiol*, 2013. **62**(4): p. 263-71.
4. Lam, C.S.P. and D.L. Brutsaert, *Endothelial Dysfunction A Pathophysiologic Factor in Heart Failure With Preserved Ejection Fraction*. *Journal of the American College of Cardiology*, 2012. **60**(18): p. 1787-1789.
5. Savoji, H., et al., *Cardiovascular disease models: A game changing paradigm in drug discovery and screening*. *Biomaterials*, 2019. **198**: p. 3-26.
6. Duval, K., et al., *Modeling Physiological Events in 2D vs. 3D Cell Culture*. *Physiology (Bethesda)*, 2017. **32**(4): p. 266-277.
7. Rasheena, E., et al., *Three-Dimensional Cell Culture Systems and Their Applications in Drug Discovery and Cell-Based Biosensors*. *ASSAY and Drug Development Technologies*, 2014. **12**(4): p. 207-218.
8. Benam, K.H., et al., *Small airway-on-a-chip enables analysis of human lung inflammation and drug responses in vitro*. *Nat Methods*, 2016. **13**(2): p. 151-7.
9. Marturano-Kruik, A., et al., *Human bone perivascular niche-on-a-chip for studying metastatic colonization*. *Proc Natl Acad Sci U S A*, 2018. **115**(6): p. 1256-1261.
10. Zhang, Y.S., et al., *Multisensor-integrated organs-on-chips platform for automated and continual in situ monitoring of organoid behaviors*. *Proc Natl Acad Sci U S A*, 2017. **114**(12): p. E2293-E2302.
11. Ajami, N.E., et al., *Systems biology analysis of longitudinal functional response of endothelial cells to shear stress*. *Proceedings of the National Academy of Sciences*, 2017. **114**(41): p. 10990-10995.

12. Liu, M.C., et al., *Electrofluidic pressure sensor embedded microfluidic device: a study of endothelial cells under hydrostatic pressure and shear stress combinations*. Lab Chip, 2013. **13**(9): p. 1743-53.
13. Maoz, B.M., et al., *Organs-on-Chips with combined multi-electrode array and transepithelial electrical resistance measurement capabilities*. Lab Chip, 2017. **17**(13): p. 2294-2302.
14. Junaid, A., et al., *An end-user perspective on Organ-on-a-Chip: Assays and usability aspects*. Current Opinion in Biomedical Engineering, 2017. **1**: p. 15-22.
15. Ehgartner, J., et al., *Online analysis of oxygen inside silicon-glass microreactors with integrated optical sensors*. Sensors and Actuators B-Chemical, 2016. **228**: p. 748-757.
16. Vulto, P., et al., *Phaseguides: a paradigm shift in microfluidic priming and emptying*. Lab Chip, 2011. **11**(9): p. 1596-602.
17. Wang, H. and Y. Wang, *Measurement of water flow rate in microchannels based on the microfluidic particle image velocimetry*. Measurement, 2009. **42**(1): p. 119-126.
18. Tovar-Lopez, F., et al., *A Microfluidic System for Studying the Effects of Disturbed Flow on Endothelial Cells*. Frontiers in Bioengineering and Biotechnology, 2019. **7**(81).
19. van Duinen, V., et al., *96 perfusable blood vessels to study vascular permeability in vitro*. Sci Rep, 2017. **7**(1): p. 18071.
20. Skaftø-Pedersen, P., et al., *Multi-channel peristaltic pump for microfluidic applications featuring monolithic PDMS inlay*. Lab Chip, 2009. **9**(20): p. 3003-6.
21. Saw, S.N., et al., *Characterization of the in vivo wall shear stress environment of human fetus umbilical arteries and veins*. Biomech Model Mechanobiol, 2017. **16**(1): p. 197-211.
22. Wang, F., et al., *Oscillating flow promotes inflammation through the TLR2-TAK1-*IKK2* signalling pathway in human umbilical vein endothelial cell (HUVECs)*. Life Sciences, 2019. **224**: p. 212-221.
23. Katritsis, D., et al., *Wall shear stress: theoretical considerations and methods of measurement*. Prog Cardiovasc Dis, 2007. **49**(5): p. 307-29.
24. Santiago, J., et al., *A particle image velocimetry system for microfluidics*. Exp Fluid. Experiments in Fluids, 1998. **25**: p. 316-319.
25. Meinhart, C., S. T. Wereley, and J. Santiago, *PIV measurements of a microchannel flow*. Experiments in Fluids, 1999. **27**: p. 414-419.

Supplementary Figures



Supplementary Figure 1 | Continual measurement of oxygen within the integrated microvessels-on-chips after the incubator was set to 3.4% O₂.

Chapter VII

Discussion and Conclusion

Discussion

In general, microvascular disease is the result of the chronic exposure of the microvasculature to adverse metabolic and hemodynamic risk factors such as hypertension, hyperglycemia or the uremic toxins associated with renal failure. Progressive loss of tissue capillaries can continue for years without clinical manifestations until tissue-ischemia and consequent fibrosis reaches a threshold after which loss of organ function is manifested, making loss of microvascular integrity a main driver of morbidity.

Microvascular disease has an unmet clinical need for new therapeutics, with few to no therapies available yet. So far, researchers have mainly focused on using conventional cell culture systems or animal models to study microvascular diseases. However, conventional cell culture systems lack sufficient complexity to assess the functionality of the microvascular system and animal models often do not accurately mimic human pathophysiology. For these reasons, there is a broad need for alternative ways to model microvascular diseases *in vitro* to study disease mechanisms and to develop interventions to modulate or stop them. This thesis is focused on the development of microfluidic cell culture devices that mimic the microarchitecture and functions of human microvessels, using so called 'Organs-on-Chips'. These devices can host and combine different human cell and tissue types to study molecular- and cellular-scale activities that underlie the human blood vessels and specific disease states. Moreover, it gives the ability to identify and study new therapeutic targets *in vitro* [1-4]. Therefore, this platform offers an alternative way to study microvascular diseases that promotes personalized medicine by cultivating human microvessels that overcome key limitations in the fields of tissue engineering, vascular biology, immunometabolism and drug discovery. It serves as a 3D cell culture system that overcomes several shortcomings of 2D cell culture such as direct contact of cells with plastic, lack of perfusion and culturing cells for a short period [5]. Organs-on-Chips are now in the forefront of biotechnology with a promising future to truly mimic the human physiology and diseases. The research question discussed in this thesis:

How can we use a microfluidic 3D cell culture platform to develop a reliable robust and physiological relevant 'microvessel-on-a-chip' platform, that may serve as an attractive and versatile replacement for a significant fraction of animal models in vascular homeostasis?

Development and applications perspective

In **Chapter II** we reviewed the recent developments in the organ-on-a-chip field. Elegant platforms have been reported that cover almost all human organs, including the lung, intestine, kidney, skin, bone marrow, brain and vasculature, among others. Organs-on-Chips have developed from an academic research concepts to commercially available products. End-Users are interested in using these devices for functional and biochemical assays in the lab. Unfortunately, none of the published organ-on-a-chip models fully satisfy end-user usability requirements including assay compatibility, ease of handling and throughput. Furthermore, the majority of available systems are single chip-based models, with external pumping and use immunohistochemical stains as primary read-out. This severely limits the sensitivity, throughput and scalability.

In order to provide a more robust system, it is of utmost importance for engineers to make sure that their products are easy to use, high-throughput, simple to operate microfluidic platform for robust screening assay and compatible with other equipment in the lab, including liquid handlers and high-content imaging systems. And this should also require the availability of proper molecular read-outs including omics such as metabolomics to answer clinical questions.

We predict that in the coming years the organ-on-a-chip industry will become a competitive market, comparable to the smartphone industry, where third parties will review the products of organs-on-chips industries based on criteria's that meets the end-user needs. Such criteria's could include design, technology and integration [6]. We look forward in seeing this new era of competition and strategy and the impact it might have on drug research.

Mimicking microvascular disease using patients' plasma

In **chapter III** we used the organ-on-a-chip technology of MIMETAS, the OrganoPlate, to create miniaturized microvessels. For this device, we designed a novel chip structure, T-junction, that enables easy generation of 96 leak-tight microvessels and we aimed to use the platform to screen vascular destabilization factors in blood. The chip also allows endothelial cells to grow on soft substrate with a modifiable physiological stiffness. More importantly, we can measure microvessel permeability in real-time that allows the phenotypic screening of compounds.

Exposure of the microvessels to permeability factors such as TNF α , thrombin and VEGF, reconstituted vascular leakage of microvascular destabilization.

Next to that, we developed a method to prepare human plasma samples from whole blood and perfuse them through the microvessels-on-chips. To prevent coagulation for the isolation and storage of plasma samples, blood was decalcified by EDTA. As this tetravalent molecule leads to a loss of intercellular contact, we performed detailed studies to inhibit complement activation, thrombin and the intrinsic pathway of the coagulation cascade. This allowed recalcification of the plasma samples while retaining the morphology of healthy microvessels. Furthermore, the microvessels perfused with human blood plasma were as leak-tight as those with culture medium. This changed when the plasma samples were spiked with factors destabilizing the microvasculature, thereby inducing vascular leakage. We also compared our results with TEER measurements carried out in the Electric Cell-substrate Impedance Sensing (ECIS). This is a real-time, label-free and impedance-based method to study the activities of cells cultured in 2D. TEER measurements with the ECIS were significantly influenced by biological and environmental factors and 2D cell culture, thereby making the endothelial cells very sensitive to cytokines and growth factors. On the contrary, our microfluidic platform showed greater resemblance to *in vivo* tissue-like physiological responses, because it is an integrated system with excellent control and standardization of prepared 3D microvessels.

Our results indicate the possibility of using the microvessels-on-chips to study the mechanism behind microvascular destabilization. Importantly, we demonstrated the resemblance of the microvascular structure *in vitro* and the diffusion of albumin, thus representing the human microvessels. The microvessels-on-chips will be a tool to discover the effect of circulatory factors in patient blood samples on microvascular destabilization and to identify endothelial factors released by the destabilizing microvessels. In our current system, the microchambers contain two phaseguide-defined lanes. These allow cell-cell contact, cell-ECM contact and diffusive transport of molecules from the microvessel to the ECM. Using collagen gel in one lane and creating monolayer of cultured endothelial cells in the other lane, we can generate series of perfusable microvessels that can be used to model certain cellular aspects of microvascular destabilization as it is occurring *in vivo*. Our system represents a unique platform to study the pathophysiology of microvascular diseases in a manner that, differently from previously reported 2D models, allows to study changes in 3D conformation of

endothelial cells and abnormalities in their function. Moreover, the strong association between functional data in the microvessels-on-chips and *in vivo* microvessels parameters indicates that this system may be used as a platform to identify new biomarkers of microvascular destabilization in response to various stimuli and to test toxicity of new drug compounds.

In drug research, there is a big need for robust human *in vitro* models as animal models can differ from humans and translation of results from animal models to humans with regards to efficacy and safety are often a challenge. In addition, by using *in vitro* models, the human variability in genotypes and phenotypes can be taken into account. In this endeavor, the evidence from our study suggest that the microvessels-on-chips platform will have a major beneficial impact. Our microvessels-on-chips platform is especially suitable for detailed parallel optical interrogation of endothelial barrier function and inflammatory responses. Since the platform integrates both perfusion and the generation of biomolecular gradients, the microvessels-on-chips can be used as a tool to study angiogenesis *in vivo* [7]. The platform may have wide applications in toxicology as, e.g. an off-target effect of a drug candidate on microvascular integrity can be measured by high-throughput image analyses of phenotypic alterations. In addition, perfusing microvessels with human plasma samples is a valuable tool to identify disease-associated circulating plasma factors that cause microvascular destabilization and help diagnosis and clinical management of patients at risk for microvascular disease related complications, such as neurodegenerative diseases [8]. These findings can then be translated to patients and back.

We acknowledge that the microvessel-on-a-chip platform has some limitations, including the fact that it does not include pericytes yet. To develop a full picture of the microvasculature, additional studies will be needed in creating a co-culture of endothelial cells and pericytes. This will for example enable us to assess the functional properties of human pericyte-EC interactions in patients with constitutive endothelial Ang-2 release and patients with haploinsufficiency for the RNA-binding protein Quaking [9].

To explore the application limits of the microvessels-on-chips for further approaches in personalized medicine, future work should focus on developing patient's microvessels by using blood outgrowth endothelial cells (BOECs) or induced pluripotent stem cells (iPSCs) derived endothelial cells and pericytes. Most importantly, the derivation of cell lines from

patients suffering from microvascular diseases guarantees representation of disease heterogeneity in real-time in a dynamic system, which is not possible for example in animal studies. As several of the target diseases, for example heart failure with preserved ejection fraction (HFpEF), are significantly more frequent in woman and therefore sex-biased, our approach can also be used to explore gender-specific mechanisms [10].

Efficacy testing and drug discovery

Chapter IV describes the use of the microvessels-on-chips to recapitulate the hemorrhagic fever in Ebola disease. This disease is a major health threat for which we lack predictive tools. The Ebola virus causes vascular integrity impairment with subsequent blood loss, leading to fatal disseminated coagulopathies and hemorrhagic shock. We showed that perfusion of the Ebola VLPs induces vascular leakage in our system. The Ebola GP_{1,2} is the perpetrator in this process by perturbing the Rho/Rock pathway, causing changes in cellular mechanics. This hemorrhagic shock is treated with the Ebola disease drug candidates, melatonin and FX06.

Not all Ebola patients have signs of hemorrhagic fever with bleeding from the internal organs. Previous mouse studies have established that genetic background determines susceptibility to Ebola hemorrhagic fever [11]. Little is known about the heterogeneity in Ebola disease progression in human. This increases the death rate of vulnerable subjects and promotes Ebola virus disease to cause another global crisis. The microvessel-on-a-chip platform can serve as a chip-based diagnostic tool to quantify the severity of the Ebola disease, to diagnose or predict susceptibility at an early stage and assess the risk for healthy subjects. This can be achieved by perfusing blood plasma samples of Ebola patients to understand the dynamic in the disease progression. With this, more efficient health management strategies against Ebola can be developed.

Metabolomics as phenotypic read-out of organ-on-a-chip

The physiological read-out of endothelial function is a critical aspect in using microvessels-on-chips for disease and drug research. Metabolomics may deliver a more informative and sensitive read-out compared to relying only on morphological changes obtained with imaging analyses of phenotypic changes. It is a sensitive and robust read-out to identify metabolic markers of small molecule exposure in cells in diseased state. These properties are relevant for testing metabolic dose-response in pharmaceutical interventions and study the effect of metabolites that reflect microvascular destabilization [12].

In **Chapter V** we present an approach on using targeted liquid chromatography–tandem mass spectrometry (LC-MS/MS) metabolomics to quantify bioactive lipids that drive systemic inflammation in the microvessels, such as prostaglandins, isoprostanes, lysophosphatidic acid (LPA) classes, sphingolipids and platelet activating factor (PAF). *In vitro* studies of these bioactive lipids have been based on 2D endothelial cell cultures that, due to lack of laminar flow and the growth of the cells on plastics, often display a pro-inflammatory phenotype. Since, the microvessel-on-a-chip model resembles the physiological environment, we optimized targeted LC-MS/MS measurements of a panel of pro- and anti-inflammatory bioactive lipids to generate expression profiles both in TNF α treated 3D microvessels as well as in 2D endothelial cell cultures. Although we were dealing with very small samples and low concentration of metabolites in the microvessels-on-chips, we were able to measure bioactive lipids secreted by the endothelial cells. Furthermore, they displayed a less inflammatory response to TNF α compared to classical 2D endothelial cell cultures. This study demonstrates the possibility to use the microvessels-on-chips to study disease mechanisms, validate drug effects and drug-drug interactions, a major unmet need for research in vascular biology [13]. This allows pharmaceutical companies to reevaluate drugs, investigate on- and off-target effects of drugs that failed to meet their primary effectiveness in phase III clinical trials and repurpose them for the treatment of other diseases in an efficient and cost-effective way [14].

We have combined our microvessels-on-chips with established metabolomics platform to identify novel cellular factors that are released from destabilizing microvessels. These factors may serve as potential biomarkers *in vivo* and help to dissect cellular pathways of microvascular destabilization. We envision that in the future with metabolomics and the microvessels-on-chips we will be able to study the flux of molecules that maintain vascular

homeostasis, such as nitric oxide (NO) and glucose, in a more physiologically relevant setting. Another emerging direction promising for the microvessels-on-chips is to use single-cell metabolomics [15]. The study will give insights into the heterogeneity of cell-cell and cell-ECM interactions. These differences might have important consequences in the discovery of new biomarkers for microvascular destabilization. However, single-cell metabolomics is still in its infancy. Works still need to be done in improving the sensitivity, developing innovative cell-sampling techniques and providing robust data-processing and normalization methods.

Automated microfluidic cell culture and control of system parameters

Although a wide variety of human microvessels have been created with MIMETAS OrganoPlate, there are limited efforts so far on the integration of a pumping system and real-time oxygen sensor. A pumping system is critical for introducing controlled laminar shear stress to endothelial cells, since their response to physiological flow dynamics affects vascular health [16, 17]. Additionally, *in situ* continual measuring of oxygen is essential in precise assessment of the microenvironment and the dynamic responses of the microvessels to drugs over extended periods of time. In **Chapter VI**, we report a microfluidic pumping and oxygen sensor platform, which we developed in our lab. The platform is high-throughput and operates in an automated manner. The system was used to study the effect of static condition, bidirectional flow with the MIMETAS Rocker and unidirectional flow with our pumping system on the cytoskeleton remodeling and gene expression of the microvessels-on-chips. Our results clearly demonstrated that the laminar flow introduced with the microfluidic pumping system brings the microvessels to a more physiological state, while maintaining a stable oxygen level in the enclosed microfluidic system.

There is a growing need to automate *in vitro* experiments for improvement in accuracy, throughput and safety. Manual handling of the microvessels-on-chips greatly effects the long-term maintenance and monitoring of cells. This might become a barrier for the high-throughput and robustness of the system. In many organs-on-chips studies, the integration of laboratory automation technology has therefore been proposed [18, 19]. This system primarily consists of a liquid-handler and a robot for transposition of receptacles, allowing automated cell culture and monitor. Moreover, it accurately handles micro-scale fluid

volumes in a rapid speed, decreasing the temporal lag in extracellular response to molecules transported across cell membranes in the organs-on-chips. Therefore, the integration of robotic handling in the microvessels-on-chips will be of great value, because it will further improve the reproducibility, parallelization and longitudinal observations of the microvessels.

For further developments, the microfluidic pumping and oxygen sensor platform can be flexibly adapted to an automated cell culture platform. Together, they will be a powerful tool to enable automated cell culture, perfusion, medium addition, fluidic linking, sample collection and *in situ* monitor of cells, within a controlled temperature and oxygen environment. This should facilitate the studies of drug pharmacokinetics and pharmacodynamics (PK/PD) for an extended period of time *in vitro* [18].

Conclusion

In vitro modeling the vasculature can provide molecular and cellular insights to understand the biochemical and biophysical mechanisms of the human vascular system. The current gold standard for this are animal models and 2D cell culture. Unfortunately, these systems are significantly limited in recapitulating the human pathophysiology. Organs-on-Chips can provide a unique solution to mimic the vascular function, however, these micro-physiological systems are still in proof-of-concept stage and need further optimization to really aid in diagnosing and treating microvascular diseases. In order to utilize the full potential of the organs-on-chips for recapitulating the critical aspects of microvascular diseases, the following research question was discussed:

How can we use a microfluidic 3D cell culture platform to develop a reliable robust and physiological relevant 'microvessel-on-a-chip' platform, that may serve as an attractive and versatile replacement for a significant fraction of animal models in vascular homeostasis?

To answer this question, this thesis was focused on:

- 1) The assessment of the usability, compatibility and assay ability of the organ-on-a-chip in the light of end-user adoption aspects.

- 2) Methods to screen blood samples for the presence of inflammatory, leakage or angiogenic factors in a perfusable high-throughput microvessel-on-a-chip platform and translation to the clinic.
- 3) The use of the microvessel-on-a-chip platform for studying mechanisms in the vascular pathophysiology associated with Ebola virus disease and therapeutic interventions to suppress Ebola-induced vascular destabilization.
- 4) The application of metabolomics as a molecular read-out in the microvessels to identify biomarkers for microvascular diseases.
- 5) The development of a high-throughput microfluidic pump and *in situ* oxygen monitoring for the microvessel-on-a-chip platform in order to make it more physiological relevant.

The microvessel-on-a-chip platform represents a transformative system that can serve as an effective replacement and for some applications, improvement over the current animal model and 2D cell culture system for microvascular destabilization. The next step now is to further validate this system by using it to screen blood samples in a large clinical study on microvascular diseases. This will provide large number of samples from patients that can be analyzed in the microvessel-on-a-chip platform under various therapeutic conditions. The findings observed can then be translated back to patients to predict clinical outcome of treatments and at the same time evaluate the effectiveness of the system for speeding up drug research. We are convinced that the coming years the microengineered microvessels will have a major impact on society by accelerating the development of new drugs and advancing personalized medicine.

References

1. Phan, D.T.T., et al., *A vascularized and perfused organ-on-a-chip platform for large-scale drug screening applications*. Lab on a Chip, 2017. **17**(3): p. 511-520.
2. Zhang, B.Y., et al., *Biodegradable scaffold with built-in vasculature for organ-on-a-chip engineering and direct surgical anastomosis*. Nature Materials, 2016. **15**(6): p. 669-+.

3. Sances, S., et al., *Human iPSC-Derived Endothelial Cells and Microengineered Organ-Chip Enhance Neuronal Development*. *Stem Cell Reports*, 2018. **10**(4): p. 1222-1236.
4. Rayner, S.G., et al., *Reconstructing the Human Renal Vascular-Tubular Unit In Vitro*. *Advanced Healthcare Materials*, 2018. **7**(23).
5. Duval, K., et al., *Modeling Physiological Events in 2D vs. 3D Cell Culture*. *Physiology*, 2017. **32**(4): p. 266-277.
6. Kaushik, G., J. Leijten, and A. Khademhosseini, *Concise Review: Organ Engineering: Design, Technology, and Integration*. *Stem Cells*, 2017. **35**(1): p. 51-60.
7. van Duinen, V., et al., *Perfused 3D angiogenic sprouting in a high-throughput in vitro platform*. *Angiogenesis*, 2019. **22**(1): p. 157-165.
8. Sohn, E.H., et al., *Retinal neurodegeneration may precede microvascular changes characteristic of diabetic retinopathy in diabetes mellitus*. *Proceedings of the National Academy of Sciences of the United States of America*, 2016. **113**(19): p. E2655-E2664.
9. van der Veer, E.P., et al., *Quaking, an RNA-Binding Protein, Is a Critical Regulator of Vascular Smooth Muscle Cell Phenotype*. *Circulation Research*, 2013. **113**(9): p. 1065-1075.
10. Duca, F., et al., *Gender-related differences in heart failure with preserved ejection fraction*. *Scientific Reports*, 2018. **8**.
11. Rasmussen, A.L., et al., *Host genetic diversity enables Ebola hemorrhagic fever pathogenesis and resistance*. *Science*, 2014. **346**(6212): p. 987-991.
12. Shintu, L., et al., *Metabolomics-on-a-Chip and Predictive Systems Toxicology in Microfluidic Bioartificial Organs*. *Analytical Chemistry*, 2012. **84**(4): p. 1840-1848.
13. Wang, X., et al., *Analysis of an Integrated Human Multiorgan Microphysiological System for Combined Tolcapone Metabolism and Brain Metabolomics*. *Analytical Chemistry*, 2019. **91**(13): p. 8667-8675.
14. Esch, E.W., A. Bahinski, and D. Huh, *Organs-on-chips at the frontiers of drug discovery*. *Nature Reviews Drug Discovery*, 2015. **14**(4): p. 248-260.
15. Fessenden, M., *Metabolomics: Small Molecules, Single Cells*. *Nature*, 2016. **540**(7631): p. 153-155.
16. Mahmoud, M.M., et al., *Shear stress induces endothelial-to-mesenchymal transition via the transcription factor Snail*. *Scientific Reports*, 2017. **7**.
17. Doddaballapur, A., et al., *Laminar Shear Stress Inhibits Endothelial Cell Metabolism via KLF2-Mediated Repression of PFKFB3*. *Arteriosclerosis Thrombosis and Vascular Biology*, 2015. **35**(1): p. 137-145.
18. Novak, R., et al., *A robotic platform for fluidically-linked human body-on-chips experimentation*. *bioRxiv*, 2019: p. 569541.
19. Kane, K.I.W., et al., *Automated microfluidic cell culture of stem cell derived dopaminergic neurons*. *Scientific Reports*, 2019. **9**.

Chapter VII

VII

Chapter VIII

Summary

Nederlandse Samenvatting

Acknowledgements

Curriculum Vitae

List of Publications

Summary

In the last decades, microvascular diseases are a leading cause of mortality worldwide. Chronic activation of the endothelial cells by cardiovascular risk factors can inflict the loss of pericytes that plays a critical role in microvascular stabilization. To diagnose and treat microvascular diseases, we aim to explore the association of circulating plasma factors with microvascular integrity. As current human 2D models with cultured endothelial cells lack sufficient complexity to assess the function of microvascular endothelial-pericyte interactions, research on microvascular loss largely depends on animal models. To mimic the microarchitecture and functions of the human blood vessel in a more efficient way for drug discovery, the organs-on-chips are proposed to be an advanced 3D culture system as introduced in **Chapter I**. The scope of this thesis is to develop a human microvessel-on-a-chip that experiences mechanical fluid flow, biological and environmental sensing, which allow for analysis of organ-level microvessel physiology and pathophysiology. Furthermore, this device is high-throughput and can be used as a diagnostic and drug screening tool for drug development.

In **Chapter II**, we reviewed organ-on-a-chip efforts published over the last two years in light of user friendliness, compatibility, assay ability and product readiness. This review is written to introduce organs-on-chips to scientists from various research field. Elegant platforms from a single chip to microtiter plate format with various integrated sensors were reported. Also, functional assays for angiogenesis, calcium imaging of neurons and neuro-muscular contractility were notified. The system is gaining its momentum in compatibility with standard analysis techniques such as sequencing, fluorescent activated cell sorting and mass spectrometry. Organs-on-Chips is rapidly shifting from academic proof-of-concept studies to real-world solutions.

The development of models that effectively recapitulate the human blood vessel is important for studying the pathogenesis and therapeutic approaches for microvascular diseases. In order to do this, in **Chapter III**, we engineer a perfusable human microvessel-on-a-chip with human umbilical vein endothelial cells (HUVECs) that is partly surrounded with extracellular matrix (ECM). The perfusion of VEGF, histamine and TNF α leads to increase in vessel permeability, reconstituting the microvascular leakage seen *in vivo*. To screen microvascular destabilization factors in blood, we prepared plasma samples from whole blood and treated with hirudin, corn trypsin inhibitor (CTI) and compstatin. Healthy volunteer plasma samples spiked with

VEGF, histamine and TNF α leads to vascular leakage in the microvessel-on-a-chip. These findings strengthen the idea that our assay can be used for analysing human microvascular pathophysiology and possibly carrying out preclinical drug evaluations.

As an example, in **Chapter IV** we show that a perfusable, endothelialized microvasculature-on-a-chip featuring a collagen hydrogel that minimally mimics the ECM of host tissue allows the modeling of Ebola-induced vascular phenotypes and provides an *in vitro* platform for drug studies. Luminal infusion of Ebola virus-like particles (VLPs) leads to albumin leakage from the engineered vessels. Mechanistically, we demonstrate that this process involves the Rho/ROCK pathway. The Ebola glycoprotein (GP_{1,2}) plays a key role in this process. Finally, we demonstrate the applicability of this platform for studying the efficacy of potential drugs by measuring the potency of the recently developed experimental drug FX06 and melatonin, in phenotypic rescue.

Besides imaging analyses of phenotypic changes in the microvessels, metabolomics may deliver a more informative readout of endothelial function. As an exploratory study, in **Chapter V** we assessed whether the 3D microvessels display a less inflammatory phenotype compared to 2D endothelial cell cultures. In order to do this, we use an optimized targeted liquid chromatography–tandem mass spectrometry measurements of a panel of pro- and anti-inflammatory bioactive lipids to generate expression profiles both in TNF α treated microvessels as well as in 2D endothelial cell cultures. We demonstrate that bioactive lipid profiles can be readily detected from 3D microvessels-on-a-chip and display a more dynamic, less inflammatory response to TNF α , that resembles more the human situation, compared to classical 2D endothelial cell cultures.

In vivo, the microvessels experience physical stress associated with laminar blood flow and it plays a central role in maintaining vascular integrity and homeostasis. **Chapter VI** reports the microvessels-on-a-chip with integrated multi-channel microfluidic pumping and *in situ* oxygen monitoring system. This system is used to study the effect of flow on the cytoskeleton remodeling and the expression of flow responsive genes in the microvessels-on-a-chip. Our results demonstrate that the generated unidirectional flow changes the orientation of angle of endothelial cells and increase the expression of flow responsive genes *in vitro* compared to bidirectional flow.

Chapter VIII

In conclusion, as illustrated in this thesis, the microvessels-on-chips may serve as a unique tool for microvascular destabilization studies as well as for the development of novel therapeutic strategies to combat microvascular complications. In the future, with the developed method to perfuse plasma samples in the microvessels, destabilizing profile of patients can be developed in order to predict ongoing microvascular rarefraction and risk of complications.

Nederlandse samenvatting

In de laatste decennia zijn microvasculaire aandoeningen wereldwijd een belangrijke oorzaak van sterfte. Chronische activering van de endotheelcellen door cardiovasculaire risicofactoren kan leiden tot het verlies van pericyten die een cruciale rol spelen bij microvasculaire stabilisatie. Om microvasculaire aandoeningen te identificeren en behandelen, willen we de associatie van circulerende plasmafactoren met microvasculaire integriteit onderzoeken. Aangezien de huidige menselijke 2D-modellen met gekweekte endotheelcellen onvoldoende complexiteit bevatten om de functie van interacties van microvasculaire endotheel-pericyte te beoordelen, hangt het onderzoek naar microvasculair verlies grotendeels af van diermodellen. Om de microarchitectuur en functies van het menselijk bloedvat op een efficiëntere manier na te bootsen voor het ontwikkelen van geneesmiddelen, wordt de 'organen-op-chips' voorgesteld als een geavanceerd 3D-kweekstelsel, zoals geïntroduceerd in **Hoofdstuk I**. Het doel van dit proefschrift is het ontwikkelen van een menselijke microvaat-op-een-chip die mechanische vloeistofstroom ervaart, biologische en omgevingsdetectie, die analyse van de vatfysiologie en pathofysiologie op orgaan-niveau mogelijk maakt. Bovendien heeft dit apparaat een hoge doorvoersnelheid en kan het worden gebruikt als een diagnostisch en medicijnscreeningsinstrument voor het ontwikkelen van geneesmiddelen.

In **Hoofdstuk II** hebben we de orgaan-op-een-chip uitvindingen van de afgelopen twee jaar besproken in het licht van gebruiksvriendelijkheid, compatibiliteit, experimentele testvermogen en productgereedheid. Deze review is geschreven om organen-op-chips te introduceren aan wetenschappers uit verschillende onderzoeksgebieden. Elegante platformen van een enkele chip tot microtiterplaatformaat met verschillende geïntegreerde sensoren werden besproken. Daarnaast werden functionele testen voor angiogenese, calciumbeeldvorming van neuronen en neurospiercontractiliteit besproken. Het systeem wint zijn momentum in compatibiliteit met standaardanalysetechnieken zoals sequencing, fluorescent geactiveerde celsortering en massaspectrometrie. Organen-op-Chips verschuiven snel van academische 'proof-of-concept' studies naar oplossingen in de praktijk.

De ontwikkeling van modellen die het menselijke bloedvat effectief na bootsen is belangrijk voor het bestuderen van de pathologie en therapeutische behandelen van microvasculaire aandoeningen. Om dit te doen, construeren we in **Hoofdstuk III** een perfuseerbare menselijke microvaat-op-een-chip met menselijke navelstreng endotheelcellen die gedeeltelijk omgeven

is met extracellulaire matrix (ECM). De perfusie van VEGF, histamine en TNF α leidt tot een toename van de permeabiliteit van het vat, waardoor de *in vivo* waargenomen microvasculaire lekkage wordt nagebootst. Om microvasculaire destabilisatiefactoren in bloed te screenen, hebben we plasmamonsters uit volbloed bereid en behandeld met hirudine, maïs-trypsineremmer en compstatin. Gezonde vrijwillige plasmamonsters verrijkt met VEGF, histamine en TNF α leiden tot microvasculaire lekkage in het microvaat-op-een-chip. Deze bevindingen versterken het idee dat onze model kan worden gebruikt voor het analyseren van menselijke microvasculaire pathofysiologie en mogelijk preklinische geneesmiddelenevaluaties.

Als voorbeeld laten we in **Hoofdstuk IV** zien dat een perfuseerbare, endotheel microvaat-op-een-chip met collageenhydrogel die de ECM van gastheerweefsel minimaal nabootst, het modelleren van door Ebola veroorzaakte vasculaire fenotypes mogelijk maakt en een *in vitro* platform voor geneesmiddelen studies aanbiedt. Luminal infusie van Ebola-virusachtige deeltjes leidt tot albumine-lekkage uit de geconstrueerde vaten. Mechanisch laten we zien dat dit proces het Rho/ROCK signaalweg omvat. Het Ebola-glycoproteïne (GP1,2) speelt een belangrijke rol in dit proces. Ten slotte tonen we de toepasbaarheid van dit platform voor het bestuderen van de werkzaamheden van potentiële medicijnen door het meten van de potentie van het recent ontwikkelde experimentele medicijn FX06 en melatonine, voor fenotypische redding.

Naast beeldvormende analyses van fenotypische veranderingen in de microvaten, kan metabolomics een meer informatieve uitlezing van de endotheel functie leveren. Als een verkennend onderzoek hebben we in **Hoofdstuk V** beoordeeld of de 3D-microvaten een minder inflammatoir fenotype vertonen in vergelijking met 2D-endotheelcelculturen. Om dit te doen, gebruiken we een geoptimaliseerde gerichte vloeistofchromatografie - tandem massaspectrometriemetingen van een paneel van ontsteking bioactieve lipiden om expressieprofielen te genereren, zowel in TNF α behandelde microvaten als in 2D-endotheelcelculturen. We tonen aan dat bioactieve lipidenprofielen gemakkelijk kunnen worden gedetecteerd uit 3D-microvaten-op-een-chip en een meer dynamische, minder ontstekingsreactie door TNF α vertonen, die meer op de menselijke situatie lijkt in vergelijking met klassieke 2D-endotheelcelculturen.

In vivo, ervaren de microvaten fysieke stress geassocieerd met laminaire bloedstroom en het speelt een centrale rol bij het handhaven van vasculaire integriteit en homeostase. **Hoofdstuk VI** beschrijft de microvaten-op-een-chip met geïntegreerd geminiaturiseerd pomp en zuurstofmonitorsysteem *in situ*. Dit systeem wordt gebruikt om het effect van stroming op de remodelering van het cytoskelet en de expressie van stromingsgevoelige genen in de microvaten-op-een-chip te bestuderen. Onze resultaten tonen aan dat de gegenereerde unidirectionele stroom het oriëntatie van de hoek van endotheelcellen veranderen en de expressie van stroomgevoelige genen *in vitro* verhoogt in vergeleken met bidirectionele stroom.

Concluderend, zoals geïllustreerd in dit proefschrift, kunnen de microvaten-op-chips dienen als een uniek hulpmiddel om microvasculaire destabilisatie te onderzoeken en voor het ontwikkelen van nieuwe therapeutische strategieën om microvasculaire complicaties te bestrijden. In de toekomst, met het ontwikkelde methode om plasmamonsters in de microvaten te perfuseren, kan een destabiliserend profiel van patiënten worden weergegeven om voortdurende microvasculaire rarefactie en het risico op microvasculaire complicaties te voorspellen.

Acknowledgements

I really enjoyed the freedom Prof. dr. Thomas Hankemeier, Prof. dr. Anton Jan van Zonneveld, Dr. Alireza Mashaghi and Dr. Janine van Gils gave me in carrying out my research. I am impressed by their patience, motivation and immense knowledge in this thesis process.

I would like to thank Dr. Paul Vulto, Dr Henriëtte Lanz and Dr. Sebastiaan Trietsch from MIMETAS, as well as Ankur Kislaya MSc from TU Delft and Dr. Mettine Bos from LUMC for giving me access to their laboratory and research facilities, and the stimulating discussions.

I would also like to thank the volunteers who provided the sample material for the studies described in this thesis. I sincerely valued our working relationship and the positive impact it had in widening out my research.

I am grateful to Dr. Amy Harms, Loes Beijersbergen and Cathy Robbers for their daily support, meeting and travel arrangements made during my PhD.

Huge gratitude goes out to Wendy Stam and Raphaël Zwier. Both of you supported me greatly in my work and together we produced wonderful results.

To all the past and present members of Systems Biomedicine and Pharmacology, BMFL at Leiden University and Eindhoven Laboratory at LUMC, thank you for your help, collaboration and the great time we had during my PhD.

Finally, I wish to thank my parents, Taiwo and Modupe, and my brothers, Daniel and John, for their support and encouragement throughout my study. And my wife Peace and baby girl Kharis, I want to thank you both for your help and support in finishing my PhD and working towards the future together.

Curriculum Vitae

Abidemi Junaid was born on August 15, 1990 in Ibadan, Nigeria. He obtained his secondary school degree in Biology, Chemistry and Physics at Dalton Den Haag, The Hague, The Netherlands in 2008. Subsequently, he started a Bachelor in Biometrics at the Zuyd University of Applied Sciences in Heerlen.

Between 2013 – 2015, Abidemi pursued a Master in Biomolecular Sciences at the VU University Amsterdam, specifically the Molecular Cell Biology, with excellent grades. His first master internship, in the group of Dr. Chirlmin Joo at TU Delft, was on elucidating the biophysical rule behind how microRNAs find their targets. In 2015, he started with a second master internship in the laboratory of Dr. Derk ten Berge at the Erasmus MC, to investigate the type of enhancer LIMES cells use to maintain their pluripotency.

In August 2015, Abidemi started his PhD at the Division of Systems Biomedicine and Pharmacology, LACDR, Leiden University and Einthoven Laboratory, Department of Nephrology, Leiden University Medical Center, on the investigations described in this thesis. This research was funded by the Dutch Heart Foundation and was performed under the supervision of Prof. Dr. Thomas Hankemeier, Prof. Dr. Anton Jan van Zonneveld, Dr. Alireza Mashaghi and Dr. Janine van Gils at Leiden University and Leiden University Medical Center. Work described in this thesis has been presented at several national and international congresses, where Abidemi was awarded with travel grants from The Metabolomics Society and Society for Laboratory Automation and Screening (SLAS). Moreover, he received the best oral presentation award by the Dutch Cardio Vascular Conference.

Currently, Abidemi is working at Leiden University and Leiden University Medical Center. Together with Erasmus University Medical Center, he aims to use his technology to discover biomarkers for early microvascular changes in sepsis and COVID-19 in order to improve survival from these diseases.

List of Publications

1. **Junaid A**, Mashaghi A, Hankemeier T and Vulto P. An end-user perspective on Organ-on-a-Chip: Assays and usability aspects. *Current Opinion in Biomedical Engineering*. 2017;1:15-22.
2. **Junaid A**, Tang HQ, van Reeuwijk A, Abouleila Y, Wuelfroth P, van Duinen V, Stam W, van Zonneveld AJ, Hankemeier T and Mashaghi A. Ebola Hemorrhagic Shock Syndrome-on-a-Chip. *Iscience*. 2020;23.
3. Zhang HY, Vreeken D, **Junaid A**, Wang GQ, Sol WMPJ, de Bruin RG, van Zonneveld AJ and van Gils JM. Endothelial Semaphorin 3F Maintains Endothelial Barrier Function and Inhibits Monocyte Migration. *Int J Mol Sci*. 2020;21.
4. **Junaid A**, Schoeman J, Yang W, Stam W, Mashaghi A, van Zonneveld AJ and Hankemeier T. Metabolic response of blood vessels to TNF alpha. *Elife*. 2020;9.

